Winter 12-4-2013

Marine Diatom Assemblage Variation Across Pleistocene Glacial-Interglacial Transitions and Neogene Diatom Biostratigraphy of Site C9001, NW Pacific Ocean

Marcella K. Purkey
University of Nebraska-Lincoln, marciepurkey@gmail.com

MARINE DIATOM ASSEMBLAGE VARIATION ACROSS PLEISTOCENE GLACIAL-INTERGLACIAL TRANSITIONS AND NEOGENE DIATOM BIOSTRATIGRAPHY OF SITE C9001, NW PACIFIC OCEAN

by

Marcella K. Purkey

A THESIS

Presented to the Faculty of

The Graduate College at the University of Nebraska

In Partial Fulfillment of Requirements

For the Degree of Master of Science

Major: Earth and Atmospheric Sciences

Under the Supervision of Professor David M. Harwood

Lincoln, Nebraska

November, 2013

MARINE DIATOM ASSEMBLAGE VARIATION ACROSS PLEISTOCENE GLACIAL-INTERGLACIAL TRANSITIONS AND NEOGENE DIATOM BIOSTRATIGRAPHY OF SITE C9001, NW PACIFIC OCEAN

Marcella K. Purkey, M.S.

University of Nebraska, 2013

Adviser: David M. Harwood

In 2006, *D/V-Chikyu* cruise CK06-06 drilled Hole C9001C at Site C9001 in the Northwest Pacific Ocean, 80 km east of the Shimokita Peninsula, Japan. An existing chronostratigraphic framework provides a continuous glacial-interglacial (GI) climate record from which a diatom record of paleoenvironmental changes was developed across several GI cycles. Species counts, diatom temperature values, calculated sea-surface temperatures (SST) and factor analysis were produced for each sample and calibrated to prior diatom studies in this region. These features were used to characterize and compare interglacial maxima of Marine Isotope Stages (MIS) 1, 5e, 9 and 11 and transitions from the preceding glacial maxima. MIS 9 was the warmest with a peak temperature of 20.2°C. Peak temperatures in MIS 1 are calculated at 14.9°C and are only 1°C cooler than peak SSTs calculated for MIS 11 and 5e; however, the temperature trend for MIS 1 continues on a linear trajectory toward warmer temperatures. A lead/lag relationship between SST and the benthic oxygen isotope record of ice volume was observed at the onset and reversals of major GI cycles. The highest four factors derived from factor analysis of the diatom assemblages explain 88.7% of the total variance and are attributed to diatom preference for specific watermasses. Factor 1 is dominated by *Melosira*

albicans, which does not show a consistent environmental preference through every interval. Factor 2 is dominated by a north-temperate species, and Factors 3 and 4 are both dominated by species indicating sea-ice influence.

Integrated Ocean Drilling Program (IODP) Expedition 337 returned to Site C9001, drilled a new hole in 2012, and extended the total depth at Site C9001 to 2466 meters below sea floor (mbsf). Diatom biostratigraphic analysis presented here confirmed an Early Miocene age at 1246.5 mbsf. These new diatom results, combined with palynological analysis suggest a Late Oligocene-Early Miocene age at the base of the hole. These ages are younger than those predicted by seismic correlations prior to drilling.

This work is dedicated to my parents,

who always encouraged me to build my own future.

Special acknowledgement and thanks for the expertise offered by my adviser and committee members Drs. David Harwood, Tracy Frank, Sherilyn Fritz and David Watkins; as well as Tatiana Davila and Drs. Cara Burberry, Itsuki Suto and Diane Winter.

Support for my participation in Integrated Ocean Drilling Program Expedition 337 and subsequent research on this project was provided to the University of Nebraska-Lincoln through the U.S. Science Support Program.

TABLE OF CONTENTS

Chapter 1
Marine Diatom Assemblage Variation across Pleistocene Glacial/Interglacial Transitions

Multimedia Objects

Figures

CHAPTER 1

MARINE DIATOM ASSEMBLAGE VARIATION ACROSS PLEISTOCENE GLACIAL-INTERGLACIAL TRANSITIONS

ABSTRACT

In 2006, *D/V-Chikyu* cruise CK06-06 drilled Hole C9001C at Site C9001 in the Northwest Pacific Ocean, 80 km east of the Shimokita Peninsula, Japan. An existing chronostratigraphic framework provides a continuous glacial-interglacial (GI) climate record from which a diatom record of paleoenvironmental changes was developed across several GI cycles. Species counts, diatom temperature values, calculated sea-surface temperatures (SST) and factor analysis were produced for each sample and calibrated to prior diatom studies in this region. These features were used to characterize and compare interglacial maxima of Marine Isotope Stages (MIS) 1, 5e, 9 and 11 and transitions from the preceding glacial maxima. MIS 9 was the warmest with a peak temperature of 20.2°C. Peak temperatures in MIS 1 are calculated at 14.9°C and are only 1°C cooler than peak SSTs calculated for MIS 11 and 5e; however, the temperature trend for MIS 1 continues on a linear trajectory toward warmer temperatures. A lead/lag relationship between SST and the benthic oxygen isotope record of ice volume was observed at the onset and reversals of major GI cycles. The highest four factors derived from factor analysis of the diatom assemblages explain 88.7% of the total variance and are attributed to diatom preference for specific watermasses. Factor 1 is dominated by *Melosira albicans*, which does not show a consistent environmental preference through every interval. Factor 2 is dominated by a north-temperate species, and Factors 3 and 4 are both dominated by species indicating sea-ice influence.

1. Introduction

Characterizing and comparing the magnitude and timing of past interglacial stages and glacial-interglacial (GI) transitions is particularly relevant to help understand our present interglacial and in predicting our future climate trajectory (Yin and Berger, 2012). GI cycles through the Pleistocene are generally thought to be paced by astronomically induced insolation changes that drive Earth System feedbacks toward periods of more or less ice on Earth. Since the Mid-Pleistocene Transition, at about 900 ka, climate variation has been controlled by the 100 k.y. eccentricity cycle; and since about 430 ka, the amplitude of GI transitions has increased substantially, as recorded by marine oxygen isotope and Antarctic ice core records (Yin and Berger, 2012).

Marine Isotope Stage (MIS) 11 has been considered the best analogue for the Holocene in terms of orbital forcing (Berger and Loutre, 2003), but a recent modeling study by Yin and Berger (2012) now shows that MIS 19 is a closer analogue based on greenhouse gas (GHG) concentrations, insolation distribution pattern, and temperature response.

Insolation plays a more important role in northern high latitudes than GHG, and high eccentricity induces more solar radiation in high, Northern Hemisphere (NH) latitudes. Insolation also explains most of the variation of the summer sea-ice area in the Arctic. Together, insolation and elevated GHG contributed to the warmest MISs, including, but not limited to MIS 1, 5e, 9, 11 and 19 (Yin and Berger, 2012).

Recognizing that past records of paleoclimate and paleoenvironmental change will guide our ability to predict future changes, this study was designed to examine the

diatom record across several GI transitions at Site C9001 in the Northwest Pacific Ocean near Japan. This site provides an expanded sedimentary archive of diatom variation, which can be compared directly to the benthic foraminiferal-based oxygen isotope record, in order to characterize and compare the timing of surface water changes in this region to global ice volume changes across several Late Pleistocene GI transitions and interglacial stages.

In order to better understand the nature and range of possible paleoenvironmental changes in this region, and how diatoms responded to changes in paleoceanographic and paleoclimatic conditions, this study initially examined the entire and most recent glacial-interglacial cycle (spanning the last ~140 ky). Specifically, this study compares the Last Glacial Maximum (LGM)-to-Holocene (MIS 2/1) transition with prior GI transitions leading to interglacials MIS 5e, 9 and 11.

Diatoms can be used to identify the variable influence of ocean currents over a given region through time and characterize the response of surface water to climate shifts. Previous studies from the North Pacific Ocean provide valuable records for comparison of LGM and post-LGM paleoenvironmental changes in this region. Studies evaluating the Late Pleistocene history of surface water changes; however, are limited. The present study applies methods used in the previous studies of Koizumi et al. (2004, 2006) and Koizumi (2008) and expands existing research by developing the diatoms as a useful proxy in older geologic sediments.

This historical perspective may help to develop new insight on our present interglacial period, specifically on how the North Pacific region responded and will respond to climate change in terms of timing, magnitude and duration of interglacial

conditions. Comparative timing and magnitude of local changes in SST and global changes in the $\delta^{18}O$ data (ice volume) may provide new information of how this region responds to, or influences, global climate patterns and ice growth.

1.1 Geological and Oceanographic Setting

In 2006, as part of the Integrated Ocean Drilling Program (IODP), the *D/V Chikyu* Shakedown Cruise (CK06-06) drilled three holes at Site C9001 (41°10.5983′N, 142°12.0328′E, 1180 m water depth). This site is located ~80 km east of the Shimokita Peninsula, northeastern Honshu, Japan, near the mouth of the Tsugaru Strait (Fig. 1.1). Although Cruise CK06-06 was designated primarily to implement System Integration

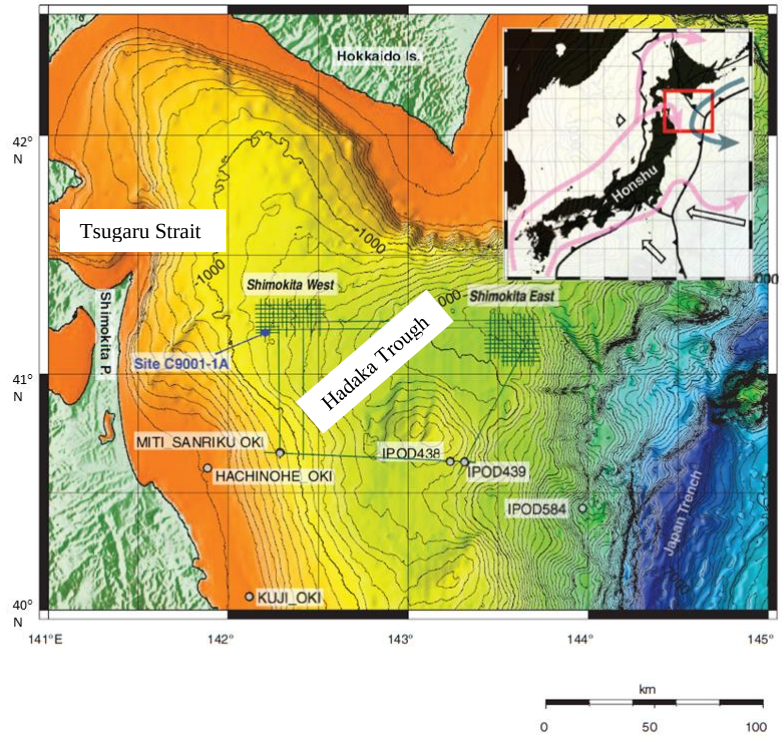

Figure 1.1. Regional map of the Shimokita region and Hadaka Trough showing bathymetry, seismic survey track lines and location of Site C9001, including other existing drill holes. Inset map shows site location relative to the Japanese Islands and basic modern ocean current circulation (after Inagaki et al., 2010).

Tests for deep water riser drilling and associated operations rather than for scientific investigation, a scientific party was organized to study the recovered marine sediments (Aoike, 2007). Drilling operations at Site C9001 recovered sediment cores from Hole C9001C between 0 and 365 meters below seafloor (mbsf) and sediment cuttings from Hole C9001D between 527 and 647 mbsf. Recovery of geological materials from Hole C9001B was unsuccessful.

Site C9001 is situated in a forearc basin formed by subduction of the Pacific Plate (moving westward ~8 cm/yr) beneath northeastern Honshu, Japan, forming the northernmost segment of the Japan Trench. The drilling area is located in the Hadaka Trough, a sedimentary basin formed by subsidence originating just offshore of southwest Hokkaido and extending to the Japan Trench (Aoike et al., 2010; Inagaki et al., 2010) (Fig 1.1). Sediments from Hole C9001C are composed primarily of diatom-rich, hemipelagic silty clay intercalated with volcanic tephra and sand layers. A disturbance around 150 mbsf, identified as a slump, marks the boundary between two designated lithologic units marked by a change in lithology and physical properties. Preliminary biostratigraphic age models indicate high sediment accumulation rates, ranging between 54 to 95 cm/k.y., and an approximate core bottom age of 640 ka in Hole C9001C. An approximate total depth age of 1.6 Ma is assigned to Hole C9001D (Aoike, 2007). Sediment cores from Hole C9001C are very well constrained in time due to the tuning of benthic foraminiferal $\delta^{18}O$ records to the Lisieki and Raymo (2004) global stack by Domitsu et al. (2010). Hole C9001D was re-entered and drilled to a total depth of 2466 mbsf in 2012 as part of IODP Expedition 337 (Expedition 337 Scientists, 2013) [See Chapter 2].

Site C9001 is influenced by two major ocean currents: the Tsugaru Warm Current (TWC) and the cold Oyashio Current (OC) (Fig. 1.2). The TWC is sourced from the Tsushima Warm Current that flows into the Japan Sea from the East China Sea through the Tsushima Strait between Kyushu, Japan and Korea. It continues northeastward along the western coastline of Honshu Island and diverges slightly southwest of the Tsugaru

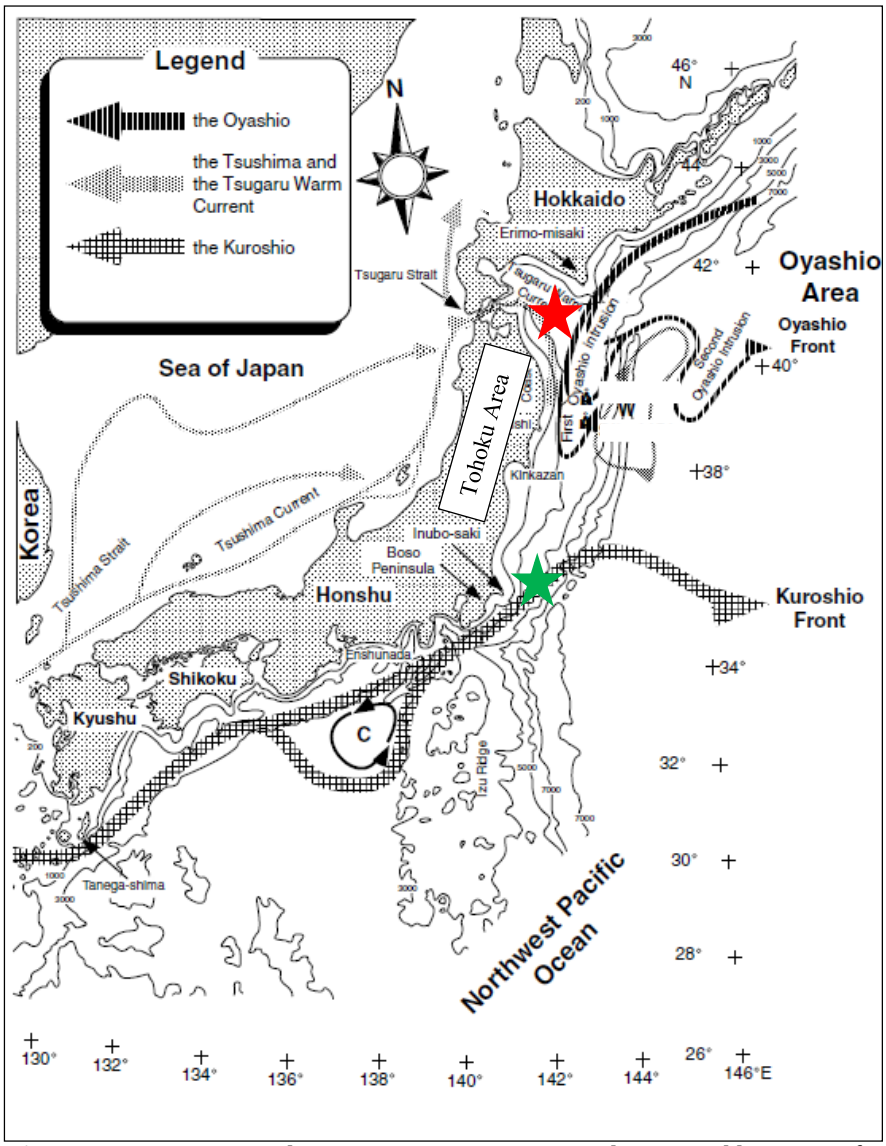

Figure 1.2. Major regional ocean current systems around Japan and locations of Site C9001 (red star), MD01-2421 (green star) and Tohoku Area (after Koizumi & Sakamoto, 2003).

Strait where the majority of the current flows through the Tsugaru Strait to become the TWC, flowing south in to the Pacific Ocean to approximately Lat. 38°N. The OC is derived from the Bering and Okhotsk seas and flows south along the southeast coast of Hokkaido and east coast of northern Honshu to about Lat. 41°N where it turns eastward (Koizumi et al., 2006). A third current, the Kuroshio Current (KC), is located to the south of the study region and does not presently influence Site C9001, although it may have in the past. The Kuroshio Current is derived from the East China Sea and flows northeast along the southwest coast of Honshu Island to approximately Lat. 35°N where it also turns east and flows into the Pacific Ocean (Koizumi et al., 2004).

Paleoceanographic reconstructions suggest that the TWC and OC have oscillated in strength throughout the Holocene (Koizumi et al., 2006), and the variable interactions are recorded in the diatom record at Site C9001 and documented herein. During glacial periods the TWC weakened and nearly stopped, because the shallow East China and Japan seas are sensitive to sea-level fall, whereby the OC became the dominant current at Site C9001 and mixed the water column. In contrast, the TWC was strong during interglacial periods, and it stratified over the OC (Koizumi et al., 2006).

1.2 Previous Work

Hole C9001C was cored continuously for 365 m with over 100% recovery. (Aoike, 2007). These cores penetrate through Marine Isotope Stage (MIS) 18 (~640 ka) with little to no drilling disturbance and only one identified geologic disturbance around 150 mbsf. Previous paleoenvironmental studies on this core or in this region include: 1) a 27 kyr reconstruction of paleoceanographic changes based on planktonic foraminiferal

assemblages from Hole C9001C (Kuroyangi et al., 2006); 2) a diatom-based paleoceanographic history spanning a similar time interval from cores around the Tsugaru Strait (Koizumi et al., 2006); and 3) a diatom-based paleoceanographic reconstruction of the last 150 ky (Koizumi et al., 2004) from Hole MD01-2421 located ~6° latitude farther south (Fig. 1.2).

1.3 Significance of Diatoms

Diatoms are photosynthetic, unicellular, siliceous algae with golden-brown chloroplasts. They are extremely sensitive to environmental conditions but are able to inhabit virtually any environment that provides moisture and sunlight (Crosta and Koç, 2007). Marine diatoms thrive in turbulent, cold, nutrient-rich waters where silicic acid is not limiting, such as the polar regions, coastal and equatorial upwelling systems and along coastal areas (Crosta and Koç, 2007; Romero and Armand, 2010).

Diatoms recently have been developed as precise tools for reconstructing paleoceanographic and paleoclimatic conditions. Three main applications include: 1) biostratigraphy, 2) paleoecology and 3) paleoceanography. Species- and statistics-based methods and transfer functions each uniquely process diatom data to reconstruct past environment and track changes through time (Crosta and Koç, 2007). This study takes a multi-proxy approach employing Q-mode factor analysis, a statistical method, and species-based methods, comparing frequencies of multiple species' occurrences to determine SST.

2. Materials and Methods

Cores recovered during CK06-06 are divided into four lithological units, A-D. Unit A (0~158 mbsf) is characterized by diatomaceous silty clay that is frequently intercalated with tephra and sand and has higher magnetic susceptibility (MS). Unit B (158~340 mbsf) is characterized by diatomaceous silty clay that is nearly devoid of tephra/sand intercalations and has lower MS. Unit C (340~348 mbsf) is composed of unconsolidated fine sands, and Unit D (348~365 mbsf) is similar in lithology to Unit A (Aoike, 2007; Domitsu et al., 2010).

2.1 Quantitative Sample Preparation

Sixty-six diatom-bearing sediment samples were collected from select glacial-interglacial transition intervals in Hole C9001C (Table A1). Marine Isotope Stages (MIS) 1 through the glacial maximum in MIS 6, and the transitions of MIS 10/9 and MIS 12/11 were sampled at an average age resolution of 4 ky.

Samples were allowed to air dry for several days before preparation. Approximately 0.5 gram of dry sediment was measured on a digital balance. Samples were then softened in deionized water before being treated with 40 mL each of 30% hydrogen peroxide and 10% hydrochloric acid to remove organic and calcareous material, respectively. After reactions stopped, the remaining sediment was rinsed several times in deionized water and centrifuged at 1500 rpm for 5 minutes in 50 mL centrifuge tubes. Some samples required treatment with a dilute *Calgon* (sodium

hexametaphosphate) solution to further disaggregate sediments, followed by rinsing as described above. Disaggregated sediment was retained in water.

A random settling method was used to prepare two quantitative slides per sample for microscope analysis. Depending on the density of the suspension after thorough re-suspension, a measured volume of randomized suspension (between 0.5 to 8 mL) was extracted and added to a small beaker containing 40 mL of deionized water to allow for good dissemination. The contents of this beaker were then poured into a petri dish and allowed to freely settle over the area of the petri dish (1430 mm^2), including over two prepared 22 x 22 mm cover slips that were attached to the bottom. Sediment was allowed to settle for 30 minutes at which time thin short strips of absorbent paper towel were inserted into the water and attached to the edge of each petri dish, and draped over the outside wall in order to drain the water through capillary action and expedite drying. Coverslips were dried on a hot plate before mounting to glass slides using *Norland* Optical Adhesive #61.

One slide per sample was examined using light microscopy. Random traverses were made across the coverslip until at least 450 diatom valves were counted for each sample (Chang, 1967). Species were counted at 750x magnification, and identifications checked at 1250x magnification using an *Olympus* BH2 microscope. Following the methods described by Schrader and Gersonde (1978), diatoms were counted when at least half of a valve was present and were identified to the species level unless distinguishing features had been broken or dissolved, in which case they were categorized at the generic level. Terrestrial diatoms were counted as one group. Diatoms from lineolate genera, such as *Thalassiothrix* and *Thalassionema*, were often only observed as fragments, in

which case two apices counted as one valve (Akiba, 1986). Resting spores of the genus *Chatoceros* were included in the count data as they contribute value to environmental interpretation. All taxa and abundance data by sample are tabulated in the Appendix (Table A1).

2.2 Diatom Abundance

Microfossils per gram of sediment was calculated using the following formula:

$$n = (V \cdot (v \cdot (x \cdot A/a)^{-1})^{-1}) \cdot m^{-1}$$

where: *V* is the total volume of the sample suspension after chemical treatment; *v* is the volume of the aliquot of the sample left for evaporation in a Petri dish; *x* is the number of microfossils counted; *A* is the area of the Petri dish in which the cover slips were evaporated; *a* is the area examined on a coverslip; and *m* is the original mass of the sample processed (Witkowski et al., 2012) (Table A2).

2.3 Diatom Temperature (Td') Values

The original *Td* ratio of Kanaya and Koizumi (1966) was derived from 118 widely distributed deep marine ocean core tops between the latitudes of 55°N and 55°S and the 220 diatom taxa representing modern diatom distributions related to surface water circulation. Species defined for calculating the *Td* ratio in the North Pacific were chosen as representative of diatom assemblages in different areas of the Pacific, because their distributions are more or less restricted, and because their occurrences are consistent (Kanaya and Koizumi, 1966). The *Td* ratio is defined as: $Td = [Xw/(Xw+Xc)]*100$, where *Xw* is the frequency of warm-water species and *Xc* is the frequency of cold-water species.

Td values can range from 0 to 100. From the subarctic to tropical region, *Td* values become systematically larger and show a positive correlation with SST.

This original method included warm- and cold-water diatom species from a variety of environmental settings in the North Pacific region. Koizumi et al. (2004) redefined the *Td* values as *Td'* values, for application strictly to oceanic holoplanktonic diatoms: *Td'*=[(*Xw*+XW)/(*Xw*+XW+*Xc*+XC)]*100. *Xw* and *Xc* are the frequency of warm- and cold-water species, respectively, as originally defined by Kanaya and Koizumi (1966), while XW and XC are the frequencies of warm- and cold-water species as supplemented by Koizumi et al. (2004) (Table 1.1). The *Td'* ratios more precisely reflect oceanic holoplanktonic associations than the originally proposed *Td* ratio (Koizumi et al., 2004). Abundance of warm- and cold-water species and *Td'* ratios are tabulated in Table A2.

2.4 Estimating Paleo Sea Surface Temperature

Koizumi (2008) performed regression analysis between the *Td'* ratio of 123 surface sediment samples and the mean annual SST (°C) at core sites in the northwest Pacific Ocean, along the Japan coastline, and in the Japan Sea in order to calibrate a proxy for calculating paleo SST (°C) (Fig. 1.3a). One equation was derived for the Tohoku Area in the NW Pacific at ~Lat. 39°N (Fig. 1.2) and the Japan Sea, both of which produce strong correlation coefficients (*R*=0.90 for the Tohoku area and *R*=0.89 for the Japan Sea) indicating that there is no systematic bias in the equations derived from the data

Table 1.1. Ecological and biogeographical categories of diatom species

Taxa	Category	Geographic Range
Actinocyclus curvatulus Janisch, in Schmidt	*Xc*	North temperate-subarctic
Actinocyclus ochotensis Jousé		North temperate
Asteromphalus robustus Castracane		North temperate
Bacteriosira fragilis Gran		Arctic-subarctic (sea ice)
Chatoceros furcellatus Bailey		Arctic-subarctic
Coscinodiscus marginatus Ehrenberg		North temperate
Coscinodiscus oculus-iridis Ehrenberg		North temperate
Neodenticula seminae (Simonsen & Kanaya) Akiba & Yanagisawa		North temperate
Fragilariopsis cylindrus (Grunow) Krieger, in Helmck & Krieger		Subarctic (sea ice)
Porosira glacilis (Grunow) Jorgensen		Arctic-northtemperate
Rhizosolenia hebetata (Bailey) Gran f. *hiemalis* Gran		North temperate
Thalassiosira gravida Cleve		Subarctic (sea ice)
Thalassiosira hyalina (Grunow) Gran		Arctic-temperate
Thalassiosira nordenskioeldii Cleve		Arctic (sea ice)
Thalassiosira trifulta Fryxell, in Fryxell & Hasle		Subarctic-north temperate
Fragilariopsis oceanica (Cleve) Hasle	XC	Subarctic (sea ice)
Alveus marinus (Grunow) Kaczmarska & Fryxell	*Xw*	Tropical-subtropical
Asteromphalus imbricatus Wallich		Tropical-subtropical
Azpeitia nodulifera (Schmidt) Fryxell & Sims, in Fryxell, Sims & Watkins		Tropical
Fragilariopsis doliolus (Wallich) Medlin & Sims		Tropical
Planktoniella sol (Wallick) Schütt		Tropical
Rhizosolenia bergonii Peragallo		Tropical-subtropical
Roperia tesselata (Roper) Grunow		Tropical-subtropical
Thalassiosira leptopus (Grunow) Hasle & Fryxell		Tropical
Asteromphalus flabellatus (Brébisson) Greville	XW	Tropical-subtropical
Azpeitia tabularia (Grunow) Fryxell & Sims, in Fryxell, Sims & Watkins		South temperate
Nitzschia interruptestriata (Heiden) Simonsen		Tropical-subtropical
Nitzschia kolaczekii Grunow		Warmer
Pseudosolenia calcar-avis (Schültze) Sundstrom		Tropical-subtropical
Rhizosolenia acuminata (Peragallo) Gran		Subtropical-temperate
Rhizosolenia hebetata (Bailey) Gran f. *semispina* (Hensen) Gran		Warmer
Thalassiosira oestrupii (Ostenfeld) Hasle		Subtropical

w: oceanic warm-water species and *c*: oceanic cold-water species as defined by Kanaya & Koizumi (1966). W: oceanic warm-water species and C: oceanic cold water species supplemented by Koizumi et al. (2004). Geographic range reflects Northern Hemisphere distributions.

(Koizumi, 2008). Although the correlation between the *Td'* ratios and measured mean annual SST is not linear, annual paleo SST can be reasonably be estimated using the corresponding slope equations by substituting a *Td'* value for "x". The equation for the Tohoku Area is the one applied in this study and is: y=6.5711*x^(0.27300).

Error associated with calculating SST decreases as temperature (°C) decreases. For temperatures ≤ 11°C, the margin of error is ±2.5°C; for temperatures between 11°C and 14°C, the margin of error increases to ±3°C; and for temperatures ≥ 14°C, the margin of error is ±3.5°C (Fig. 1.3b).

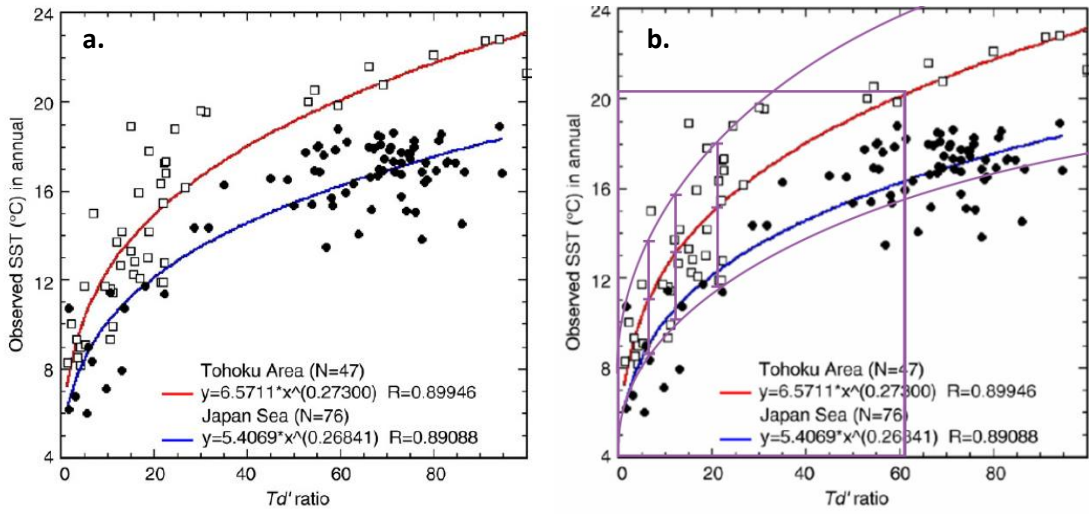

Figure 1.3. a) Regression analysis between *Td'* ratios and calculated annual sea surface temperatures (SST) (°C) which is the mean of the observed SST (°C) in summer and winter in the Tohoku Area and Japan Sea. The paleo-SST (°C) can be estimated using the equations obtained by the regression analysis. Open squares: Tohoku Area; filled circles: Japan Sea (From Koizumi, 2008). **b)** Error associated with Tohoku Area data decreases as temperature (°C) decreases: ±2.5°C for temperatures ≤11°C, ±3°C for temperatures between 11°C and 14 °C and ±3.5°C for temperatures ≥14°C. Purple box indicates the maximum value calculated in this study.

2.5 Q-mode Factor Analysis

Factor analysis determines variation in diatom assemblages representing ecological shifts in a given region (Koizumi, 2004). In order to decipher environmental conditions through time in samples from Site C9001, Q-mode factor analysis was conducted to distinguish combinations of co-varying diatom taxa throughout the samples. In total, 84 samples and 93 species were processed. Factor scores and loadings are regarded as species composition (assemblages) and the contribution of each assemblage to each sample, respectively (Koizumi et al., 2004, 2006). The numbers derived from the highest scoring components explaining the most variance were extracted for each sample and plotted individually downhole to compare co-variance of species and interpret environmental changes through time.

The method applied by Koizumi et al. (2004, 2006) is applied here and results from each location were compared to calibrate the accuracy of the method. Once verified, the method was applied to all samples downhole.

3. Results

3.1 Calculated Paleo Sea-Surface Temperature

The diatom temperature record presented here estimates sea surface conditions at this site, whereas the benthic oxygen isotope record of Domitsu et al. (2010) represents predominantly a global ice volume signal, but also local bottom water temperature changes. The set of samples used in this study were selected based on the pattern of the

benthic $\delta^{18}O$ record which enables a clear identification of MISs (Fig 1.13). In order to calibrate the diatom record in this study to that of Koizumi et al. (2004), samples from this study represent initially only MISs 6 through 1 (~140 ky). Subsequently, examination of the diatom records representing GI transitions between MIS 12/11 and 10/9.

3.1.1. MIS 6 through 1 (77.2-0.1 mbsf)

Samples included in this interval were collected between the depths of 77.2 and 0.1 mbsf (Fig. 1.4). Diatom-inferred temperatures through this interval average ~10°C, but peak warming in MIS 5e and MIS 1 and peak cooling in MIS 6 and MIS 2 is clear in the diatom surface temperature record (this study) and also in the benthic oxygen isotope record from this hole (Domitsu et al. 2010). The comparative timing and magnitude of local changes in SST and global changes in the $\delta^{18}O$ data (ice volume) provide new information of how this region responds to, or influences, global climate patterns and ice growth. In the surface record, maximum temperatures range between 14 and 16°C, and minimum temperatures range between 6 and 8°C.

Peak warming in MIS 1 is observable at 3.8 mbsf in sample 902-C9001C-3H-1, 99-100cm where the calculated SST is 14.9°C. This sample is interpreted as the interglacial maximum. At 19.9 mbsf, in sample 902-C9001C-3H-3, 57-58 cm, a SST of 0°C is calculated. Although it is unlikely that the true SST was 0°C, it is likely that this sample could represent the glacial maximum; and all samples above this level display a relatively linear warming trend (Fig. 1.4).

Peak warming associated with MIS 5e is observed at approximately 67.8 mbsf and SST is calculated to be 16.6°C. Warm temperatures persist between 67.8 and 64.2

mbsf and are immediately followed by low calculated SST of 6.3°C at 64 mbsf. Peak cooling associated with MIS 6 is calculated to be 8.5°C and is identified at 70.6 mbsf.

The $\delta^{18}O$ record through this interval displays a typical saw-toothed pattern of sharp transitions from glacial to interglacial maxima and a gradual decline between the termination of MIS 5e and the LGM. The surface temperature record, though, shows a rapid transition out of the warmest temperatures associated with MIS 5e, and then SSTs remaining relatively steady between 7°C and 12°C through to the LGM at 20 mbsf.

Koizumi's (2008) SST equation developed for the Tohoku Area was applied to Koizumi's (2004) *Td'* values produced from his data from Hole MD01-2421, located about 5° latitude south of Site C9001 (Fig 1.2), and compared to that produced for Hole C9001C (Fig. 1.4). Peaks and troughs associated with multiple glacial/interglacial periods, including minor climate excursions, but especially those of MISs 6, 5e and 2, can be correlated between the two records. Both SST records show the same general pattern between MIS 5e and MIS 2, and temperatures from Hole MD01-2421 average ~17°C; ~7°C higher than Hole C9001C. In contrast to the SST curve through MIS 1 produced for Site C9001C, the SST curve produced from Koizumi's (2004) data, shows a slight trend toward cooler temperatures in sediments above 8 m (Fig. 1.4). Hole C9001C was recovered by riser drilling techniques, which likely removed several meters of the uppermost (youngest) stratigraphic sequence.

Although the MD01-2421 record is of higher temporal resolution, both records show similar responses through GI cycles. Glacial and interglacial maxima are evident in

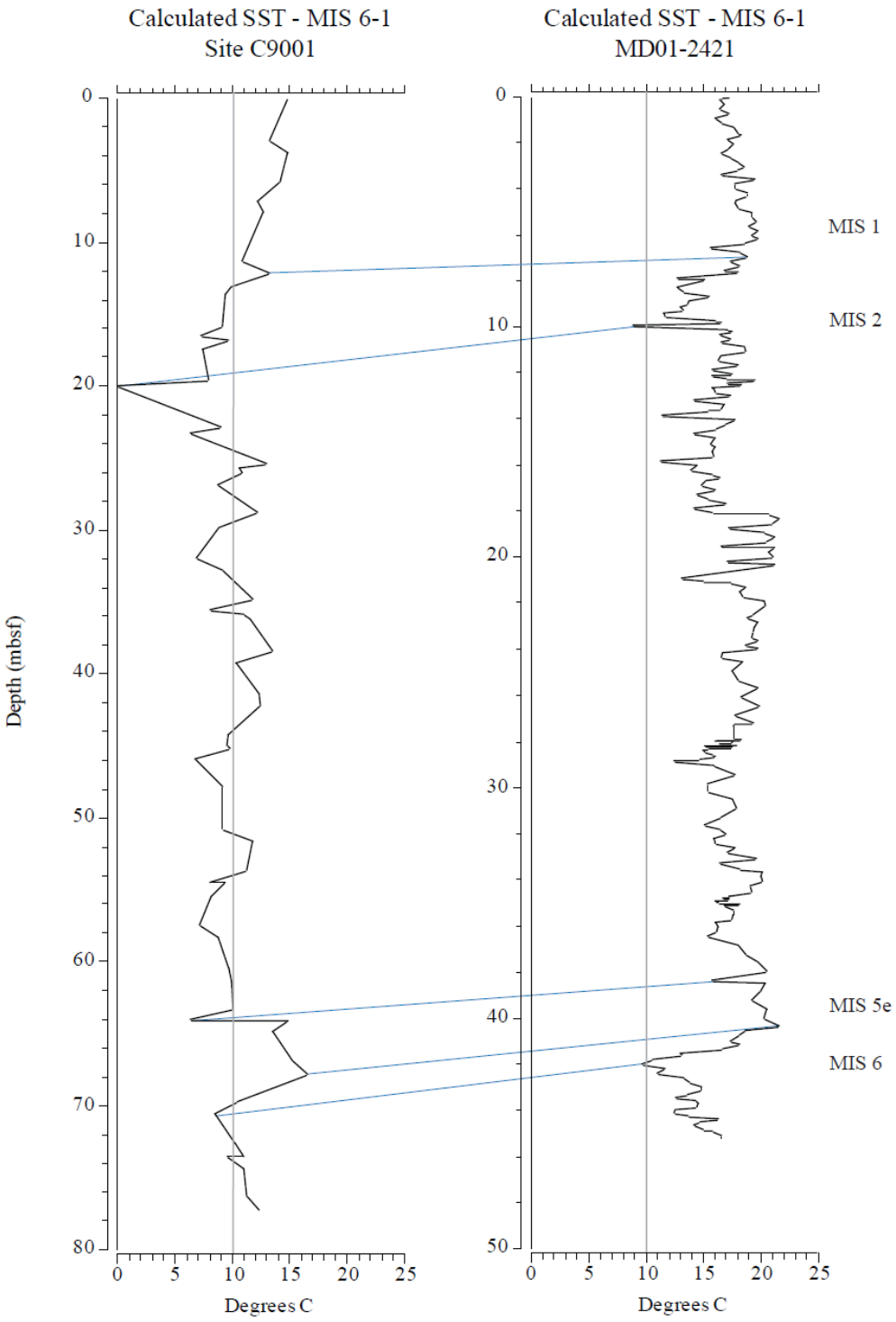

Figure 1.4. SST profiles through the last ~150 kyr produced from C9001C (left) and Koizumi's (2004) data from the MD01-2421 core (right). Blue lines provide tie points between warm and cold events. Vertical gray line is drawn at 10°C for a reference point.

both the MD01-2421 and C9001C temperature curves, and post-interglacial maximum temperatures decrease only slightly and remain steady until the next glacial maximum.

3.1.2. MIS 2/1 Transition (19.9-0.1 mbsf)

Calculated SSTs for the transition from the LGM (MIS 2) into Holocene MIS 1 produce a warming trend up-core, with a minimum calculated temperature of 0°C at 19.9 mbsf and maximum temperature of 14.9°C at 3.8 mbsf (Fig 1.5a). Calculated temperature of the youngest sample is 14.8°C at 0.1 mbsf.

3.1.3. MIS 6/5e Transition (77.2-64.2 mbsf)

Calculated SSTs for the MIS 6/5e transition increase from 8.5°C at 70.6 mbsf to 15.8°C at 67.8 mbsf (Fig 1.5c). The interval of peak temperatures through MIS 5e extends from 67.8 mbsf up through 64.2 mbsf.

3.1.4. MIS 10/9 Transition (202.5-190.7 mbsf)

Diatom assemblages from this interval yield the highest calculated SSTs of all intervals in this study, with an average temperature of 17.6°C and a maximum temperature of 20.2°C at 198.2 mbsf (Fig 1.5c). The benthic oxygen isotope record (Fig 1.13) indicates that the glacial maximum occurred at approximately 200 mbsf; however, the SSTs through this interval show sustained warm values above 16°C, the warmest temperatures estimated in this study.

During MIS 9 the abundance of warm-water species doubles relative to all other intervals examined herein, and the abundance of cold-water species is relatively low in comparison to all other intervals (Fig. 1.6).

The lowest temperature calculated from samples preceding peak warming is 16.1°C, much higher than other glacial intervals, indicating the MIS 10/9 transition was not observed and likely resides below the sampled interval. Initial sample selections were guided by the $\delta^{18}O$ record; however, SST cooling through the MIS 10/9 transition may lead the $\delta^{18}O$ shift at this site by ~5 m. Future sampling and analysis will extend the record for this interval in order to capture the reversals into and out of the warm temperatures associated with interglacial stage 9.

3.1.5. MIS 12/11 Transition (238.5-227.3 mbsf)

MIS 11 is known for its prolonged duration and increased SSTs in high latitudes (Howard, 1997) both of which are evident in the calculated SST and $\delta^{18}O$ data (Fig 1.5d, 1.13). Calculated temperatures for the interval 235.6 to 231 mbsf average around 15°C, and the maximum temperature calculated is 15.4°C at 234.8 mbsf increasing from 6.8°C at 237.6 mbsf.

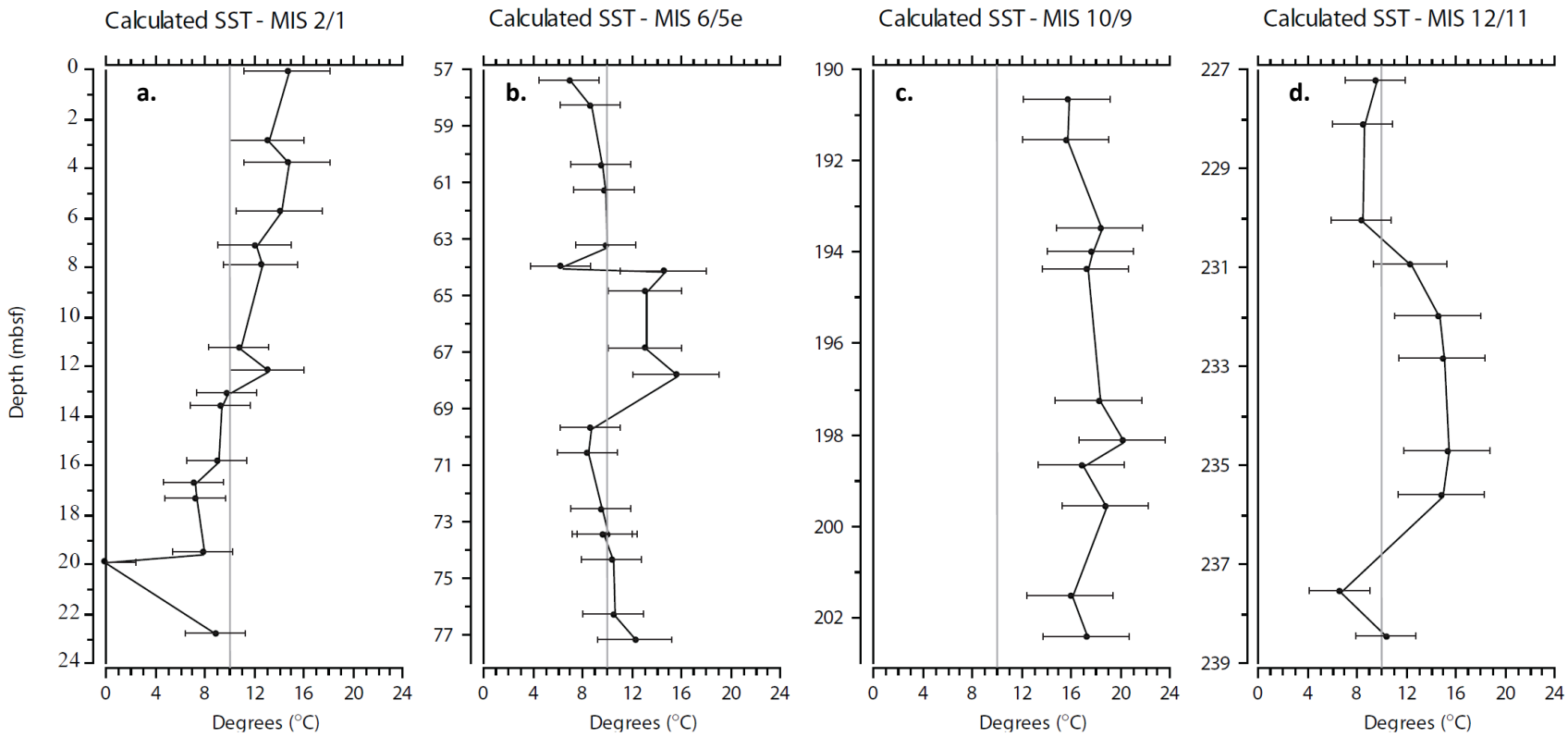

Figure 1.5. SST profiles produced for select GI transitions including error determined from regression analysis. Depth in mbsf, calculated SST in °C. **a)** MIS 2/1 (0.1-23.3 mbsf), **b)** MIS 6/5e (57.4-77.2 mbsf), **c)** MIS 10/9 (190.7-202.5 mbsf) and **d)** MIS 12/11 (227.3-238.5 mbsf).

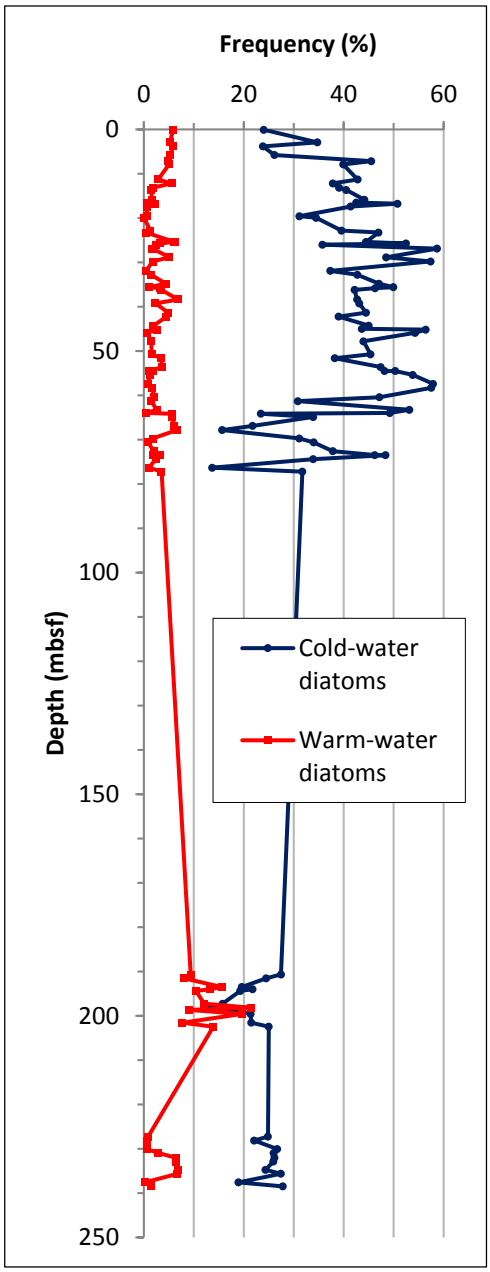

Figure 1.6. Abundance of warm- and cold-water diatoms through all sample intervals in Hole C9001C.

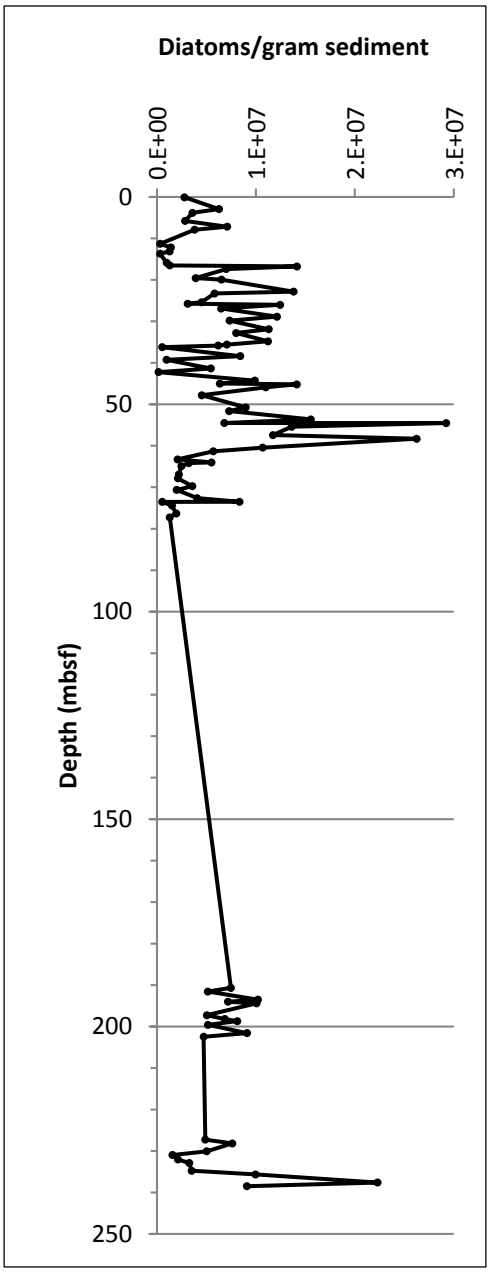

Figure 1.7. Total diatom abundance (10^7) through all sample intervals in Hole C9001C.

3.2 Factor Analysis

The highest four Factors explain 88.7% of the total variance in Hole C9001C (Table 1.2). The five highest scoring taxa from each Factor are shown in Table 1.3, and variation of each Factor loading by interval is shown in Figures 10-14. Species representing Factors 1-3 in this study also resulted from the Factor Analysis of Koizumi et al. (2006), although not in the same order.

Table 1.2. Individual and cumulative % variance for the top four Factors.

Factor	1	2	3	4
% variance explained	68.92	11.44	5.09	3.24
Cumulative % of variance explained	68.92	80.36	85.45	88.69

Table 1.3. Scores of 5 highest scoring diatom species in each Factor.

Factor 1		Factor 2		Factor 3		Factor 4	
Score	Taxa	Score	Taxa	Score	Taxa	Score	Taxa
9.41	*Melosira albicans*	-8.65	*Thalassionema nitzschioides*	-6.51	*Thalassiosira nordenskioeldii*	-6.79	*Thalassiosira antarctica*
1.01	*Thalassiosira jouseae*	-2.39	*Odontella aurita*	-4.26	*Thalassiosira hyalina*	-3.23	*Bacteriosira fragilis*
1.01	*Thalassionema nitzschioides*	-1.65	*Neodenticula semiae*	-3.25	*Fragilariopsis oceanica*	2.27	*Thalassiosira nordenskioeldii*
0.96	*Stephanopyxis turris*	-1.34	*Thalassiosira eccentrica*	-2.54	*Bacteriosira fragilis*	-2.22	*Fragilariopsis oceanica*
0.90	*Thalassiosira leptopus*	-1.13	*Thalassiosira nordenskioeldii*	-2.01	*Fragilariopsis cylindrus*	-2.10	*Thalassiosira gravida*

Factor 1 is comprised almost exclusively of the extinct species *Melosira albicans*, which was originally described by Sheshukova-Poretzkaya (1964) from the Pliocene Ust-Kamtschatica, on the east side of Kamchatka Peninsula. The environmental preference and biostratigraphic range of this species is poorly understood. The occurrence of *M. albicans* is highly variable in these data and does not display a consistent environmental

preference in the Factor Analysis. This factor was identified as Factor 5 in Koizumi et al. (2006).

Factor 2 is dominated by the cosmopolitan, neritic holoplanktonic species *Thalassionema nitzschioides*. This species represents Factor 1 in Koizumi et al. (2006). It is a common, widespread northern temperate species, often found in great numbers in coastal locations around the Japanese islands (Koizumi, 2006). A second contributor to Factor 2, *Odontella aurita*, is a littoral-neritic species with a wide distribution, which mostly flourishes in Arctic and Boreal seas. Increased abundance of *O. aurita* may indicate a local increase in productivity at the boundary between coastal and offshore waters (Koizumi, 2006).

Factor 3 is predominated by *Thalassiosira nordenskioeldii*, an Arctic species that tends to occur in large numbers. An additional Arctic species contributing to Factor 3 is *Thalassiosira hyalina*. Both of these species are defined as cold-water species useful for determining the *Td'* ratio and are indicative of sea-ice influence (Koizumi, 2006; Barron et al., 2009). *T. nordenskioeldii* represents Factor 2 in Koizumi et al. (2006).

Factor 4 is dominated by *Thalassiosira antarctica*, which is a sub-arctic species associated with sea-ice. Two additional components of Factor 4 are the arctic/subarctic species *Bacteroisira fragilis* and *Fragilariopsis oceanica* that are both indicative of sea-ice influence (Koizumi, 2006; Barron et al., 2009).

3.2.1. MIS 6 through 1 (77.2-0.1 mbsf)

Factor 1 loadings are highly variable through this interval and do not apparently correspond to warm or cold periods (Fig 1.8). The abrupt increase in Factor loading that

occurs between ~16-20 mbsf, after consistently low scores from the top of the hole, parallels a marked increase in the abundance of *M. albicans* in this hole (Table A1). Neither positive nor negative scores indicate whether *M. albicans* is fluctuating in response to glacial or interglacial conditions. At both the peak cooling at 19.9 mbsf and the peak warming at 67.8 mbsf, *M. albicans* displays relatively high positive scores.

Factor 2 displays an inverse relationship with Factors 3 and 4 during GI transitions. Factor 2 scores become more negative during interglacial periods and more positive during glacial periods, whereas the opposite is true for Factors 3 and 4.

Factor scores between the depths of ~25-60 mbsf, with the exception of Factor 1, are variable, but remain relatively linear in the same way as the calculated SST for this same interval.

3.2.2. MIS 10/9 Transtion (202.5-190.7 mbsf)

In contrast to the calculated SST profile for this interval, the loadings for each Factor produce relatively smooth curves (Fig. 1.11). The relationship between Factors 2, 3 and 4 are the same as in GI 1, and Factor 1 tends to show higher scores during warmer periods and lower scores during colder periods, and is for the most part consistent with abundance.

3.2.3. MIS 12/11 Transition (238.5-227.3 mbsf)

This sample interval displays some characteristics that differ from the other intervals (Fig. 1.12). Factors 1 and 2 have nearly parallel curves and tend to have more positive values during intervals of decreased SST. Similarly, Factor 4 values become

more positive during colder intervals. Factor 3 scores produce a nearly straight line that does not shift in response to SST change.

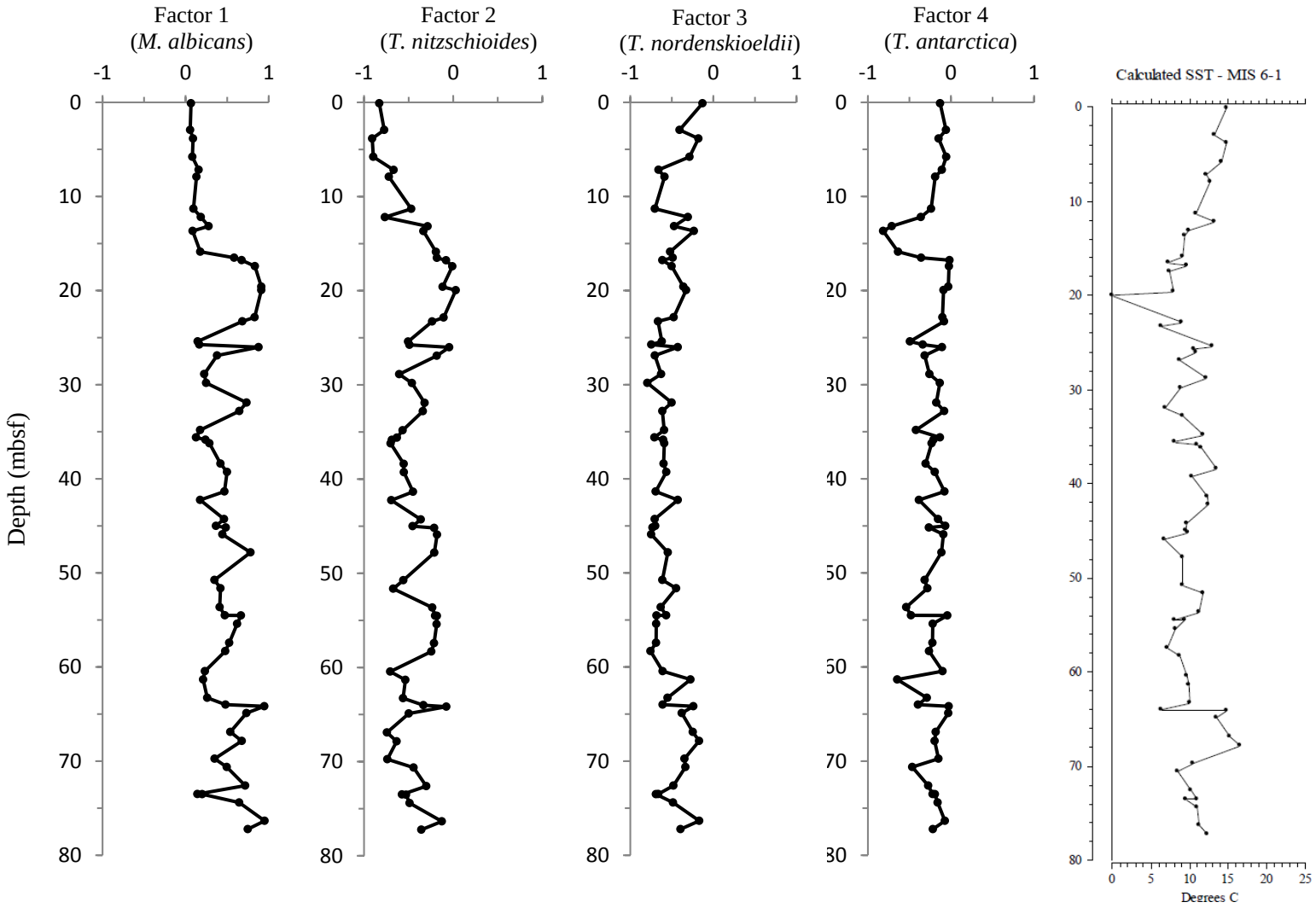

Figure 1.8. Depth variations of the loadings for each factor from Q-mode factor analysis of the diatom flora in C9001C from MIS 6 through MIS 1, and the calculated SST profile for comparison.

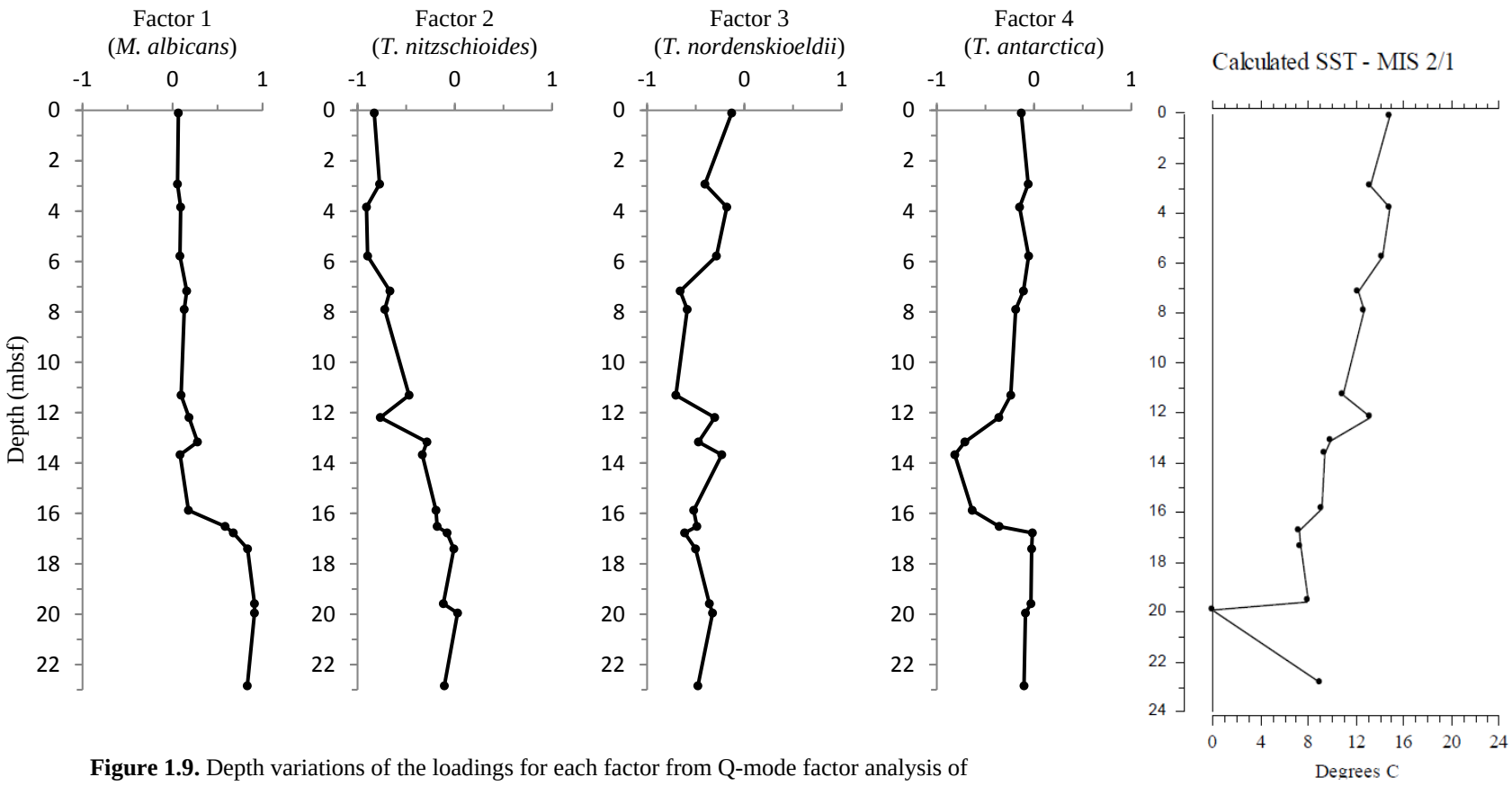

Figure 1.9. Depth variations of the loadings for each factor from Q-mode factor analysis of the diatom flora in C9001C during MIS 2/1, and the calculated SST profile for comparison.

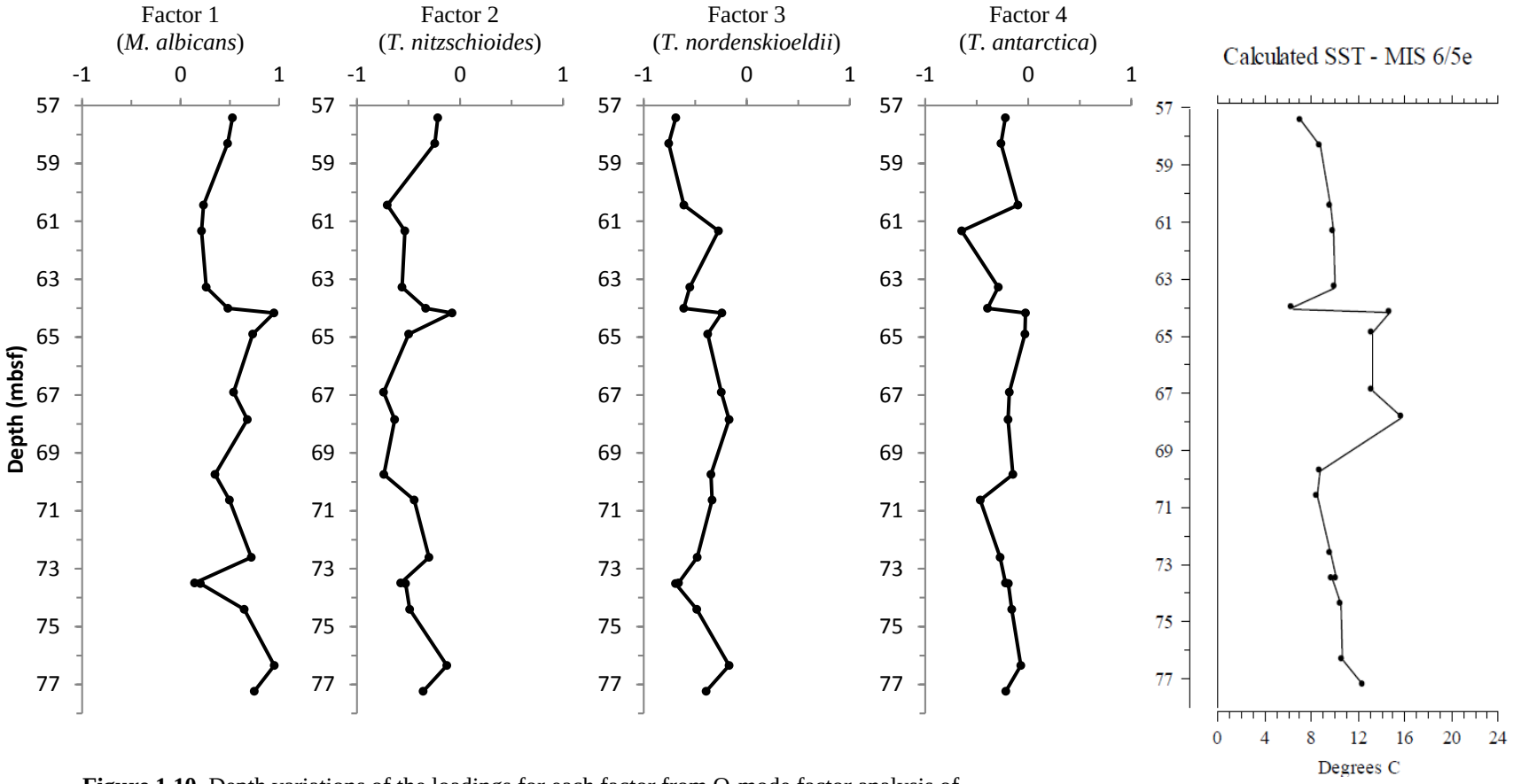

Figure 1.10. Depth variations of the loadings for each factor from Q-mode factor analysis of the diatom flora in C9001C during MIS 6/5, and the calculated SST profile for comparison.

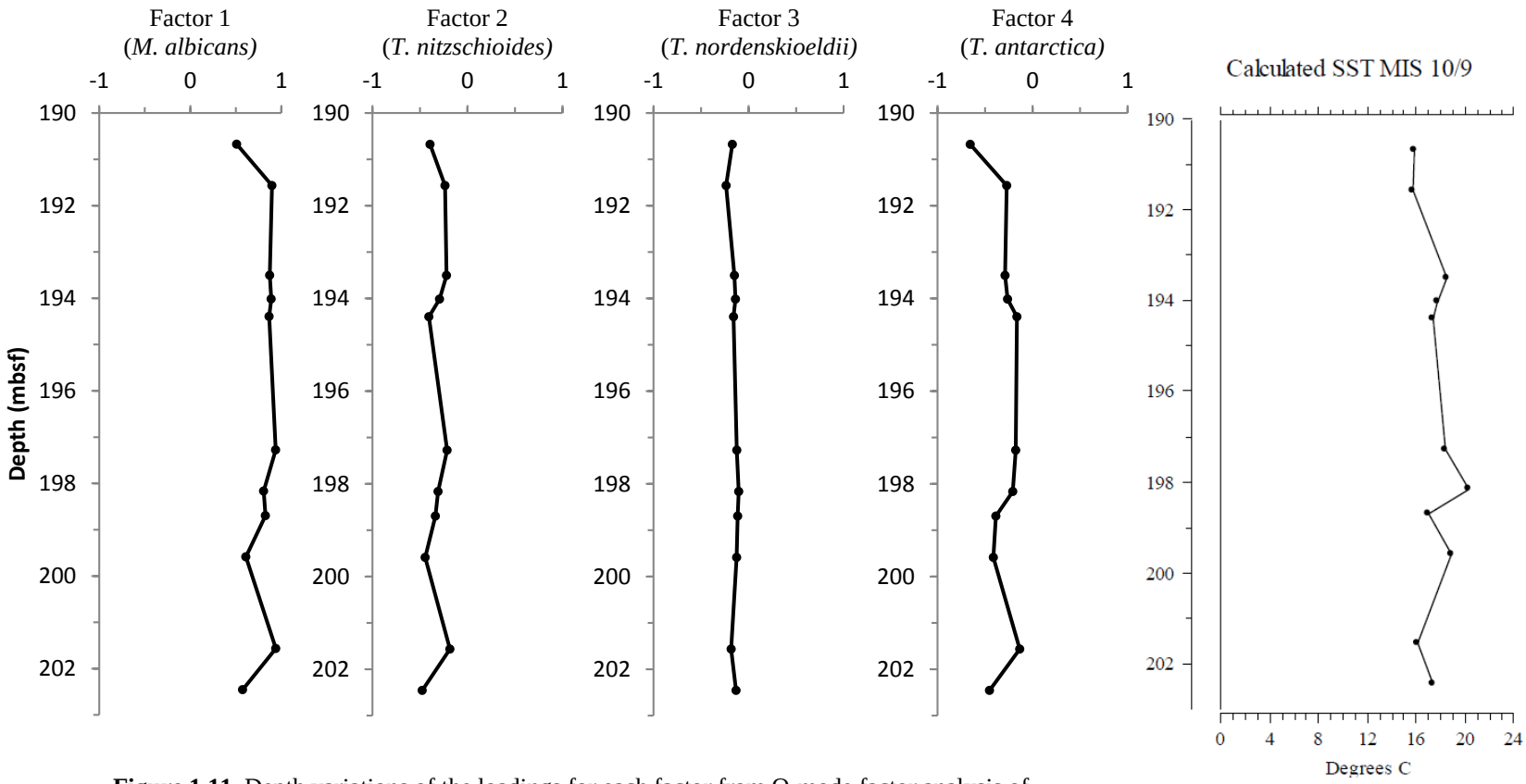

Figure 1.11. Depth variations of the loadings for each factor from Q-mode factor analysis of the diatom flora in C9001C during MIS 10/9, and the calculated SST profile for comparison.

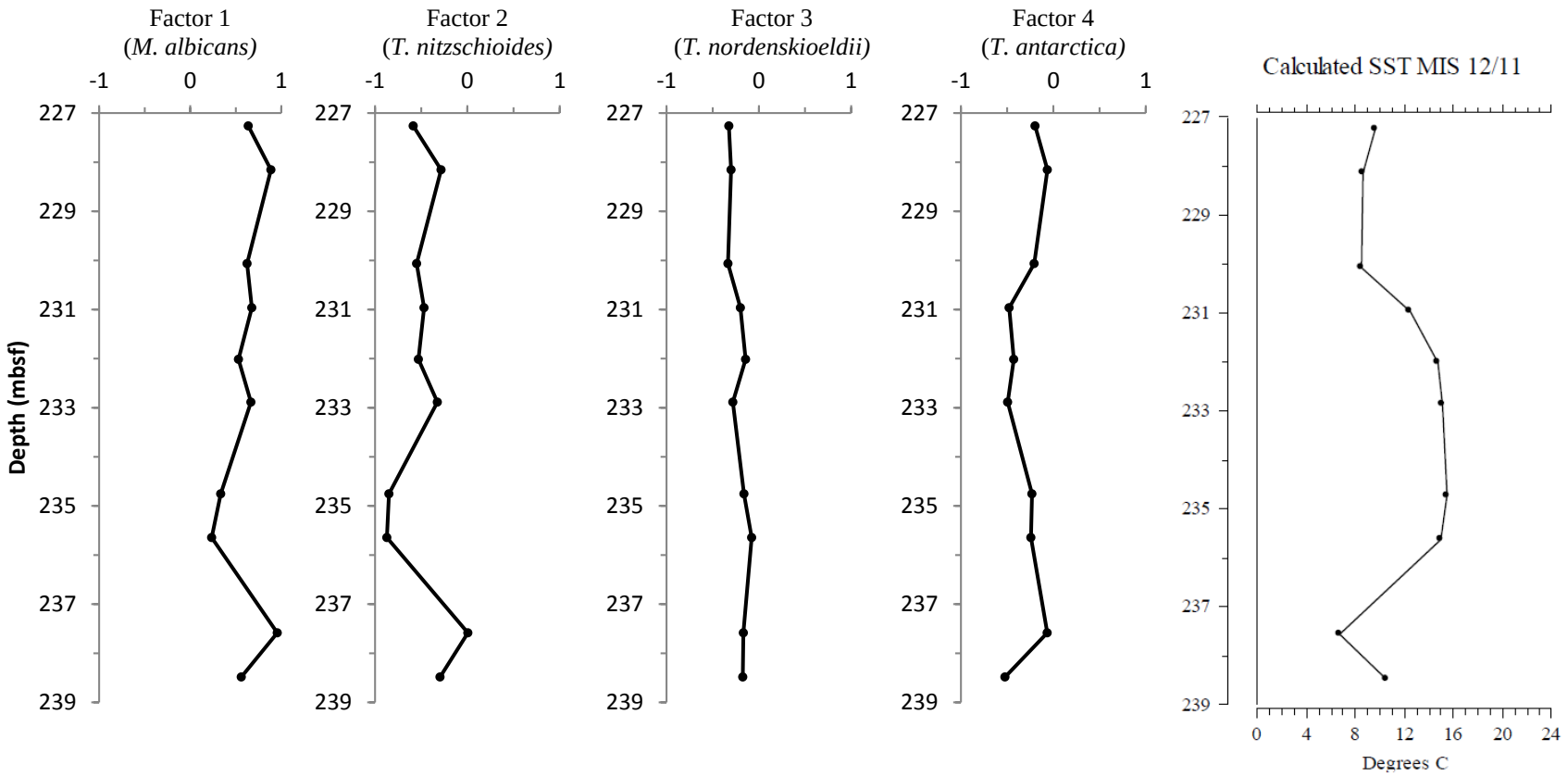

Figure 1.12. Depth variations of the loadings for each factor from Q-mode factor analysis of the diatom flora in C9001C during MIS 12/11, and the calculated SST profile for comparison.

4. Discussion

4.1 Calculated Paleo Sea-Surface Temperature

4.1.1. MIS 6 through MIS 1 (77.2-0.1 mbsf)

Site C9001 is located at 41°N, where observed diatom assemblages predominantly include cold-water species, and *Td'* values become less reliable due to the inherently smaller value of *Xw* (Koizumi and Sakamoto, 2003). This dichotomy is apparent through Hole C9001C, particularly in sample 902-C9001C-3H-3, 57-58 cm at 19.9 mbsf where 0°C was calculated for one sample due to a complete absence of warm-water species. There are multiple properties associated with this sample that offer some explanation for this 0°C SST calculation: 1) it is completely devoid of all defined warm-water species; 2) color core photos show that this sample was taken within an approximately 5cm-thick layer of dark gray to black sediment. The visual core description simply describes it as "silty clay", but the color is suggestive of organic matter content; 3) a spike in magnetic susceptibility at this depth (Aoike, 2007) indicates an arid atmosphere containing elevated amounts of dust, characteristic of glacial periods; and 4) diatom abundance decreases by 47% between this sample and the next deepest one (902-C9001C-3H-5, 44-45cm) at 22.8 mbsf.

Koizumi et al. (2006) examined samples from two piston cores from the Tsugaru Strait region, near Site C9001 and determined that between 30-20 cal kyr BP, a correlative time-period for 3H-3, 57-58 cm, a colder, less-saline oceanic water mass

flowed west through the Tsugaru Straight into the Japan Sea causing stratification of the water column and producing thinly laminated layers in the Japan Sea. The dark layer observed in core 3H-3 is similar to several others slightly deeper in core 3H-7 that likely represent this event that stretched into the shallow waters of the Japan Sea and offshore SE Hokkaido. Koizumi et al. (2006) also suggested that a fall in sea-level and the intensification of the Oyashio Current caused erosion of sediments in this region east of the Tsugaru Strait. Although it is highly unlikely that the SST was 0°C in this mid-latitude setting as calculated for this sample, this sample is centered within the coldest interval associated with the cooling that predated MIS 2 and likely reflects the coldest period in this interval.

4.1.2. MIS 10/9 Transition (202.5-190.7 mbsf)

The calculated SSTs associated with MIS 9 were by far the warmest to influence this region over the last ~420,000 years (Fig. 1.13). Diatom assemblages throughout this interval yield consistently higher abundances of warm-water species (~10-20%) and lower abundances of cold-water species (~15-25%) (Fig. 1.6). Modern distributions of warm-water species identified in these samples are known from subtropical and tropical waters of the Pacific Ocean including the equatorial zone (Kanaya and Koizumi, 1966). High abundances of these species this far north are an indicator of a northward shift in the surface water temperature gradient. Alternative explanations are: 1) the Kuroshio Current flowed farther north during this time; 2) sea-level was higher and a greater volume of warm water from the Sea of Japan flowed eastward through the Tsugaru Strait over this Site; 3) global ice volume was low, preventing an environment unsuitable for many cold-

water and sea-ice related taxa, or 4) The cold Oyashio Current was substantially warmer, and allowed lower latitude taxa to migrate north.

Samples for this interval come from cores 21H through 22H, based on the $\delta^{18}O$ record which shows the MIS 10/9 transition occurring within core 22H. Figures 1.13 and 1.14 align critical stages through this GI transition and show a lag-time between the initial changes in surface water temperatures followed by that of the global ice volume record as expressed at this site in $\delta^{18}O$ benthic foraminifera. Surface waters may precede global ice volume by approximately 5 m in this interval. The sample set examined to this point in this study did not extend deep enough to capture the SST cooling associated with the MIS 10/9 transition nor did it extend up high enough to capture the transition out of the warmest period. It is likely that only the interglacial period was observed in the calculated SST record, but not in its entirety. The $\delta^{18}O$ record indicates that MIS 9 was long in duration, longer than MIS 11. More samples will be required to document the SST changes associated with this interval. Guided by the lead of SST before $\delta^{18}O$ exhibited in other GI cycles, this interval could extend between ~185 and 210 mbsf.

4.1.3. MIS 12/11 Transition (238.5-227.3 mbsf)

MIS 11 is known for its duration and increased SSTs in high latitudes (Howard, 1997). The temperature profile as recorded in Site C9001C manifests the duration; however, maximum and average SSTs leading into and during this interglacial are much lower than SSTs calculated for warming associated with MIS 9. SST warming associated with the transition from the MIS 12 glacial maximum to the MIS 11 interglacial

maximum occurs rapidly between 237.6 and 235.6 mbsf and mimics very closely that of the MIS 6/5 transition in terms of temperature range (average 14.5°C).

Interglacial maxima for MIS 11 and 5 both show diatom abundance peaks higher than in any other sample (Fig. 1.7). Koizumi et al. (2004) also noted this in Core MD01-2421 and suggested that obliquity-driven seasonal amplification played a role in nutrient availability and diatom abundance.

4.1.4 Potential diatom species to supplement Td' *ratio*

Synedropsis recta Hasle, Medlin & Syvertson 1994 has the potential to be a useful and reliable cold-water species for determining *Td',* calculating SST and determining paleoceanographic conditions in the NW Pacific Ocean. Hasle et al. (1994) observed distribution of this species through ice samples, including sub-ice, pack-ice, sea ice and fast ice. Quantitative diatom count data collected from the sediments from Hole C9001C show this species co-occurring with multiple ice-related species and in samples where SST was calculated below 10°C. The paleoenvironmental preference and occurrence of this species in the NW Pacific Ocean would need to be confirmed in order to add it to the *Td'* ratio.

4.2 Factor Analysis

Three of the four Factors in this study (Factors 1-3) are the same as those produced by Koizumi et al. (2006). A comparison of the trajectories of each of these Factors between Holes C9001C and MD01-2409 (the closest site sampled by Koizumi et

al., 2006) are relatively the same through 30 kyr, showing that the applied methods and results produced in this study accurately depict the data.

A reconstruction of paleoceanographic changes based on relationships between planktonic foraminifers over the last 27 kyr in the Shimokita Peninsula conducted by Kuroyanagi et al. (2006) used sediments from Hole C9001C. They determined that the Oyashio Current affected both surface and subsurface waters between 26.9-15.7 ka, after which water masses progressively stratified.

In this study, the inverse relationship between Factor 2 and Factors 3 & 4 are most indicative of watermass influence. Scores for Factors 3 and 4 remain negative throughout all intervals, and increasingly negative scores occur during periods identified to be cold/glacial. Based on the oceanography, the Oyashio Current dominates during cold, interglacial periods therefore these Factors represent a strengthening Oyashio Current and mixed water column. In contrast, increasingly negative Factor 2 scores occur during warm/interglacial periods indicating a strengthening TWC, warmer surface waters and a stratified water column.

4.2.1. MIS 6 through MIS 1 (0.1-77.2 mbsf)

Concomitant with the studies by Koizumi et al. (2006) and Kuroyanagi et al. (2006), results from this interval indicate stratified water masses above about 13 mbsf (~10 kyr) as Factor 2 scores are strongly negative and Factor 4 scores are strongly positive; both are consistently stable. Increasingly positive Factor 3 scores further support a subsiding Arctic water mass. Between the depths of ~13-65 mbsf, these Factor relationships are not as strong and suggest a stronger influence of the Oyashio Current

and mixed water column. Strong indirect relationships between Factor 2 and Factors 3 and 4, suggesting stratified water masses, can again be observed between approximately 71-65 mbsf in the MIS 5e interval.

4.2.2. MIS 10/9 Transition (190.7-202.5 mbsf)

Throughout the MIS 9 interval, Factors 3 and 4 show persistent suppression of Arctic and Subarctic watermass influence; however, Factor 2 doesn't indicate strong influence of the TWC. If the Kuroshio Current flowed farther north during this period, as was suggested earlier in the Discussion, and distributed subtropical and equatorial species to the C9001 area, the primary heat contributor may not be recognized by these factors in this analysis.

4.2.3. MIS 12/11 Transition (227.3-238.5 mbsf)

In MIS 11, only a short interval between ~237-234 mbsf indicates strongly stratified watermasses, where Factor 2 values are strongly negative and Factors 3 and 4 are less negative.

4.3 Lead/lag relationship between SST and global ice volume ($\delta^{18}O$)

The curves produced by SST and $\delta^{18}O$ records are relatively parallel to each other, but mostly asynchronous through GI transitions. In this study, a lead/lag relationship between SST and $\delta^{18}O$ is observed in every interval at varying magnitude

(Figs 1.13, 1.14). Through the transitions of MIS 2/1 and 10/9, a lead of SST before $\delta^{18}O$ is observed, but the opposite occurs through the transitions of MIS 6/5e and 12/11.

Through MIS 2/1, SST leads the glacial termination as seen in the $\delta^{18}O$ record by about 5 meters, and peak temperatures and minimum ice volume co-occur at ~4 mbsf (Fig 1.14). Based on the existing data, the GI transition through this interval appears to be the most gradual, but this may be due to less-compacted sediments at the top of Hole C9001C.

Through MIS 6/5e, $\delta^{18}O$ reached its most positive value ~2 meters (~71.5 mbsf) before temperatures reached a peak minimum (~70 mbsf), but peak warm temperatures and the most negative $\delta^{18}O$ value occurred rapidly and coincided soon after at ~68 mbsf. The depth of GI transitions in $\delta^{18}O$ and cold to warm transitions is offset by ~3 meters, with $\delta^{18}O$ leading. A reversal to higher $\delta^{18}O$ values occurs between 68 to 63 mbsf. SSTs remain high until ~64 mbsf where cooling reaches a minimum temperature that coincides with the termination of MIS 5e (Fig 1.14).

As mentioned previously, the MIS 10/9 GI transition was not observed in this study, and lies below the sampled interval. The SST curve that was produced represents an interval of warm temperatures associated with the MIS 9 interglacial stage. The $\delta^{18}O$ record shows a peak positive value, representing a glacial maximum, occurring at 202 mbsf; however, SSTs persist at or above 16°C. This indicates that SST preceded global ice growth through this transition. The $\delta^{18}O$ record shows an abrupt negative shift reflecting termination of glacial MIS 10 between ~201-202 mbsf. The end of MIS 9 is identified by a reversal in $\delta^{18}O$ at ~185 mbsf (Fig 1.14).

In the MIS 12/11 interval, a global ice volume increase, as inferred from the $\delta^{18}O$ record, declines gradually from MIS 12 to MIS 11, between ~238 to 236 mbsf. SST and $\delta^{18}O$ occur concomitantly through the transition from coldest to warmest calculated SSTs, but isotope values did not reach a minimum until the end of the warmest interval (that persisted for 5 meters, ~236-231 mbsf), after which $\delta^{18}O$ values rapidly increase (Fig 1.14).

Regarding the transition from glacial to interglacial maxima based on these data, MIS 12/11 and MIS 2/1 have the most similar characteristics, in that through a gradual transition SSTs become warmer before global ice volume decreases and maximum temperature and minimum ice volumes eventually co-occur (Fig. 1.14). If the relationship between these two transitions makes MIS 12/11 an accurate analogue for this region, then one reasonable expectation for future climate may be the beginning of declining SSTs, while the reduction of global ice volume continues for another few thousand years before a reversal.

The lead/lag relationship between SST and $\delta^{18}O$ suggests that at a given time, one of these factors may regulate the other. For example, a lead in SSTs before $\delta^{18}O$ suggests that warming oceans and an increasingly warm and humid atmosphere may cause deterioration of global ice supply, or may cause increased snowfall downstream over the ice sheets causing them to grow. In the case where $\delta^{18}O$ leads SST, seasonal variation caused by orbital forcing may lead to reduction in ice volume and driving change in SST.

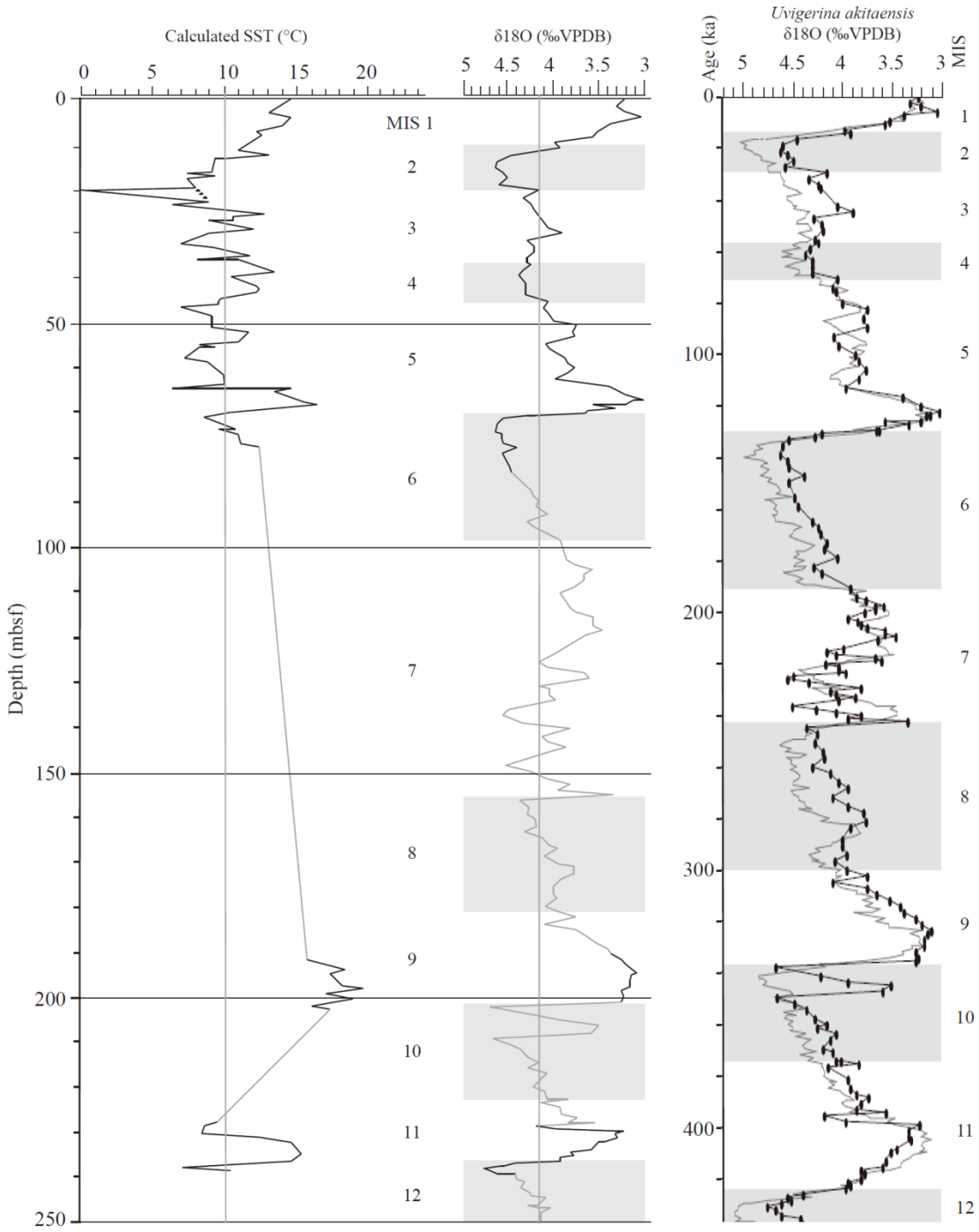

Figure 1.13. Left: the C9001C SST curve with sample intervals drawn in black. Gray line between profiles indicates no data. Gray vertical line at 10°C is drawn for reference and corresponds to the vertical gray line in the middle graph drawn at 4.15‰. **Middle:** the C9001C benthic oxygen isotope record (after Domitsu et al., 2010) with approximate sample intervals drawn in black. Gray line between profiles indicates no data. Both of these curves are aligned by depth with additional lines at 50 meter intervals. **Right:** the C9001C benthic oxygen isotope record of Domitsu et al. (2010) tuned to LR04 global benthic oxygen isotope stack with glacial periods shaded in gray.

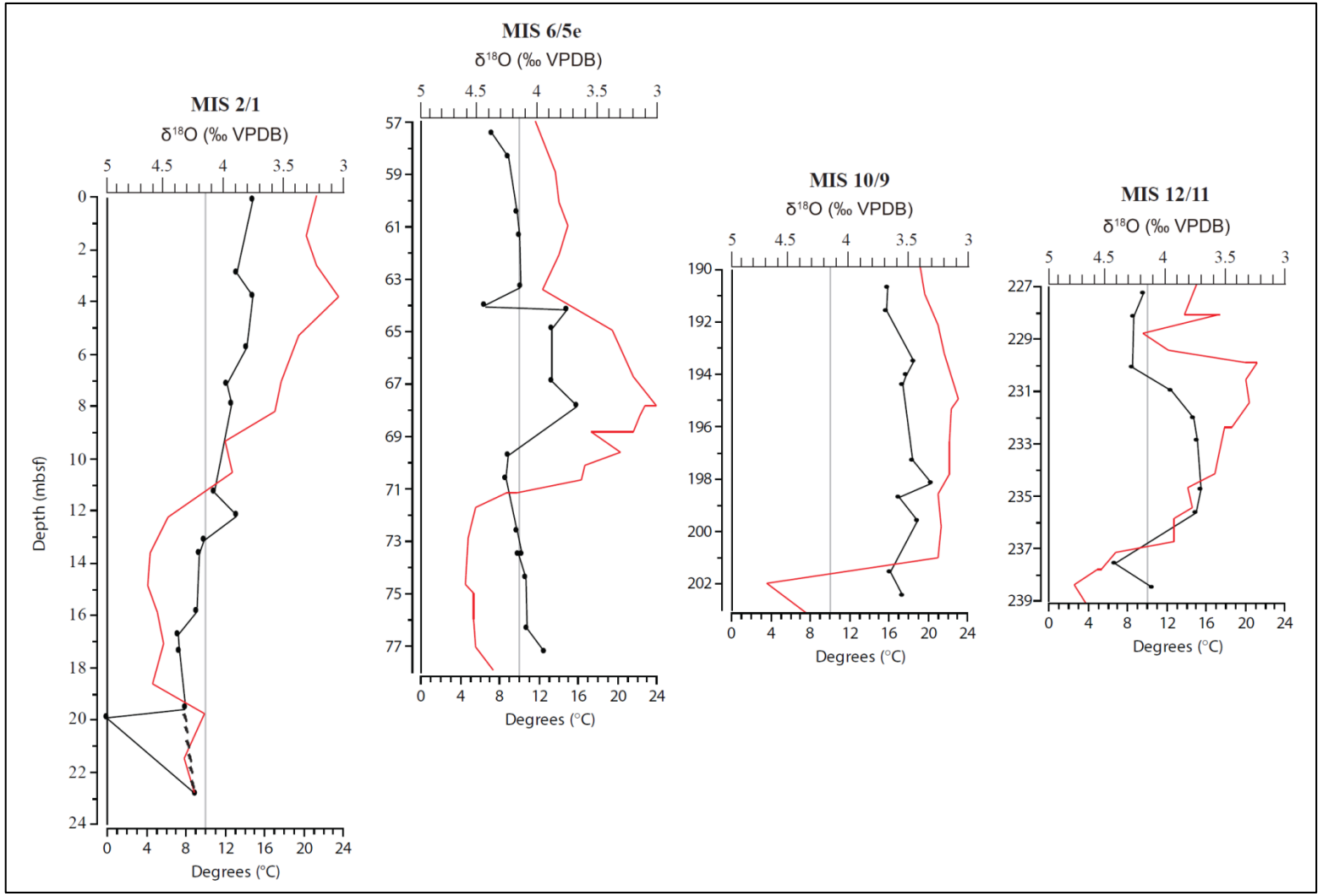

Figure 1.14. SST and $\delta^{18}O$ profiles overlain for each interval. $\delta^{18}O$ corresponds to the smooth red line and the scale on the top horizontal scale. SST (°C) corresponds to the dotted black line and the bottom horizontal scale. Vertical gray line is at 10°C and ~4.2‰ for a reference point. Each profile has been stretched/compressed for a consistent two-meter interval width, and profiles are aligned by greatest $\delta^{18}O$ values (glacial maximum).

5. Conclusions

There is value in comparing the magnitude and timing of the LGM/Holocene transition to previous Late Pleistocene GI transitions in order to assess the current position of modern climate and help predict its future trajectory. Based on the data from this study, the following conclusions can be drawn.

Sea-surface temperature can reasonably be estimated by applying *Td'* values to Koizumi's (2008) regression analysis slope equations; however, *Td'* values are inherently inaccurate in higher latitudes where warm-water diatom assemblages are fundamentally scarce or even absent.

A lead/lag relationship between SST and global ice volume in the North Pacific Ocean is observable through each sample interval at varying magnitude from Hole C9001C. Because of this lag of ice volume (as expressed in the $\delta^{18}O$ record) behind SST at this site, only the middle portion of sustained warm temperatures through MIS 9 was captured.

Comparison of the most recent GI transition in Hole C9001C to those of past GI cycles indicates that modern SSTs nearly match those of MISs 5e and 11, and that the relationship between SST and $\delta^{18}O$ is most similar between MIS 11/12 and 2/1. The maximum temperature calculated from the youngest sediments in MIS 1 is only about 1°C cooler than the maximum temperatures calculated for MIS 5e and 11.

MISs 9 was the warmest interglacial to influence this region. The high calculated SSTs produced for this interglacial at this site supports the assumption that this

interglacial was influenced by both GHG and high insolation. In addition to high calculated SSTs, $\delta^{18}O$ values are low; a combination that further supports this assumption as high-to-mid latitude environments would become unsuitable for most cold-water and sea-ice organisms.

Factor analysis using the diatom data in this study identified 3 taxa useful in determining watermass influence in the North Pacific regions where Site C9001 is located. The inverse relationship between Factor 2 and Factors 3 & 4 approximates shifting watermasses. Increasingly negative scores occur during cold/glacial periods when the Oyashio Current dominates therefore representing a strong Oyashio Current and mixed water column. In contrast, increasingly negative Factor 2 scores occur during warm/interglacial periods indicating a strong TWC and a stratified water column. Relatively intermediate scores between each of these Factors indicates transition between stratified to mixed watermasses and a shift in influence between the Tsugaru Warm Current and the Oyashio Current derived from Arctic/Subarctic latitudes.

Finally, *Melosira albicans* may have existed up to the LGM in the North Pacific region based on its record from Hole C9001C and from other holes drilled around the Tsugaru Strait and Japan Sea. Constraining this biostratigraphic datum has the potential to serve as a valuable measure of characterizing environmental conditions during a certain period in geologic history, and it may have the potential to be developed as a useful biostratigraphic marker.

Diatoms were successfully applied in this study as tools for reconstructing paleoenvironmental and paleoceanographic conditions in the NW Pacific Ocean. In only about the last century, diatoms have rapidly been developed as paleoenvironmental

proxies and biostratigraphic tools, largely in part due to various ocean drilling projects. Based on the data and the results produced from this study, continued development of diatoms as precise paleoenvironmental and biostratigraphic tools will prove to be a valuable effort.

6. Floral List

Taxonomic references to diatom taxa tabulated in Hole C9001C are listed below in alphabetical order in groups of marine taxa and non-marine genera. Chief references utilized in this study for species identification include Akiba (1986), Akiba and Yanagisawa (1986), Koizumi (1968, 2008), Sancetta (1982), and Winter et al. (2004). These works should be consulted for taxonomic reference and synonymy. All species and their occurrences are tabulated by sample in Appendix Table A1.

Marine Diatoms

Actinocyclus curvatulus Janisch, in Schmidt 1878
Actinocyclus ingens Rattray 1890
Actinocyclus ochotensis Jousé 1968
Actinocyclus oculatus Jousé 1968
Actinocyclus tenellus (Brébisson) Andrews 1976
Actinoptychus senarius (Ehrenberg) Ehrenberg 1843
Actinoptychus vulgaris Schumann 1867
Alveus marinus (Grunow) Kaczmarska & Fryxell 1996
Amphora costata Smith 1853
Asterolampra sp. 1
Asteromphalus flabellatus (Brébisson) Greville 1859
Asteromphalus hookeri Ehrenberg 1844
Asteromphalus imbricatus Wallich 1860
Asteromphalus parvulus Karsten 1905
Asteromphalus robustus Castracane
Azpeitia nodulifera (Schmidt) Fryxell & Sims, in Fryxell, Sims & Watkins 1986
Azpeitia tabularia (Grunow) Fryxell & Sims, in Fryxell, Sims & Watkins 1986
Bacteriastrum hyalinum Lauder 1864
Bacteriosira fragilis Gran 1900
Biddulphia biddulphiana (Smith) Boyer 1900
Chatoceros furcellatus Bailey 1856
Chatoceros septentrionalis Oestrup
Cocconeis antiqua Tempère & Brun in Brun & Tempère 1889
Cocconeis costata Gregory 1855
Cocconeis scutellum Ehrenberg 1938
Coscinodiscus marginatus Ehrenberg 1841
Coscinodiscus oculus-iridis Ehrenberg 1839
Coscinodiscus radiatus Ehrenberg 1839
Coscinodiscus stellaris Roper 1858
Crucidenticula Akiba & Yanagisawa 1986 spp.
Cyclotella striata (Kützing) Grunow 1880
Delphineis kippae Sancetta 1982

Delphineis surirella (Ehrenberg) Andrews 1981
Denticulopsis Simonsen 1979 spp.
Diploneis bombus Ehrenberg 1844
Diploneis smithii (Brébisson) Cleve 1894
Fragilariopsis curta (Van Heurck) Hustedt 1958
Fragilariopsis cylindrus (Grunow) Krieger, in Helmck & Krieger 1954
Fragilariopsis doliolus (Wallich) Medlin & Sims 1993
Fragilariopsis oceanica (Cleve) Hasle 1965
Grammatophora Ehrenberg 1840 spp.
Hemiaulus Heiberg 1863 spp.
Ikeba tenuis (Brun) Akiba 1986
Kisseleviella Sheshukova-Poretzkaya 1962 spp.
Lithodesmium reynoldsii Barron 1976
Melosira albicans Sheshukova-Poretzkaya 1964
Melosira sol (Ehrenberg) Kützing 1849
Neodenticula kamtschatica (Zabelina) Akiba & Yanagisawa 1986
Neodenticula koizumii Akiba & Yanagisawa 1986
Neodenticula seminae (Simonsen & Kanaya) Akiba & Yanagisawa 1986
Nitzschia capuluspalae Simonsen 1974
Nitzschia fossilis (Grunow) Grunow 1881
Nitzschia interruptestriata (Heiden) Simonsen 1974
Nitzschia kolaczekii Grunow 1877
Nitzschia rolandii Schrader emend. Koizumi 1980
Nitzschia sicula (Castracanea) Hustedt 1958
Odontella aurita (Lyngbye) Agardh 1830
Odontella longicuris (Greville) Hoban 1983
Paralia sulcata (Ehrenberg) Cleve 1873
Plagiogramma stauroforum (Gregory) Heiberg 1863
Planktoniella sol (Wallich) Schütt 1892
Porosira glacilis (Grunow) Jorgensen 1905
Proboscia curvirostris (Jousé) Jordan & Priddle
Pseudopodosira elegans (Sheshukova-Poretzkaya) Sheshukova-Poretzkaya 1964
Pseudosolenia calcar-avis (Schültze) Sundstrom 1986
Raphoneis amphiceros Ehrenberg 1884
Raphoneis cf. *isachaboensis* (Grunow) Mertz
Rhizosolenia acuminata (Peragallo) Gran 1905
Rhizosolenia acuminata (Peragallo) Gran 1905
Rhizosolenia bergonii Peragallo 1892
Rhizosolenia borealis Sundstrom 1986
Rhizosolenia hebetata (Bailey) Gran f. *hiemalis* Gran 1905
Rhizosolenia hebetata (Bailey) Gran f. *semispina* (Hensen) Gran 1904
Rhizosolenia imbricata Brightwell 1858
Rhizosolenia setigera Brightwell 1858
Rhizosolenia styliformis Brightwell 1858
Roperia tesselata (Roper) Grunow 1881
Stephanopyxis turris (Greville) Ralfs in Pritchard 1861
Synedropsis lata Hasle, Medlin & Syvertsen 1994
Synedropsis recta Hasle, Medlin & Syvertsen 1994
Thalassionema bacillaris (Heiden & Kolbe) Kolbe 1955
Thalassionema hirosakiensis (Kanaya) Schrader 1973
Thalassiosira sp. A
Thalassiosira antarctica Comber 1896
Thalassoisira sp. B
Thalassiosira decipiens (Grunow) Jørgensen 1905
Thalassiosira eccentrica (Ehrenberg) Cleve 1904
Thalassiosira ferelineata Hasle & Fryxell 1977
Thalassiosira gravida Cleve 1896
Thalassiosira hyalina (Grunow) Gran 1897
Thalassiosira jouseae Akiba 1986
Thalassiosira kryophila (Grunow) Jørgensen 1905
Thalassiosira lacustris (Grunow) Hasle in Hasle & Fryxell 1977
Thalassiosira leptopus (Grunow) Hasle & Fryxell 1977
Thalassiosira lineata Jousé 1968
Thalassiosira manifesta Sheshukova-Poretzkaya 1964
Thalassiosira nidulus (Tempère & Brun) Jousé 1961
Thalassiosira nordenskioeldii Cleve 1873
Thalassiosira oestrupii (Ostenfeld) Hasle 1972
Thalassiosira pacifica Gran & Angst 1931
Thalassiosira punctigera (Castracane) Hasle 1983

Thalassiosira trifulta Fryxell, in Fryxell & Hasle 1979
Thalassiothrix longissima Cleve & Grunow 1880
Thalssionema nitzschioides Grunow 1881

Nonmarine Genera
Amphora Ehrenberg ex Kützing 1844 spp.
Aulacoseira Thwaites spp.
Cyclotella (Kützing) Brébisson 1838 spp.
Cymbella Agardh 1830 spp.
Epithemia Kützing 1844 spp.
Eunotia Ehrenberg 1837 spp.
Gomphonema Ehrenberg 1832 spp.
Surirella Turpin 1828 spp.
Tetracyclus Ralfs 1843 spp.

Marine and Nonmarine Genera
Achnanthes Bory de Saint-Vincent 1822 spp.
Cocconeis Ehrenberg 1837 spp.
Diploneis Ehrenberg ex Cleve 1894 spp.
Navicula Bory de Saint-Vincent 1822 spp.
Pinnularia Ehrenberg 1843
Pleurosigma Smith 1852 spp.

6.1 Taxonomic and Biostratigraphic Notes

6.1.1 Thalassiosira leptopus (Grunow) Hasle & Fryxell 1977

Existing data show that some species of the genus *Thalassiosira* produce polymorphs in relation to environmental conditions (Fryxell, 1986, Wood et al., 1987). Throughout the samples used in this study, two varieties of *T. leptopus* were observed (Plate 1.3). This species typically displays nearly straight rows of areolae across the valve face, whereas the variety has rows “slightly bent, oblique, and decussating” (Rattray, 1890). The variety fits the description of a species formerly known as *Coscinodiscus leptopus* var. *discrepans* Rattray 1890, a name that is now synonymized with *T. leptopus* Hasle & Fryxell 1977; Pl. 1-4, p. 49-52. In order to confirm whether the forms observed here could fall within the morphological range of *T. leptopus*, measurements, including the diameter of the valve face and number of areolae in 10 μm, were taken of each morphotype and compared to the original description (Fig. 1.15). A strictly qualitative number of specimens were measured for this investigation, but it becomes apparent that

the variety with oblique rows of areolae tends to occur when the valve diameter is smaller. In addition to the other defining characteristics of *T. leptopus*, all measurements fit within the species description. Given the synonomy of the names, specimens of each variety are all tabulated under *T. leptopus.* The reader is referred to Hasle and Fryxell (1977) and Rattray (1890) for detailed taxonomic description and illustration of this species.

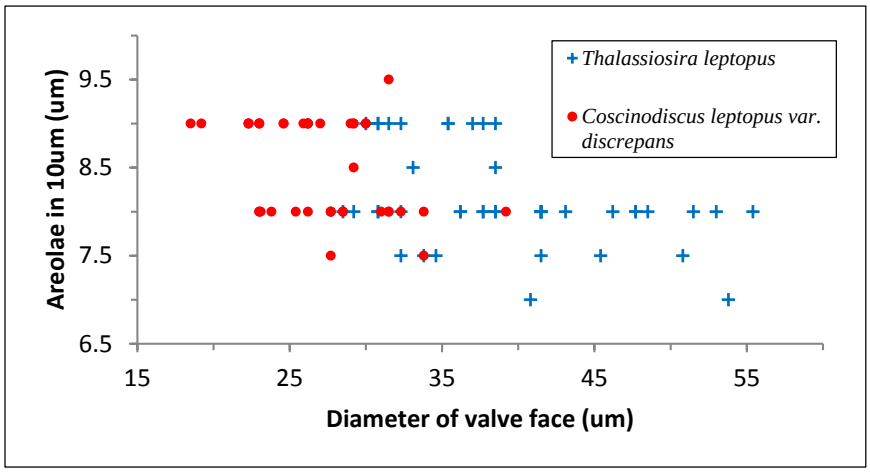

Figure 1.15. Morphometric data for two morphological varieties of *Thalassiosira leptopus.*

6.1.2 Thalassiosira punctigera (Castracane) Hasle 1983

Thalassiosira punctigera was identified throughout Hole C9001C and originally identified as an informal taxon, *Thalassiosira* sp. D, described and illustrated by Akiba (1986). Hasle (1983) clarified the concept of *T. punctigera* and synonymized 8 taxa, including the transfer of *Ethmodiscus punctiger* Castracane into *Thalassiosira.* Akiba's (1986) illustration of *Thalassiosira* sp. D (Pl. 11. Fig. 8) is identical to the specimens of

Thalassiosira punctigera observed in this study. The reader is referred to Akiba (1986), Hasle (1983) and Tomas (1996) for detailed description and further illustration.

6.1.3 Biostratigraphic occurrence of Melosira albicans *Sheshukova-Poretzkaya 1964*

Melosira albicans was originally described from the Pliocene Ust-Kamchatka, on the east side of Kamchatka Peninsula. It was also found in the Pliocene Tatsunokuchi Formation in Fukushima and Miyagi Prefectures (Koizumi, 1972, 1973b), and its last occurrence is documented at the Pleistocene *Proboscia curvirostris* Zone, (MIS 9/8 boundary at 300 ka) in the middle- to high-latitudes (Koizumi, 1973a, 1992). However, Koizumi and Yamamoto (2008) note that the species concept used to identify *M. albicans* should be re-examined, because its last occurrence appears to be younger in off-shore sections than in on-land sections. In this study, *M. albicans* was noted consistently up to 16.5 mbsf (~16 ka) above which its abundance declined to the lowest tabulated values within all sample intervals (Table A1). Similarly, Koizumi et al. (2006) show consistent records of *M. albicans* maintaining high values up to ~16 ka in the Tsugaru Straight and ~18 ka in the Japan Sea. The consistent highest appearance of this taxon into the LGM may suggest a new biostratigraphic datum for the offshore North Pacific Ocean region.

PLATES

Plate 1.1. Warm-water species observed in Hole C9001C as described by Kanaya and Koizumi (1966) (*Xw)* and supplemented by Koizumi et al. (2004) (XW).

1. *Asteromphalus flabellatus* (Brébisson) Greville 1859
2. *Asteromphalus imbricatus* Wallich 1860
3. *Alveus marinus* (Grunow) Kaczmarska & Fryxell 1996
4. *Thalassiosira leptopus* (Grunow) Hasle & Fryxell 1977
5. *Roperia tesselata* (Roper) Grunow 1881
6. *Thalassiosira oestrupii* (Ostenfeld) Hasle 1972
7. *Azpeitia tabularia* (Grunow) Fryxell & Sims, in Fryxell, Sims & Watkins 1986
8. *Pseudosolenia calcar-avis* (Schültze) Sundstrom 1986
9. *Nitzschia interruptestriata* (Heiden) Simonsen 1974
10. *Rhizosolenia acuminata* (Peragallo) Gran 1905
11. *Rhizosolenia bergonii* Peragallo 1892
12. *Rhizosolenia imbricata* Brightwell 1858
13. *Fragilariopsis doliolus* (Wallich) Medlin & Sims 1993
14. *Nitzschia kolaczekii* Grunow 1877
15. *Rhizosolenia hebetata* (Bailey) Gran f. *semispina* (Hensen) Gran 1904

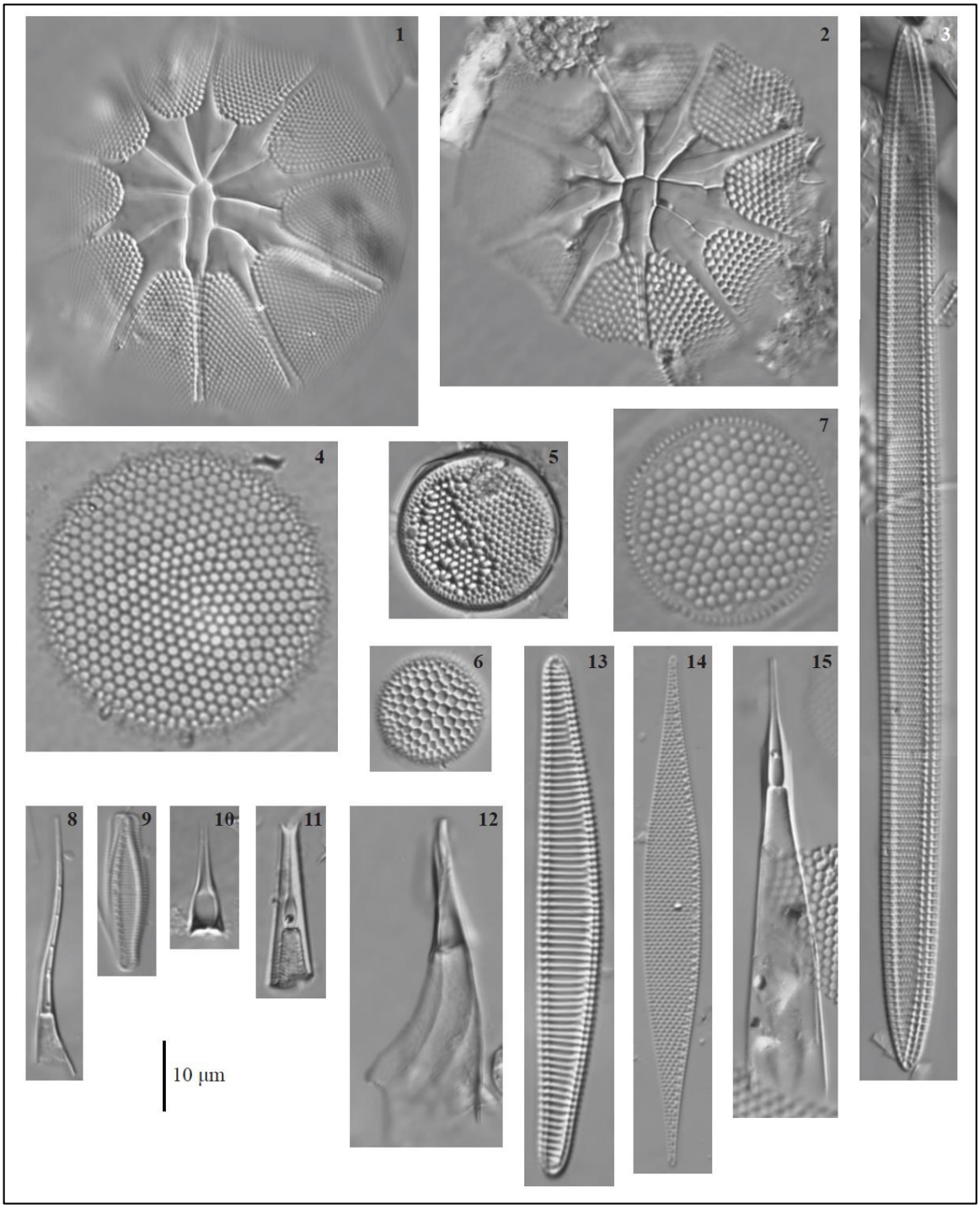
1
2
3
4
5
6
7
8
9
10
11
12
13
14
15
10 µm

Plate 1.2. Cold-water species observed in C9001C as described by Kanaya and Koizumi (1966) (*Xc)* and supplemented by Koizumi et al. (2004) (XC).

1. *Asteromphalus robustus* Castracane
2. *Thalassiosira trifulta* Fryxell, in Fryxell & Hasle 1979
3. *Thalassiosira hyalina* (Grunow) Gran 1897
4. *Coscinodiscus oculus-iridis* Ehrenberg 1839
5. *Thalassiosira gravida* Cleve 1896
6. *Fragilariopsis oceanica* (Cleve) Hasle 1965
7. *Rhizosolenia hebetata* (Bailey) Gran f. *hiemalis* Gran
8. *Chatoceros furcellatus* Bailey 1856
9. *Bacteriosira fragilis* Gran 1900
10. *Neodenticula seminae* (Simonsen & Kanaya) Akiba & Yanagisawa 1986
11. *Fragilariopsis cylindrus* (Grunow) Krieger, in Helmck & Krieger 1954
12. *Actinocyclus curvatulus* Janisch, in Schmidt 1878
13. *Coscinodiscus marginatus* Ehrenberg 1841
14. *Thalassiosira nordenskioeldii* Cleve 1873
15. *Porosira glacilis* (Grunow) Jørgensen 1905

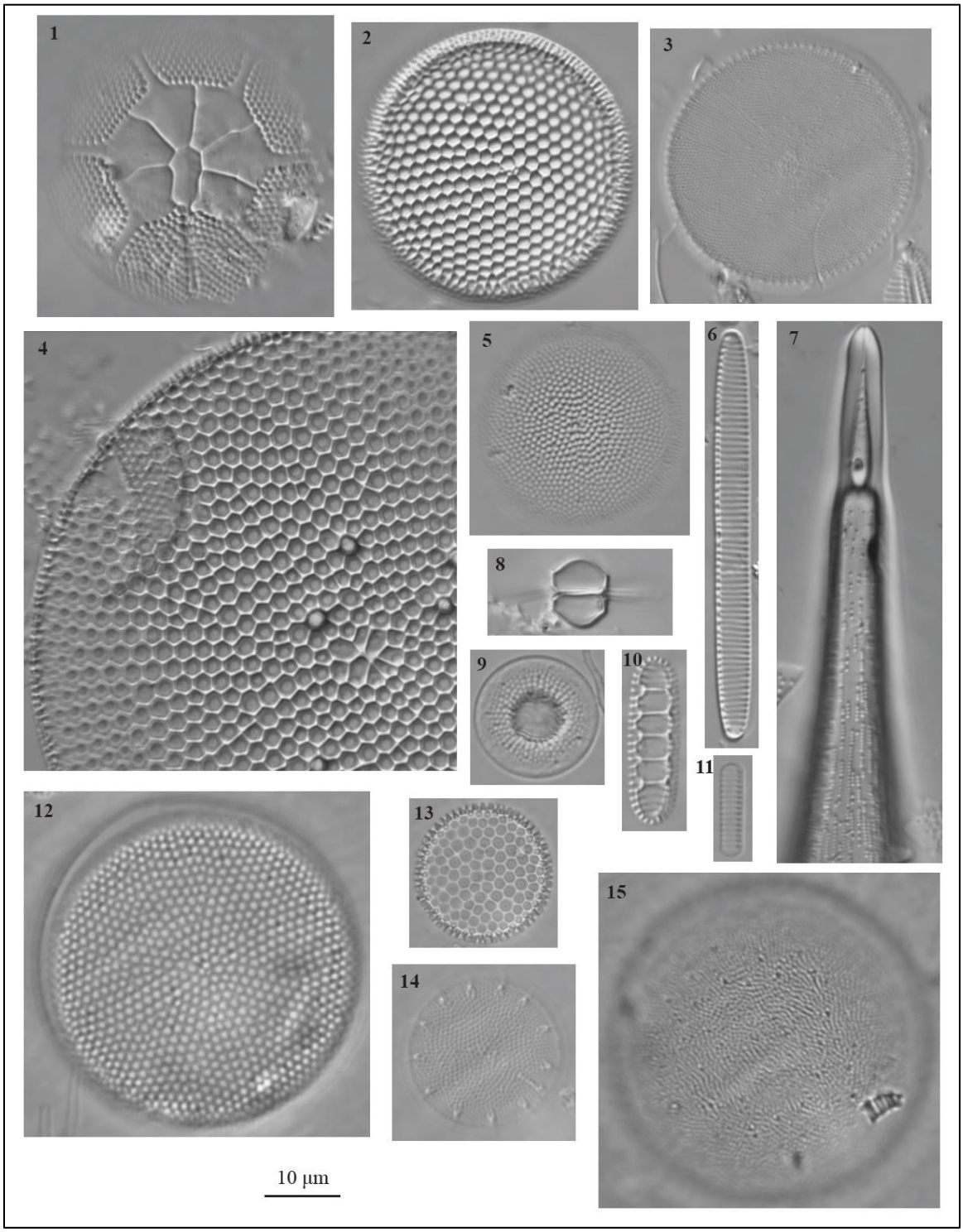
1
2
3
4
5
6
7
8
9
10
11
12
13
14
15
10 µm

Plate 1.3. Morphological variation within *Thalassiosira leptopus* and documentation of *Thalassiosira punctigera* from Hole C9001C.

1-2. *Thalassiosira leptopus* (Grunow) Hasle & Fryxell 1977. Two specimens displaying linear areolation pattern and variable valve size.

3-4. *Thalassiosira leptopus* (Grunow) Hasle & Fryxell 1977 Two specimens displaying non-linear areolation patterns and similar valve size.

5a-5c. *Thalassiosira punctigera* (Castracane) Hasle 1983. One specimen at three levels of focus: **Fig. 5a** shows labiate processes, marginal rings of strutted processes and ribs; **Fig. 5b** focuses on the occluded processes, and **Fig. 5c** is focused on the valve center to show central-radiating and fasciculated rows of fine areolae.

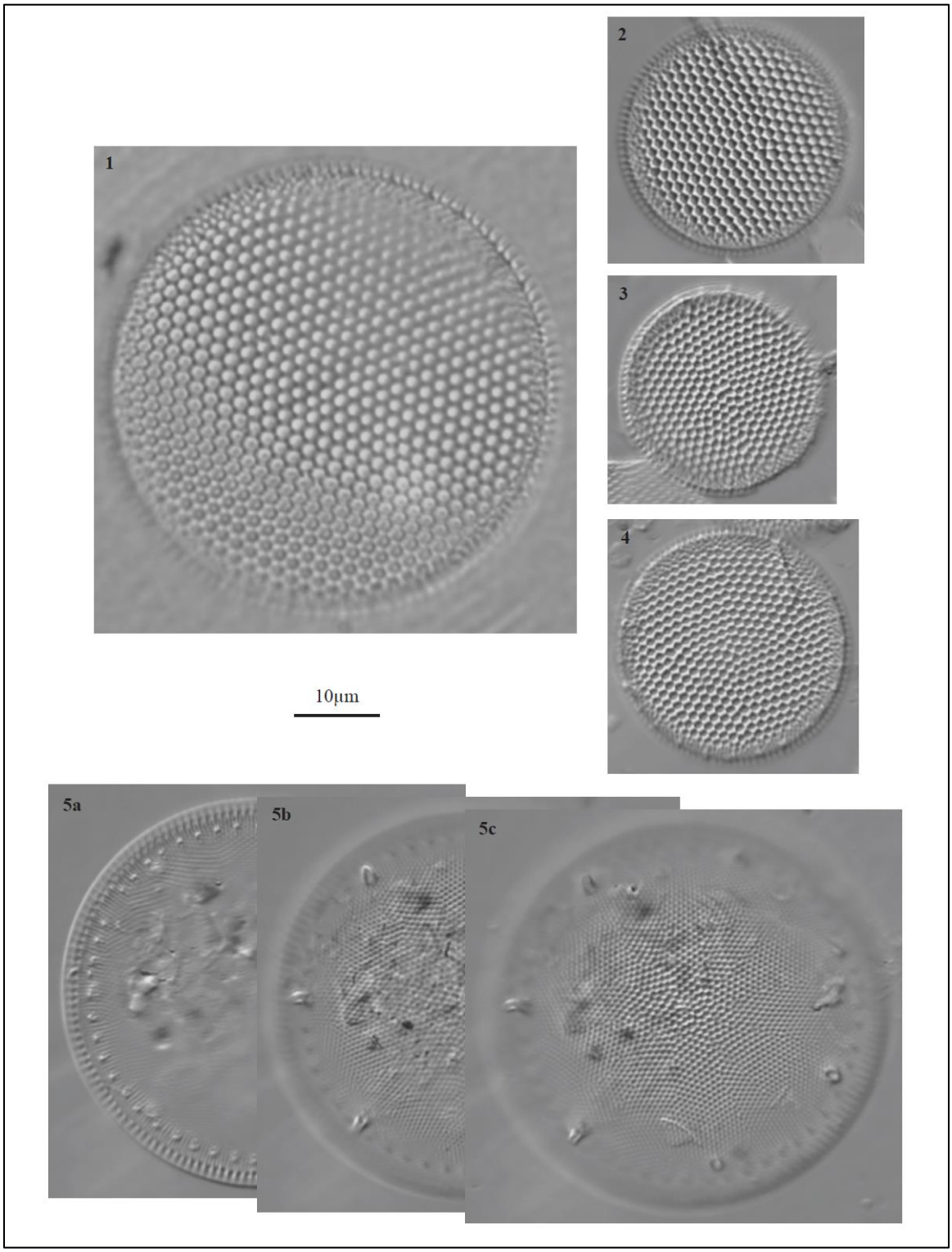
1
2
3
4
10µm
5a
5b
5c

CHAPTER 2

NEOGENE DIATOM BIOSTRATIGRAPHY AND AGE SYNTHESIS OF SITE C9001/C0020, NORTHWEST PACIFIC OCEAN[1]

ABSTRACT

Integrated Ocean Drilling Program (IODP) Expedition 337 drilled a new core in 2012 that extended the coring depth of Hole C9001D at Site C9001 below the 647 meters below seafloor (mbsf) that was penetrated in 2006 during the Chikyu Shakedown Cruise CK06-06. Drilling operations at Site C0020 (formerly Site C9001), located 80 km off the Shimokita Peninsula of northeastern Honshu, Japan, penetrated Hole C0020A to a total depth of 2466 mbsf. IODP Exp. 337 sought to explore a deep hydrocarbon system and coalbeds that, prior to drilling, were estimated to be of Eocene age. Combined shipboard diatom and palynological analyses, however, revealed unexpectedly thick sections of Pliocene and Miocene sediments, an approximately 12-13 million year hiatus at 1086.5 mud depth below sea floow (m MSF), and coalbeds younger than originally predicted. New biostratigraphic results from Hole C0020A indicate the target coalbed is Early Miocene. The age of the youngest sediments recovered in Hole C0020A is revised from Late Pliocene to Early Pleistocene, and the basal age of Hole C9001C is confirmed as Early Pleistocene. The age of the deepest sediments recovered at Site C0020 is Late Oligocene-Early Miocene. All new data are integrated with the overlying interval recovered from Holes C9001C and C9001D to produce a composite chronostratigraphic framework for Site C0020.

[1] This chapter will be submitted to the International Ocean Drilling Program and published as a data report in the scientific results volume for Expedition 337.

1. Introduction

In 2012, Integrated Ocean Drilling Program (IODP) Expedition 337 drilled Hole C0020A at Site C0020A located approximately 80 km off the Shimokita Peninsula of northern Honshu, Japan (Figure 2.1). Hole C0020A is a re-entry and continuation of Hole C9001D (Site C9001), which was drilled during the 2006 *D-V Chikyu* Shakedown Cruise (CK06-06). Hole C0020A was drilled to recover the stratigraphic interval below Holes C9001B, C and D. It penetrated from 636.5 mbsf to 2466 mbsf and recovered a diversity of lithologies that yielded microfossil groups of varying degrees of biostratigraphic utility including diatoms, calcareous nannofossils, organic-walled dinoflagellate cysts, pollen

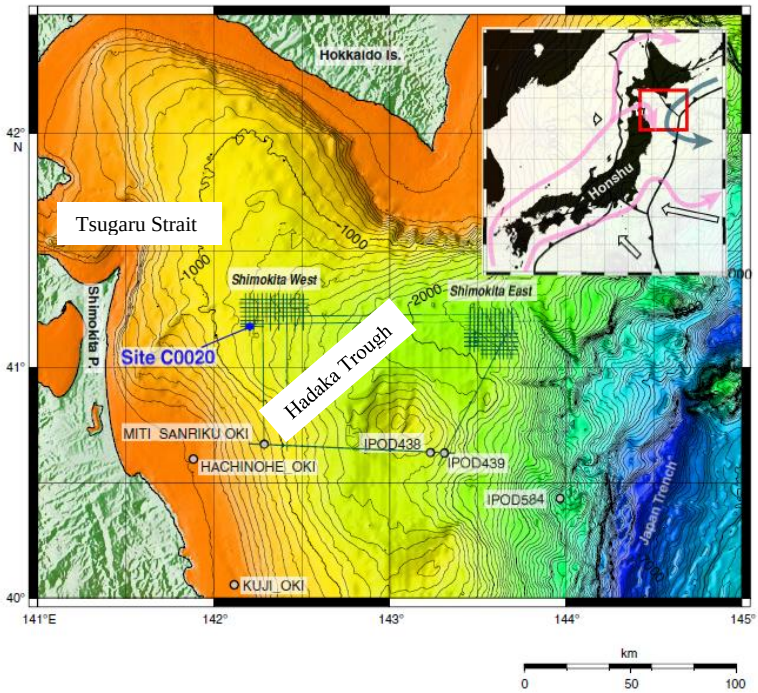

Figure 2.1. Regional map of the Shimokita region and Hadaka Trough showing bathymetry, seismic survey track lines and location of Site C0020, including other existing drill holes. Inset map shows site location relative to the Japanese Islands and basic modern ocean current circulation (after Expedition 337 Scientists, 2013).

and spores (Expedition 337 Scientists, 2013).

Based on microfossil distribution and lithology, Hole C0020A is divided into four units (Table 2.1). Unit I ranges from 636.5 to 1256.5 mud depth below seafloor (m MSF), Unit II from 1256.5 to 1826.5 m MSF, Unit III from 1826.5 to 2046.5 m MSF, and Unit IV from 2046.5 to 2466 m MSF. Unit I was entirely rotary cored, and samples were provided from cuttings. Units II-IV were spot-cored. Diatoms are present and identifiable almost entirely through Unit 1, and are the focus of this study.

Expedition 337 sought to explore a deep hydrocarbon system and coalbed that, prior to drilling, were estimated to be Eocene (Inagaki, et al 2010). In addition, a regional unconformity between marine and terrestrial sediments was predicted to mark the Eocene/Oligocene boundary at approximately 1650 mbsf (Fig. 2.2). Combined shipboard diatom and palynological analyses, however, revealed unexpectedly thick sections of Pliocene and Miocene sediments and a complete absence of Middle Miocene sediments. The oldest sediments recovered from Exp. 337 are Late Oligocene-Early Miocene (Exp. 337 Scientists, 2013).

1.1 Previous Work

Diatoms are abundant and highly diverse in the middle- and high-latitude North Pacific where they have been developed as the primary biostratigraphic tool for dating and correlating Neogene sediments (Yanagisawa and Akiba, 1998). This biostratigraphic framework was initially established through the works of Donahue (1970), Koizumi (1973a, b) and Schrader (1973a). Koizumi's (1973a, b) zonation has become the standard workable zonation through continuous revision and refinement by subsequent studies.

Table 2.1. Unit divisions in Hole C0020A, lithology and approximate age (from Expedition 337 Scientists, 2013)

Unit	Subunit	Core/Cuttings number	Depth interval MSF (m)	Thickness (m)	Lithology	Age
I	a	Samples 337-C0020A-24-SMW through 58-SMW	647–926.5	279.5	Diatom-bearing siltstone and claystone	late–middle Pliocene
	b	Samples 337-C0020A-59-SMW through 88-SMW	926.5–1116.5	190	Semiconsolidated diatom-bearing clayey siltstone with common fine sandstone	middle Pliocene/early Pliocene–late Miocene
	c	Samples 337-C0020A-92-SMW through 95-SMW	1116.5–1236.5	120	Unconsolidated to semiconsolidated sandstone and silty sandstone with rare clayey siltstone	early Pliocene–Miocene
	d	Samples 337-C0020A-97-SMW through 98-SMW	1236.5–1256.5	20	Semiconsolidated clayey siltstone with medium loose sand	early Pliocene–Miocene
II	a	Samples 337-C0020A-98-SMW through 153-SMW; Cores C0020A-1R through 6R	1256.5–1506.5	250	Sandstone and siltstone associated with marine fossiliferous material	Miocene
	b	Samples 337-C0020A-153-SMW through 216-SMW; Cores C0020A-7R through 14R	1506.5–1826.5	320	Organic-rich shale and sandstone associated with plant remains	Miocene
III		Samples 337-C0020A-216-SMW through 261-SMW; Cores C0020A-15R through 25R	1826.5–2046.5	220	Organic-rich sandstone and shale associated with coalbeds	early–middle Miocene
IV	a	Samples 337-C0020A-261-SMW through 384-SMW; Cores C0020A-26R through 29R	2046.5–2426.5	380	Shale and sandstone associated with carbonate and glauconitic material	early Miocene–late Oligocene
	b	Samples 337-C0020A-384-SMW through 391-SMW; Cores C0020A-30R through 32R	2426.5–2466	39.5	Sandstone and shale associated with coalbed	early Miocene–late Oligocene

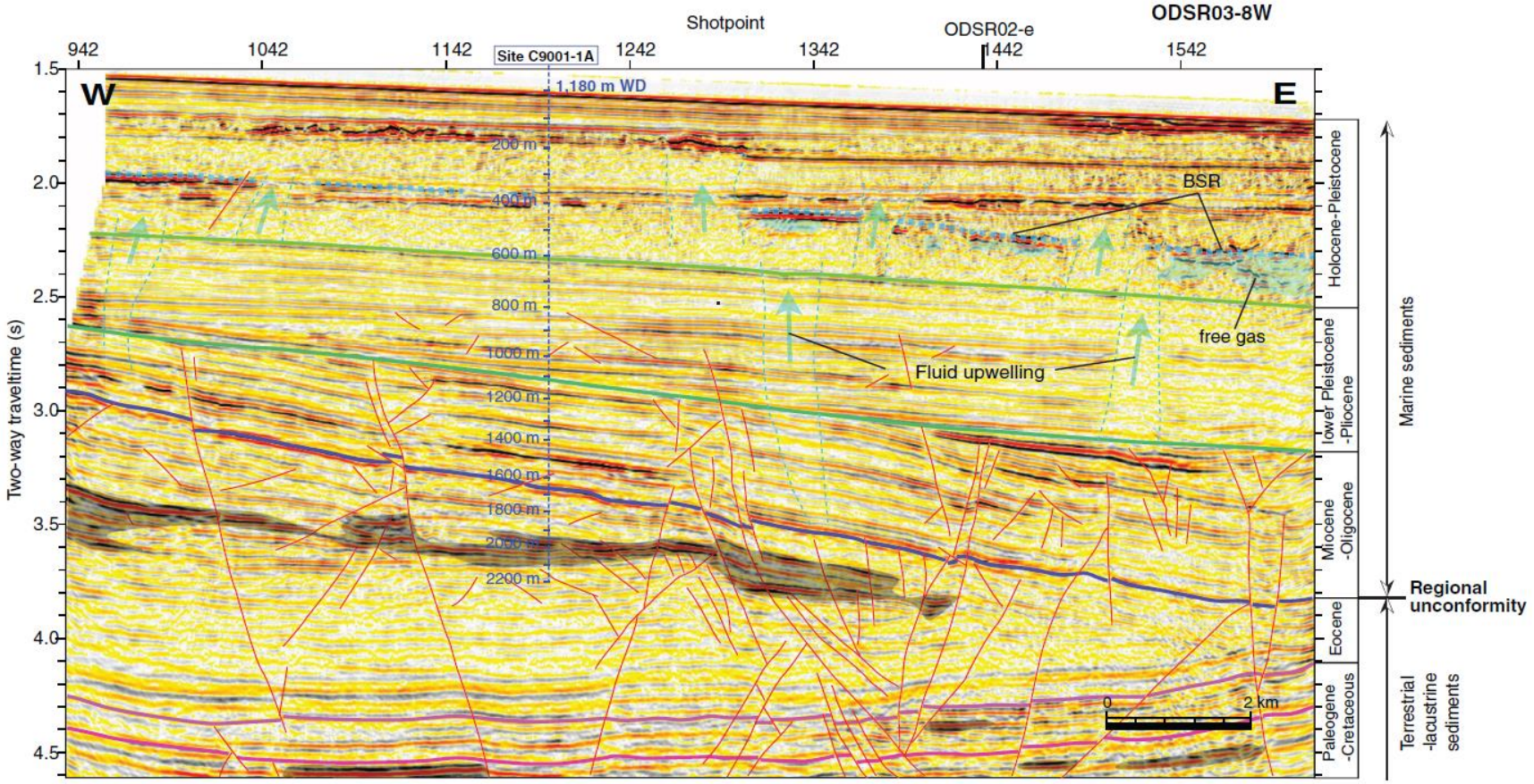

Figure 2.2. Original seismic profile produced for Site C9001/C0020A including pre-drilling interpretations of geologic features, stratigraphic boundaries and ages (from Inagaki et al., 2010).

The development of diatom biostratigraphy progressed as biostratigraphic studies of numerous continuous sequences of deep sea cores and on-land sequences facilitated detailed taxonomic and stratigraphic studies (Simonsen and Kanaya, 1961; Simonsen, 1979; Akiba and Yanagisawa, 1986) through which new species were identified and biohorizons were refined in studies including, but not limited to, Schrader (1973a, b) Maruyama (1984, 1992) and Akiba and Yanagisawa, (1986). A complete list of these studies is referenced in Yanagisawa and Akiba (1998).

In addition, Gladenkov and Barron (1995) firmly established an early Miocene through Oligocene diatom zonation. Their study directly correlated diatom zones to magnetostratigraphy and provided precise ages for Neogene primary zonal marker biohorizons, making the Neogene biostratigraphy for the middle- to high-latitude North Pacific a precise and high-resolution correlation tool (Barron and Baldauf, 1995; Motoyama and Maruyama, 1998).

Finally, Yanagisawa and Akiba (1998) presented a more refined high-resolution Neogene North Pacific diatom (NPD) biostratigraphy and zone code system for precise dating and correlation in the northwest Pacific around Japan. Yanagisawa and Akiba (1998) identified several useful secondary diatom biohorizons and updated ages for both primary and secondary biohorizons based on the geomagnetic polarity time scale of Cande and Kent (1995). The diatom-based biostratigraphy of Hole C0020A is constructed primarily on the occurrences of stratigraphically diagnostic diatoms following Yanagisawa and Akiba's (1998) NPD biostratigraphy.

2. Materials and Methods

Samples for diatom-based biostratigraphic analysis were collected from rotary core barrel (RCB) cuttings at 10-meter intervals between the depths of 636.5 m MSF and 1246.5 m MSF. These 10 m sample intervals are labeled from 24 SMW through 97 SMW for this study (Table 2.2, Fig. 2.2). "SMW" is an abbreviation describing the type of material recovered by drilling operations and refers to "solid taken from drilling mud". Of these, only large sample cuttings suitable for processing to mitigate downhole contamination were used. Each sample cutting was first washed and soaked/softened in Milli-Q water and then scraped with a razor-blade to remove the outer surface, in order to minimize surficial contamination. Freshly exposed sediment surfaces were scraped and materials sieved to a maximum 45μm size-fraction. Strewn slides were prepared qualitatively from a slurry by first stirring/shaking the sediment into suspension, immediately removing part of the upper suspension with a disposable pipette and injecting it into a droplet of Milli-Q water on a 24 x 36 mm coverslip. The strewn sample was dried on a hot plate (50°-60°C) then mounted to a glass slide using *Norland* Optical Adhesive #61 and cured under UV light. Species were identified at 750x magnification, and identifications checked at 1250x magnification using an *Olympus* BH2 microscope.

The diatom-based biostratigraphy of Hole C0020A is constructed primarily on the occurrences of stratigraphically diagnostic diatoms following the Neogene North Pacific diatom (NPD) zone code system of Yanagisawa and Akiba (1998). In order to further mitigate complications associated with downhole contamination, the last occurrences

Table 2.2. Cuttings sample intervals from Unit I used for diatom biostratigraphy in Hole C0020A including depth, age, zonal assignment, preservation and qualitative abundance of diatoms. Abundance: A=abundant, C=common, F=few, R=rare, r = reworked specimens, d = inferred downhole contaminating specimens. Preservation: G=good, M=moderate, P=poor.

Sample No. (SMW)	Depth (mBRT)	Depth TOP (m MSF)	Depth BOTTOM (m MSF)	Geo Age	NPD Zone	Abundance	Preservation	*K. ezoensis*	*D. hustedtii*	*D. katayamae*	*Denticulopsis spp.*	*Rouxia spp.*	*T. schraderi*	*N. kamtschatica*	*T. praeoestrupii*	*N. koizumii*	*T. oestrupii*	*A. oculatus*	*N. seminae*
24 SMW	1855.0	636.5	646.5	E. Pleistocene	NPD 10	A	G										R	R	C
25 SMW	1865.0	646.5	656.5			A	G										R	R	C
26 SMW	1875.0	656.5	666.5			A	G										R	R	C
27 SMW	1885.0	666.5	676.5			A	G										R	F	C
28 SMW	1895.0	676.5	686.5	L. Pliocene	NPD 9	C	G									R	R	F	C
29 SMW	1905.0	686.5	696.5			C	G									R	R	R	C
30 SMW	1915.0	696.5	706.5			C	G									F		R	F
34 SMW	1955.0	736.5	746.5			F	M											R	
35 SMW	1965.0	746.5	756.5			F	P									R			
40 SMW	2015.0	796.5	806.5			F	P									F	R	R	C
45 SMW	2065.0	846.5	856.5			C	M									R	R		R
46 SMW	2075.0	856.5	866.5			R	P									R			R
55 SMW	2105.0	886.5	896.5			F	M									R		R	R
56 SMW	2115.0	896.5	906.5		NPD 8	F	G							R		F		F	d
57 SMW	2125.0	906.5	916.5			C	M				r			R		F		F	d
58 SMW	2135.0	916.5	926.5			C	M				r			R		F			
59 SMW	2145.0	926.5	936.5			F	M							R		R		R	
60 SMW	2155.0	936.5	946.5	E. Pliocene	NPD 7Bb	C	M				r			C	R		R		
61 SMW	2165.0	946.5	956.5	L. Mio - L. Plio		C	M		r	?				C		R			d
66 SMW	2215.0	996.5	1006.5	Mio/Plio		A	G							A	R		R		d
74 SMW	2275.0	1056.5	1066.5	L. Miocene	NPD 7Ba	F	M							F	R				
79 SMW	2295.0	1076.5	1086.5			F	P					r	r	C					

Table 2.2. (Continued)

Sample No. (SMW)	Depth (mBRT)	Depth TOP (m MSF)	Depth BOTTOM (m MSF)	Geo Age	NPD Zone	Abundance	Preservation	*K. ezoensis*	*D. hustedtii*	*D. katayamae*	*Denticulopsis spp.*	*Rouxia spp.*	*T. schraderi*	*N. kamtschatica*	*T. praeoestrupii*	*N. koizumii*	*T. oestrupii*	*A. oculatus*	*N. seminae*
80 SMW	2305.0	1086.5	1096.5	E. Miocene	NPD 1-2A	R	P	R						d					
88 SMW	2325.0	1106.5	1116.5			R	P	R											
92 SMW	**2335.0**	**1116.5**	**1186.5**					**LOST ZONE**											
95 SMW	2445.0	1226.5	1236.5			R	M	R						d		d		d	
97 SMW	2455.0	1236.5	1246.5			R	M												
END UNIT I																			

(LO) of marker species were the primary biohorizons used.

Counting methods followed that described by Schrader and Gersonde (1978). Estimation of diatom abundance was qualitative and based on the following outline:

A = abundant (≥ 6 specimens per field of view [FOV] at 750x magnification)

C = common (1–5 specimens/FOV at 750x)

F = few (1–4 specimens/5 FOV at 750x)

R = rare (1–10 specimens/horizontal traverse at 750x)

Diatom preservation is recorded as G (good), M (moderate) and P (poor) based on the degree of breakage and dissolution of diatom valves as described by Akiba (1986).

3. Contamination

Considerable challenges were posed by contamination from drilling mud that affected core samples, core catchers, and especially cuttings samples for diatom analysis. In some intervals material was unsuitable for both processing and biostratigraphic analysis.

Downhole contamination worsened progressively with depth. Microfossil-bearing sediments from overlying stratigraphic intervals were incorporated into the drilling mud that recirculated through the hole, resulting in downhole contamination in nearly every sample to the base of the hole. The first major indication of contamination was observed at ~1185.5 m MSF (Table 2.2), just below the first lost interval near the base of Unit I. Downhole contamination can also be inferred in deeper cuttings samples as specimens observed and marking the top of the hole were noted as well preserved, compared to the

rest of the assemblage. Contamination proved especially problematic for core catcher samples and cuttings samples of the smallest size fraction (<1 mm). However, even samples of larger size fractions (1-4 mm) often contained contaminants, especially those possessing larger grain size or greater porosity. Cuttings samples of the smallest size fraction often contained no rock cuttings and were of a sandy or muddy consistency and therefore were completely saturated with contaminated drilling mud. Some samples, upon recovery, were washed with tap water before distribution and analysis, but these samples also contained contaminants in quantities that proved problematic. The most abundant contaminants were those of Late Miocene and Pliocene ages, including marker species *Neodenticula kamtschatica, Neodenticula koizumii* and *Neodenticula seminae.* Two Pleistocene diatoms, *Actinocyclus oculatus* and *Proboscia curvirostris*, were also identified as downhole contaminants.

4. Results

Domitsu et al. (2010) developed an age model for holes C9001C and C9001D based on the biostratigraphy of four microfossil groups including calcareous nannofossils, diatoms, foraminifera and radiolarians down to 645 mbsf for a total depth age of ~1.6 Ma within the lower Pleistocene NPD Zone 10. The upper 350 mbsf were cored continuously with over 100% recovery (Aoike, 2007). A complete oxygen isotope record from these cores was also produced using benthic foraminifera and tuned to Lisieki and Raymo's (2004) global benthic stack, providing precise age control for the upper 350 mbsf through 640 ka (Domitsu et al., 2010). The diatom-based age model for

the underlying stratigraphic interval recovered in Hole C0020A continues from NPD Zone 10 at 636.3 m MSF and continues down into the lower Miocene at 1246.5 m MSF, to the base of Unit I, where the useful diatom record stops. Diatom biohorizons constraining the age of sediments in Unit I are listed in Table 2.3, and constrain the age/depth interpretations in Table 2.2.

Biostratigraphically useful diatoms do not occur below 97-SMW at 1246.5 m MSF. Age information below this level is based on palynomorph biochronology as provided by Guy Harrington (Expedition 337 Scientists, 2013). The age interpreted at the total depth of Hole C0020A is Late Oligocene-Early Miocene.

An interval of loosely consolidated sand between the depths of 1116.5-1186.5 m MSF resulted in a significant 70 meter zone of loss. A shift in diatom assemblage from what is interpreted to be the Early Miocene *Thalassiosira fraga* NPD Zone 2A into the

Table 2.3. Diatom biohorizons used to constrain age in Unit I, Hole C0020A

Code number	Occurance	North Pacific Diatom biohorizon	Age (Ma)	Depth (m MSF)	Sample
a*	LO	*Neodenticula koizumii*	2.0	686.5 - 676.5	28 SMW
b	FO	*Neodenticula seminae*	2.4?	906.5 - 896.5	55 SMW
c*	LO	*Neodenticula kamtschatica*	2.6 - 2.7	906.5 - 896.5	56 SMW
d*	FO	*Neodenticula koizumii*	3.5 - 3.9	936.5 - 926.5	59 SMW
e	FO	*Actinocyclus oculatus*	4.0	936.5 - 926.5	59 SMW
f	LO	*Thalassiosira praeoestrupii*	5.3	946.5 - 936.5	60 SMW
g*	FO	*Thalassiosira oestrupii* s.l.	5.5	1006.5 - 996.5	66 SMW
h	FO	*Thalassiosira praeoestrupii*	6.1	1066.5 - 1056.5	74 SMW
i	FCO	*Neodenticula kamtschatica*	6.4	1086.5 - 1076.5	79 SMW
k	LO	*Kisseleviella ezoensis*	~19.0	1096.5 - 1086.5	80 SMW
m	FO	*Kisseleviella ezoensis*	~24.0	1236.5 - 1226.5	97 SMW

Code number: (*) indicates primary biohorizons

Neodenticula kamtschatica-Nitzschia rolandii NPD Zone 7Ba, is recognized between samples 80-SMW and 79-SMW at 1086.5 m MSF. This age assignment in 80-SMW is based almost solely on the marker species *Kisseleviella ezoensis. Kisseleviella carina* is also present, and although it isn't a marker species, it has a reliable biostratigraphic range from the Late Oligocene through the Early Miocene. In at least one sample, 97-SMW at the base of Unit I, *K. carina* is the only biostratigraphically useful and identifiable species present and may be indicative of an older age, perhaps NPD Zone 1.

Unfortunately, several samples between 79-SMW and 61-SMW were unsuitable for biostratigraphic investigation, offering only a rough progression through time. 79- through 74-SMW (1086.5-1056.5 m MSF) are assigned to NPD Zone 7Ba based on the common occurrence of *N. kamtschatica* and the absence of *T. oestrupii.* A specimen and fragments of *Thalassionema schraderi* and *Rouxia* spp., respectively, were observed, but are considered reworked because *T. schraderi* should not occur in this zone (Yanagisawa and Akiba, 1998), and *Rouxia* spp. fragments could not be identified to the species level due to fragmentation.

The first common occurrence (FCO) of *N. kamtschatica* is observed in 66-SMW (996.5 - 1006.5 m MSF). Along with the co-occurrences of *T. oestrupii* and *T. preaoestrupii*, this sample interval is the closest representation of the Miocene/Pliocene boundary in this hole.

Samples 66-SMW through 60-SMW are assigned to the Early Pliocene *Thalassisira oestrupii* NPD Zone 7Bb, with the exception of 61-SMW, based primarily on the abundant occurrence of *N. kamtschatica* with *T. oestrupii* and *Thalassiosira*

preaoestrupii. Sample 61-SMW yielded diatoms that range from the Late Miocene to the Late Pliocene, including species from genera *Denticulopsis* and *Neodenticula.*

The *Neodenticula koizumii-Nedenticula kamtschatica* NPD Zone 8 is represented by samples 59-SMW through 56-SMW, based on the co-occurrences of *N. koizumii* and *N. kamtschatica*. In samples 57-SMW and 56-SMW, however, *N. seminae* co-occurred with *N. kamtschatica.* The ranges of these two species are not believed to overlap, although, the FO of *N. seminae* has been documented to coincide with the LO of *N. kamtschatica* at ODP Leg 127 sites in the Japan Sea and at ODP Leg 145 sites in the North Pacific. These two species are very similar in valve morphology, and it is possible that the apparent diachroneity of the FO of *N. seminae* is a result of misidentification as suggested by Yanagisawa and Akiba (1998). In this particular case, however, the co-occurrence of *N. seminae* is considered to be an effect of downhole contamination.

Fragments from the genus *Denticulopsis* were observed in samples 58-SMW and 57-SMW. This genus existed through the Middle and Late Miocene, however, so these fragments are considered reworked here.

Samples 55-SMW through 28-SMW (896.5 - 676.5 m MSF) represent the Late Pliocene *Neodenticula koizumii* NPD Zone 9. These samples have virtually the same assemblage as that defining NPD Zone 10, but now include *N. koizumii.* The absence of *N. kamtschatica* from these samples further supports this age.

Samples 27- through 24-SMW (676.5-636.5-m MSF), the uppermost sediments recovered from Hole C0020A, are Late Pleistocene in age and are assigned to the *Actinocyclus oculatus* NPD Zone 10, based on the presence of *A. oculatus* and *N. seminae*. This age is further supported by the absence of *N. koizumii.*

5. Discussion

A two-dimensional seismic profile was produced for Site C0020A (Fig. 2.2) (Inagaki et al., 2010). Integrated with data from regional industry wells, a preliminary geologic age model was produced, and regional geologic features were identified to a depth of 2200 mbsf. New marine microfossil data presented herein revise the age of this profile. Results from the diatom assemblages reported here update those published in the IODP Expedition 337 Initial Results (Expedition 337 Scientist, 2013); misidentifications and downhole contamination caused much confusion in the diatom shipboard results. The age is revised from Late Pliocene at the top Hole C0020A (636.5 m MSF) to Early Pleistocene. Revisions to the age of seismic reflectors, stratigraphic boundaries, regional unconformities, and ultimately, of the target coalbed interval are presented on Figures 2.4a and 2.4b.

Three major stratigraphic boundaries are identified based on diatom assemblages in Unit I: 1) an unconformity between Late and Early Miocene sediments at approximately 1086.5 m MSF, between samples 80- and 79-SMW; 2) a disconformity between samples 60- and 59-SMW (NPD Zones 8 and 7Bb) at ~936.5 m MSF; and 3) the Pliocene/Pleistocene boundary between samples 28- and 27-SMW at approximately 676.5 m MSF (Fig. 2.3).

Hiatuses of varying magnitude of Middle Miocene sediments have been recognized in several deep ocean drilling cores and on-land sequences around northeastern Honshu and Hokkaido (Akiba, 1986). Akiba (1986) recognized a hiatus of Middle Miocene sediments in DSDP Hole 584 and correlated it with one in Hole 438A.

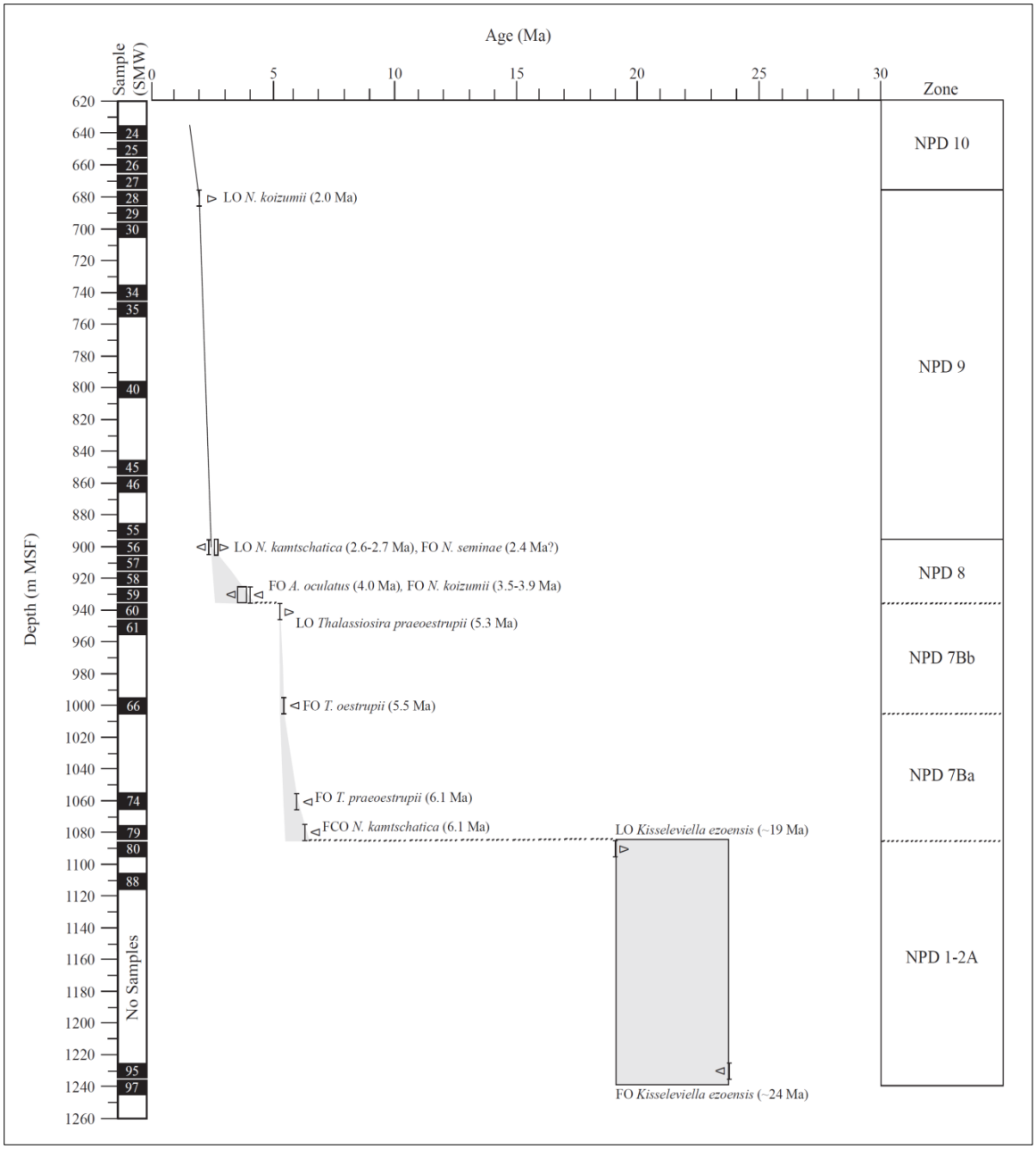

Figure 2.3. Time/depth plot and sediment accumulation rate curve showing diatom biostratigraphy through Hole C0020A Unit 1 (636.5 - 1236.5 m MSF). The column on the left beside depth, indicates which samples were used for biostratigraphic analysis. Diatom biohorizons are correlated to North Pacific Diatom (NPD) Zones on the right. The gradient through NPD 7-7Bb indicates that some biohorizons separating each subzone are inferred due to missing samples.

Both of these holes are located within approximately 150 km of Hole C0020A to the southeast near the Nankai Trough and Japan Trench.

What was predicted to be the Miocene/Pliocene boundary at 1100 m in Hole C0020A actually proved to be an unconformity representing between 2-15 m.y. between Early and Late Miocene sediments. Toward the east-center margin of the 2-D seismic profile (Inagaki, 2010), a package of eastward down-dipping reflection events below ~1100 m and 2.7 two-way travel time (TWT) is truncated and overlain by a succession of continuous reflections offering a visual explanation for the missing Middle and early Late Miocene sediments (Figs. 2.4a, 2.4b). This event was identified by the diatom biostratigraphy at ~1086.5 m MSF between samples 80- and 79-SMW.

A hiatus representing ~1.3-1.8 m.y between NPD Zones 8 (Late Pliocene) and 7Bb (Early Pliocene) was first recognized LO of *T. preaoestrupii* (5.3 Ma) in sample 60-SMW and the FO of *N. koizumii* (3.5-3.9 Ma) in sample 59-SMW around 936.5 m MSF. This disconformity is likely the effect of an erosional event, and it is represented by a low-amplitude reflection event on the seismic profile (Fig. 2.4b). Close examination of the seismic profile shows that this disconformity occurs with the first series of reflections overlaying the Miocene unconformity, which appear to be onlapping against the low-dipping unconformity boundary toward the west at ~2.7 TWT.

An integrated age model for the entire stratigraphic section drilled at Site C9001/C0020 is presented in Figure 2.5 and includes the results presented here for Hole C0020A, as well as those produced by Domitsu et al. (2010) for the overlying section in holes C9001C and C9001D and the underlying section to the total depth, which is

constrained by palynomorphs documented by Guy Harrington (Expedition 337 Scientist, 2013).

6. Conclusions

The diatom biostratigraphy of Hole C0020A presented herein yields a smooth continuation of Early Pleistocene sediments from the base of Hole C9001D (Domitsu et al., 2010) through the top of Hole C0020A (636.5 m MSF) and suggests an Early Miocene age at the base of Unit I (1246.5 m MSF) where diatoms cease to be preserved. Palynological investigations suggest an age of Late Oligocene-Early Miocene at the bottom of Hole C0020A (2466 m MSF) (Expedition 337 Scientists, 2013).

Diatoms were the most useful and most abundant microfossil group present in the upper section of Hole C0020A. In addition to successfully constraining geologic age in Unit 1, and despite many challenges due to downhole and drilling mud contamination, diatom assemblages in conjunction with the seismic profile produced for Site C0020 were successful in adjusting ages of seismic reflectors.

The target coalbed intervals for this Expedition were originally predicted to be Eocene in age, but micropaleontological investigations revealed an unexpectedly thick section of Early Miocene sediments extending from at least the base of Unit III (2046.5 m MSF), and maybe even the base of the hole (2466 m MSF), up to 1086.5 m MSF (Expedition 337 Scientists, 2013). A hiatus spanning 12-15 m.y. occurs between the Early Miocene and latest Miocene. The remaining upper Miocene sediments in this hole are only about 30 m thick. The Pliocene sediments are approximately 330 meters thick

and Pleistocene sediments compose the upper ~676 meters of sediment. Therefore, sediment accumulation rates at Site C9001/C0020 for the Late Miocene to Pleistocene was ~300 m/m.y. Most of the coalbeds, if not all, recovered from Hole C0020A are of Early Miocene age.

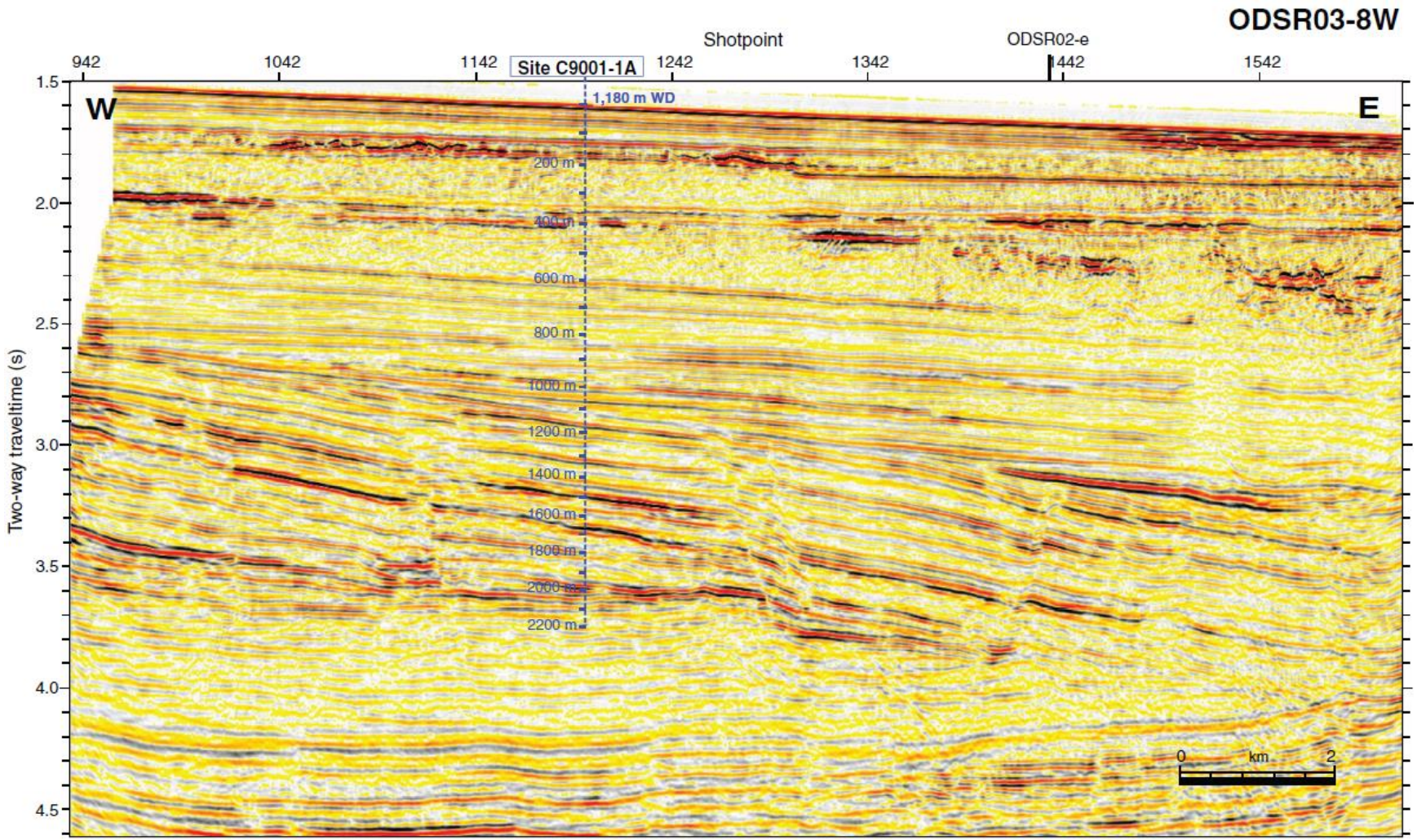

Figure 2.4a. Original seismic line ODSR03-8W and profile produced for Site C9001/C0020 (from Inagaki et al., 2010).

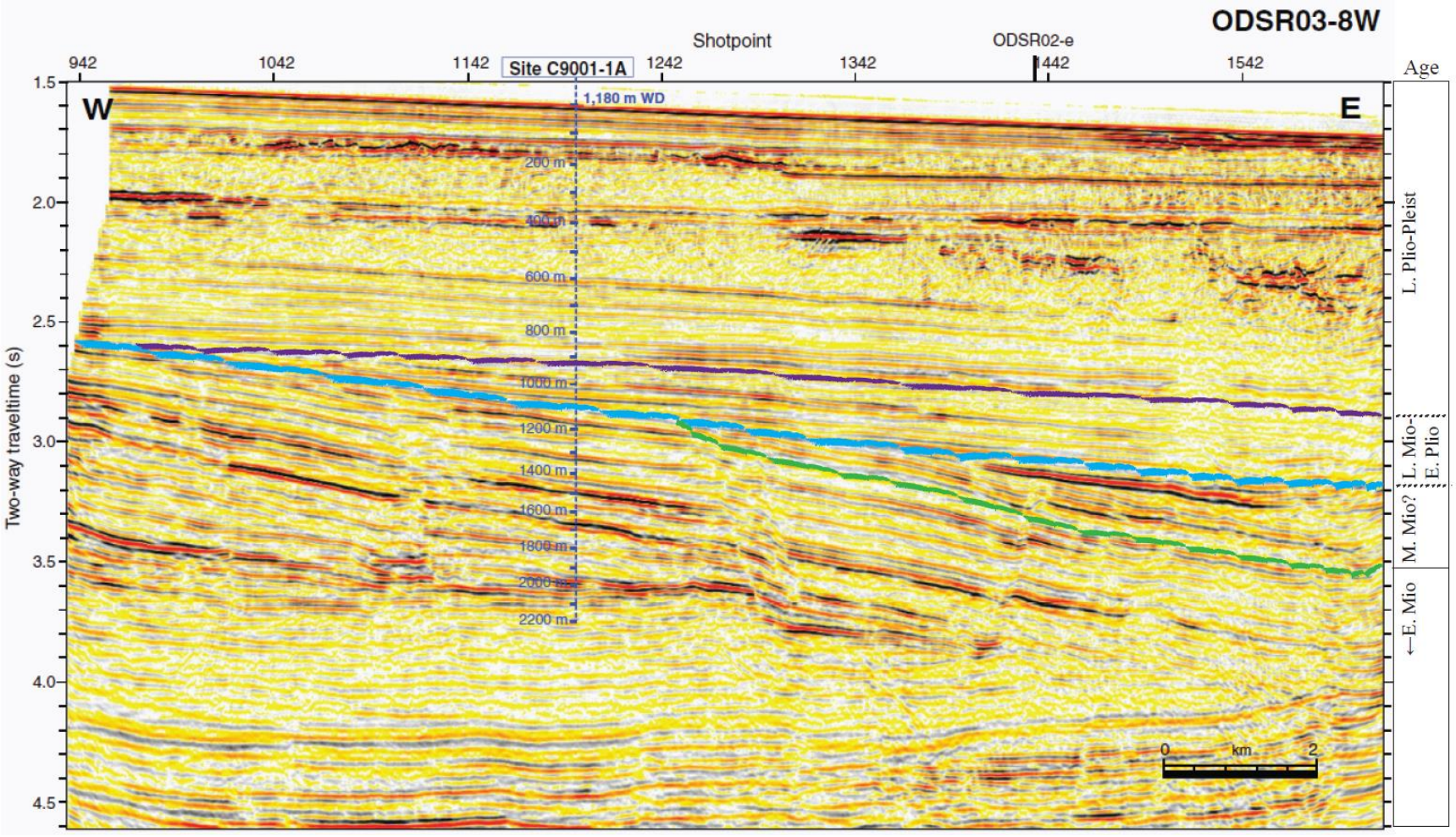

Figure 2.4b. Seismic Profile reinterpreting stratigraphic boundaries and ages based on diatom biostratigraphy. The green line outlines a package of east-ward down-dipping reflection events truncating up against the Early Miocene/Late Miocene unconformity (blue line). The Pliocene disconformity (purple line) bounds onlapping reflections between it and the unconformity (after Inagaki et al., 2010).

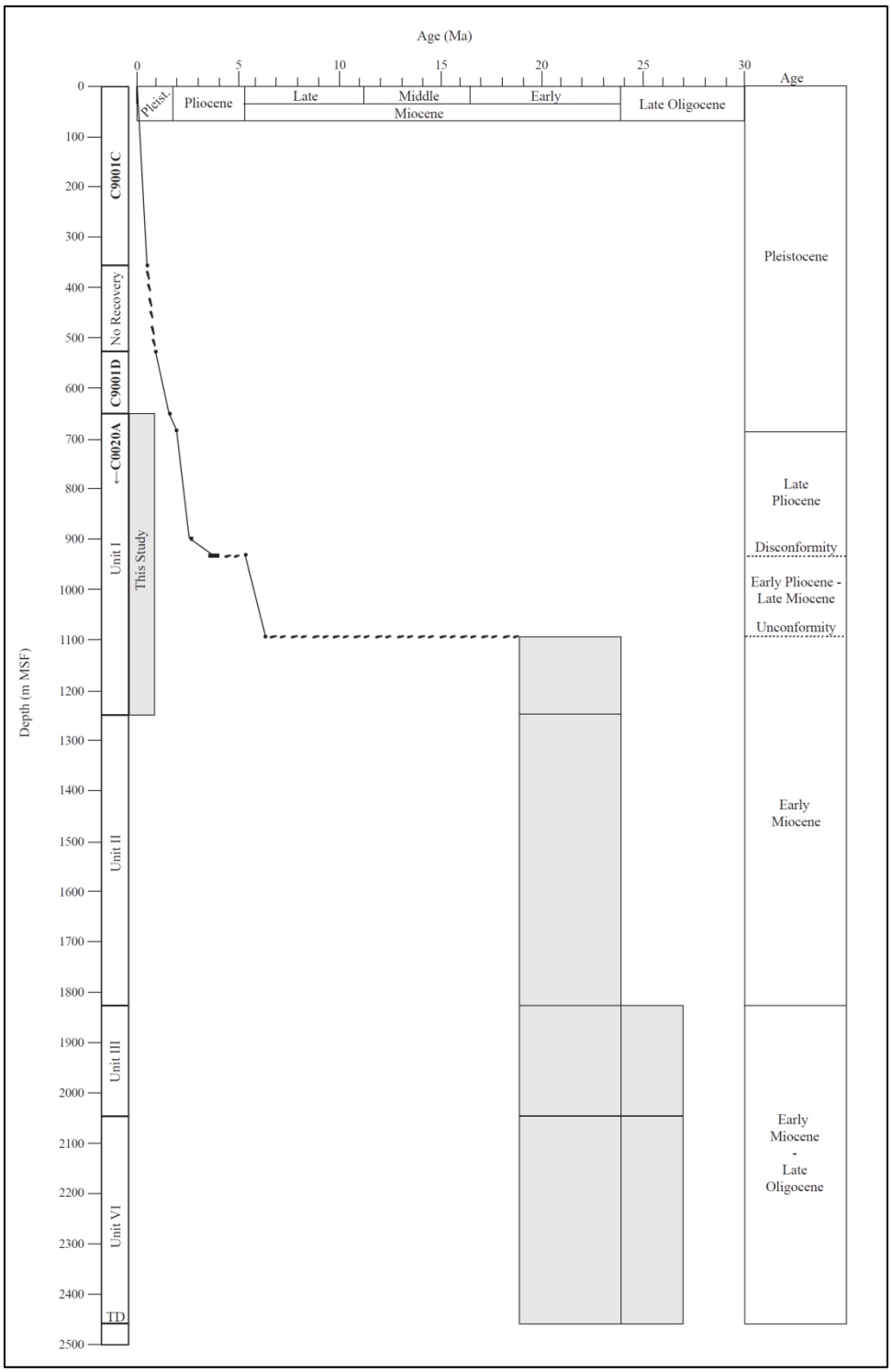

Figure 2.4. Integrated time/depth plot and accumulation rate curve based on the biostratigraphy for Site C9001/C0020A (0-2466 mbsf). Column next depth indicates the Hole and/or unit from which age was determined. Geologic eras are indicated along the x-axis and right-side column.

7. Floral List

Taxonomic references to diatom taxa tabulated in Hole C0020A are listed below in alphabetical order. Chief references utilized in this study for species identification include Akiba (1986), Akiba and Yanagisawa (1986) and Schrader (1973a). The reader should also refer to the listed author reference for the original taxon description.

Actinocyclus oculatus Jousé 1968
Denticulopsis Simonsen 1979
Denticulopsis hustedtii (Simonsen ex Kanaya) Simonsen
Denticulopsis katayamae Maruyama 1984
Kisseleviella carina Sheshukova-Poretzkaya 1962
Kisseleviella ezoensis Akiba 1986
Neodenticula koizumii Akiba & Yanagisawa 1986
Neodenticula kamtschatica (Zabelina) Akiba & Yanagisawa 1986
Neodenticula seminae (Simonsen & Kanaya) Akiba & Yanagisawa 1986
Rouxia Brun & Héribaud-Joseph *in* Héribaud 1893 spp.
Thalassionema schraderi Akiba 1982a
Thalassiosira oestrupii (Ostenfeld) Hasle 1972
Thalassiosira praeoestrupii Dumont, Baldauf & Barron 1986

PLATE

Plate 2.1. Diatom marker species used to constrain the age of Unit I of Hole C0020A.

1. *Neodenticula seminae* (Simonsen & Kanaya) Akiba & Yanagisawa 1986
2. *Actinocyclus oculatus* Jousé 1968
3. *Neodenticula koizumii* Akiba & Yanagisawa 1986
4. *Neodenticula kamtschatica* (Zabelina) Akiba & Yanagisawa 1986
5. *Kisseleviella ezoensis* Akiba 1986
6. *Thalassiosira preaoestrupii* Dumont, Baldauf & Barron 1986
7. *Thalassiosira oestrupii* (Ostenfeld) Hasle 1972

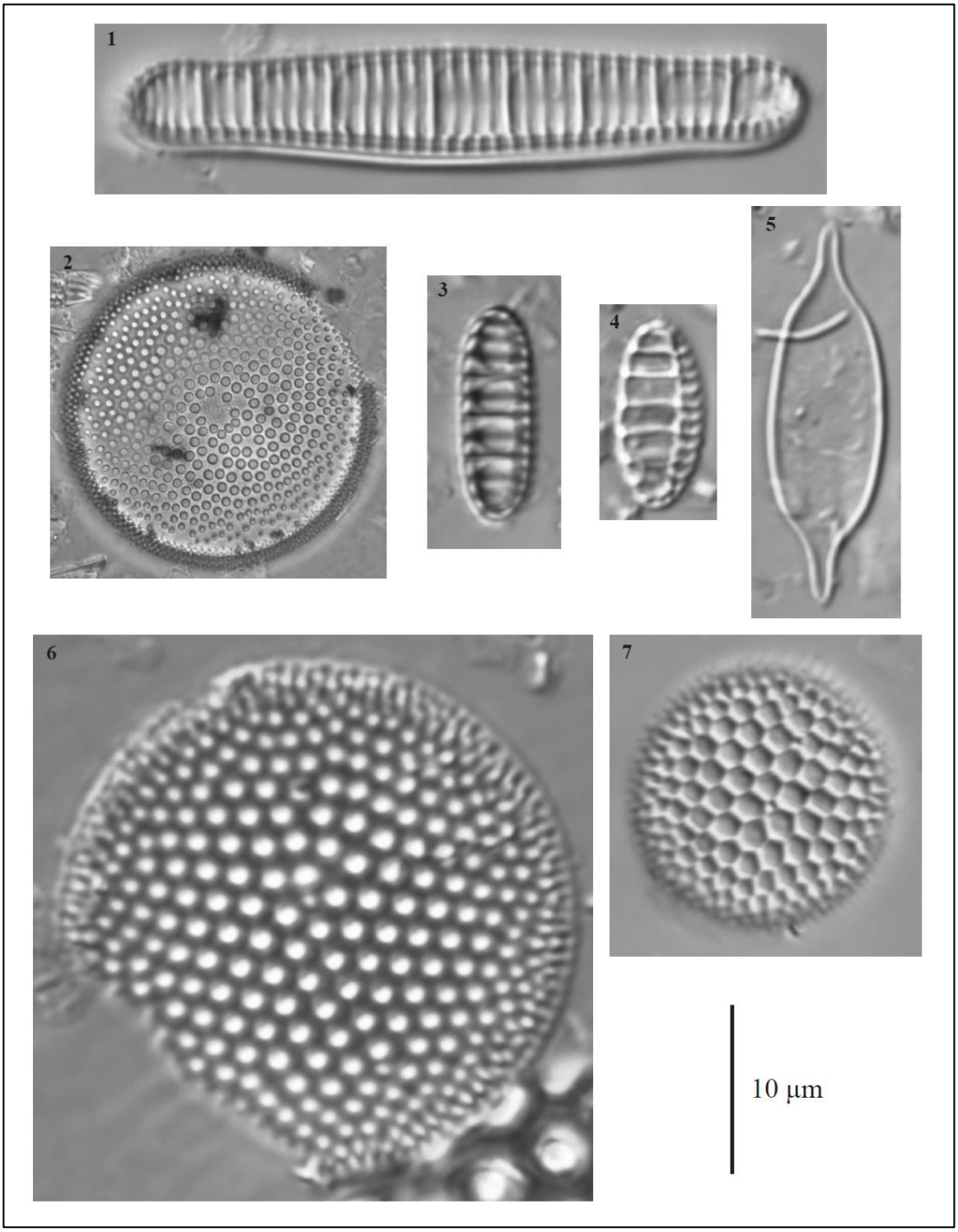
1
2
3
4
5
6
7
10 µm

REFERENCES

Akiba, F., 1986. Middle Miocene to Quaternary diatom biostratigraphy in the Nankai trough and Japan trench, and modified lower Miocene through Quaternary diatom zones for middle-to-high latitudes of the North Pacific. *In* Kagami, H., Karig, D.E., Coulbourn, W.T., et al., *Init. Repts. DSDP,* 87: Washington (U.S. Govt. Printing Office), 393-481.

Akiba, F., and Yanagisawa, Y., 1986. Taxonomy, Morphology and Phylogeny of the Neogene Diatom Zonal Marker Species in the Middle-to-High Latitudes of the North Pacific. *In* Kagami, H., Karig, D.E., Coulbourn, W.T., et al., *Init. Repts. DSDP,* 87: Washington (U.S. Govt. Printing Office), 483-554.

Aoike, K., Nishi, H., Sakamato, T., Iijima, K., Tsuchiya, M., Taira, A., Kuramato, S., Masago, H., and Shimokita Core Research Group, 2010. Paleoceanographic history of offshore Shimokita Peninsula for the past 800,000 years based on primary analyses on cores recovered by *D/V Chikyu* during the shakedown cruises. *The Palaeontological Society of Japan,* Vol. 87, p. 65-81.

Aoike, K. (Ed.), 2007. CDEX Laboratory Operation Report: CK06-06 D/V *Ckikyu* Shakedown Cruise Offshore Shimokita: *Yokohama (CDEX-JAMSTEC).* http://sio7.jamstec.go.jp/JAMSTEC-exp-report/902/CK06-06_CR.pdf

Barron, J.A. and Baldauf, J.G., 1995. Cenozoic marine diatom biostratigraphy and applications to palaeoclimatology and palaeoceanography. *In* Blome, C.D., et al., *Siliceous Microfossils, Paleontological Soc. Short Courses in Paleontology,* Vol. 8, p. 107-118.

Barron, J.A., Bukry, D., Dean, W.E., Addison, J.A., Finney, B., 2009. Paleoceanography of the Gulf of Alaska during the past 15,000 years: Results from diatoms, silicoflagellates, and geochemistry. *Marine Micropaleontology,* Vol. 72, p. 176-195.

Berger, A. and Loutre M.F., 2003. Climate 400,000 years ago, a key to the future? *In* Droxler, A., Burckle, L., and Poore, A. (eds), Earth climate and orbital eccentricity: the marine isotope stage 11 question. *Geophysical monograph* 137, American geophysical union, Washington, p. 17-26.

Cande, S.C. and Kent, D.V., 1995. Revised calibration of geomagnetic polarity time scale for the Late Cretaceous and Cenozoic. *Jour. Geophy. Res.,* Vol. 100, p. 6093-6095.

Chang, Y., 1967. Accuracy of Fossil Percentage Estimation. *Journal of Paleontology,* Vol. 41, No. 2, p. 500-502.

Crosta, Xavier and Koç, Nalan, 2007. Diatoms: From Micropaleontology to Isotope Geochemistry, *In* Hillaire-Marcel, C., and De Vernal, A. (Eds.) *Developments in Marine Geology, Proxies in Late Cenozoic Paleoceanography,* Vol 1, p. 327-358.

Domitsu, H., Nishi, H., Uchida, J., Oda, M., Ogane, K., Taira, A., and Aoike, K., 2010. Age model of core sediments taken by D/V CHIKYU during the shakedown cruises off Shimokita Peninsula, *The Palaeontological Society of Japan,* Vol. 87, p. 47-64.

Donahue, J.G., 1970. Pleistocene diatoms as climate indicators in North Pacific sediments. *In* Hays, J.D., (Ed.), *Geological investigation of the North Pacific, Mem. Geol. Soc. Am.,* no. 126, 121-138.

Expedition 337 Scientists, 2013. Expedition 337 Summary. *In* Inagaki, F., Hinrichs, K.-U., Kubo, Y., and the Expedition 337 Scientists, *Proc. IODP,* 337: Tokyo (Integrated Ocean Drilling Program Management International, Inc.). doi:10.2204/iodp.proc.337.101.2013.

Expedition 337 Scientists, 2013. Expedition 337 Summary. *In* Inagaki, F., Hinrichs, K.-U., Kubo, Y., and the Expedition 337 Scientists, *Proc. IODP,* 337: Tokyo (Integrated Ocean Drilling Program Management International, Inc.). doi:10.2204/iodp.proc.337.102.2013.

Expedition 337 Scientists, 2013. Site C0020. *In* Inagaki, F., Hinrichs, K.-U., Kubo, Y., and the Expedition 337 Scientists, *Proc. IODP,* 337: Tokyo (Integrated Ocean Drilling Program Management International, Inc.). doi:10.2204/iodp.proc.337.103.2013.

Fryxell, G.A., 1986. Polymorphism in Relation to Environmental Conditions as Exemplified by Clonal Cultures of *Thalassiosira tumida* (Janisch) Hasle. *9th Diatom Symposium,* p. 61-73.

Gersonde, R., 1990. The Paleontological Significance of Fossil Diatoms from the High-Latitude Oceans, *In* Medlin, L. and Priddle, J. (Eds.) *Polar Marine Diatoms,* p. 57-63.

Gladenkov, A.Y., and Barron, J.A., 1995. Oligocene and early Middle Miocene diatom biostratigraphy of Hole 884B. *In* Rea, D.K., Basov, I.A., Scholl, D.W. and Allan, J.F., (Eds.), *Proc. Ocean Drilling Program, Scie. Results,* College Station TX (Ocean Drilling Program), Vol. 145, p. 21-41.

Hasle, G.R., Medlin, L.K., Syvertsen, E.E., 1994. *Synedropsis* gen. nov., a genus of araphid diatoms associated with sea-ice. *Phycologia,* Vol. 33 (4), p. 248-270.

Hasle, G.R., 1983. *Thalassiosira punctigera* (Castr.) comb. nov., a widely distributed marine planktonic diatom. *Nordic Journal of Botany,* Vol. 3, p. 593-608.

Hasle, G.R., and Fryxell, G.A., 1977. The genus *Thalassiosira:* species with a linear areolae array. *Nova Hedwigia (Beih.),* Vol. 54, p. 15-66.

Howard, W.R., 1997.. A warm future in the past. *Nature*, Vol. 388, p. 418-419.

Inagaki, F., Hinrichs, K.-U., Kubo, Y., and the Expedition 337 Project Team, 2010. Deep coalbed biosphere off Shimokita: microbial processes and hydrocarbon system associated with deeply buried coalbed in the ocean. *IODP Sci. Prosp.,* 337. doi:10.2204/iodp.sp.337.2010.

Kanaya, T., Koizumi, I., 1966. Interpretation of Diatom Thanatocoenoses from the North Pacific Applied to a Study of Core V20-130 (Studies of a Deep-sea Core V20-130. Part IV). *The Science Reports of the Tohoku University,* Vol. 37, No. 2, p. 89-130.

Koizumi, I., 2008. Diatom-derived SSTs (*Td'* ratio) indicate warm seas off Japan during the middle Holocene (8.2-3.3 kyr BP). *Marine Micropaleontology,* Vol. 69, p. 263-281.

Koizumi, I., 1992. Diatom biostratigraphy of the Japan Sea: Leg 127. *In* Ingle, J.C., Jr., von Breymann, M.T., Barron, J., et al., (Eds.) *Proc. ODP, Sci Res.* College Station, TX (Ocean Drilling Program). Vol 127/128, pt. 1, p. 249-289.

Koizumi, I., 1973a. The stratigraphic ranges of marine planktonic diatoms and diatom biostratigraphy in Japan. *Mem. Geol. Soc. Japan,* no. 8, p. 35-44.

Koizumi, I., 1973b. The Late Cenozoic diatoms of Sites 183-193, Leg 19, Deep Sea Drilling Project. *In.* Creager, J.S., Scholl, D.W., et al., *Init. Repts. Deep Sea Drilling Project,* U.S. Govt. Printing Office, Washington D.C., Vol. 19, p. 805-855.

Koizumi, I., 1972. Marine diatom flora of the Pliocene Tatsunokuchi Formation in Fukushima Prefecture, northeast Japan. *Trans. Proc. Paleontol. Soc. Jpn.*, No. 86, p. 340-359.

Koizumi, I., 1968. Tertiary Diatom Flora of Oga Peninsula, Akita Prefecture, Northeast Japan. *The Science Reports of the Tohoku University,* Vol. 40, No. 3, p. 171-240.

Koizumi, I. And Yamamoto, H., 2008. Paleohydrography of the Kuroshio Extension in the Tohoku Area based on fossil diatoms. *JAMSTEC Report of Research and Development,* Vol. 7, p. 1-10.

Koizumi, I., Tada, R., Narita, H., Irino, T., Aramaki, T., Oba, T., and Yamamoto, M., 2006. Paleoceanographic history around the Tsugaru Strait between the Japan Sea and the Northwest Pacific Ocean since 30 cal kyr BP. *Palaeogeography, Palaeoclimatology, Palaeoecology,* Vol. 232, p. 36-52.

Koizumi, I., Irino, T., Oba, T., 2004. Paleoceanography during the last 150 kyr off central Japan based on diatom floras. *Marine Micropaleontology,* Vol. 53, p. 293-365.

Koizumi, I., and Sakamoto, T., 2003. Paleoceanography off Sanriku, northeast Japan, based on diatom flora. *In* Suyehiro, K., Sacks, I.S., Acton, G.D., and Oda, M. (Eds.), *Proc. ODP, Sci Results,* 186, 1-21 [Online].

Kuroyanagi, A.; Kawahata, H. and Ohkushi, K., 2006. Reconstruction of paleoceanographic changes based on the relationship between planktonic foraminiferal assemblages and water masses off Shimokita over the last 27,000 years, *The Palaeontological Society of Japan,* Vol. 79, p. 33-42.

Lisiecki, L. E. and Raymo, M. E., 2005. A Pliocene-Pleistocene stack of 57 globally distributed benthic $d^{18}O$ records. *Paleoceanography*, 20, PA1003, doi:10.1029/2004PA001071.

Maruyama, T., 1992. Diatom biometry of the Miocene index *Denticulopsis hyalina. In* Ishizaki, K. and Saito, T., (eds.), *Centenary of Japanese Micropaleontology,* Terra Scientific Publ., Tokyo, 427-437.

Maruyama, T., 1984. Miocene diatom biostratigraphy of onshore sequences on the Pacific side of northeast Japan, with reference to DSDP Hole 438A (Part 2). *Sci. Pepts. Tohoku Univ., Second Ser. (Geol.),* Vol. 55, p. 77-140.

Motoyama, I. And Maruyama, T., 1998. Neogene diatom and radiolarian biochronology for the middle-to-high latitudes of the Northwest Pacific region: Calibration to the Cande and Kent's geomagnetic polarity time scales (CK92 and CK95). *Jour. Geol. Soc. Japan,* Vol. 104, p. 171-183.

Rattray, J., 1890. A Revision of the genus *Coscinodiscus* and some allied genera. *Proceedings of the Royal Society of Edinburgh,* Vol 16.

Romero, O.E., and Armand, L.K., *In* Smol, J.P. and Stoermer (Eds.), 2010. Marine diatoms as indicators of modern changes in oceanographic conditions. *The Diatoms: Applications for the Environmental and Earth Sciences,* 2nd ed., p.373-400.

Sancetta, C., 1982. Distribution of Diatom Species in Surface Sediments of the Bering and Okhotsk Seas. *Micropaleontology,* Vol. 28, No. 3, p. 221-257.

Schrader, H.-J., 1973a, Cenozoic diatoms from the Northeast Pacific, Leg 18. *In* Kulmn, L. D., von Huene, R., et al., *Init. Repts. Deep Sea Drilling Project,* U.S. Govt. Printing Office, Washington D.C., Vol. 18, p. 673-797.

Schrader, H.-J., 1973b, Stratigraphic distribution of marine species of the diatom *Denticula* in Neogene North Pacific sediments. *Micropaleontology,* Vol. 19, p 417-430.

Schrader, H.-J., and Gersonde R., 1978. Diatoms and Silicoflagellates. *Utrecht Micropaleontological Bulletins,* Issue 17, p. 129-176.

Sheshukova-Poretskaya, V.S., 1964. New and rare diatoms in the Neogene of Sakhalin and Kamchatka. *Akad. Nauk SSSR, Bot. Inst., Novitates Systematicae Plantaru non Vaschularum* 10, p. 69-72 (in Russian with English abstract).

Simonsen, R., 1979. The diatom system: idea on phylogeny. *Bacillaria,* Vol. 2, p. 9-71.

Simonsen, R. and Kanaya, T., 1961. Notes on the marine species of the diatom genus *Denticula* Kütz. *Internat. Revue Gesam. Hydrobiol.,* Vol. 46, p. 498-513.

Tomas, C. (Ed.), 1996. Identifying Marine Diatoms and Dinoflagellates. Academic Press, Inc., San Diego, CA.

Winter, D., Arney, J., Wise, S.W., 2004. Upper Miocene-Pleistocene Diatom Biostratigraphy in the Northwest Pacific, ODP Leg 191. *Proceedings of the Ocean drilling Program, Scientific Results,* Vol. 191.

Witkowski, J., Bohaty, S., McCartney, K., Harwood, D., 2012. Enhanced siliceous plankton productivity in response to middle Eocene warming at Southern Ocean ODP Sites 748 and 749. *Palaeogeography, Palaeoclimatology, Palaeoecology,* Vol. 326-328, p. 78-94.

Wood, M.A., Lande, R., Fryxell, G.A., 1987. Quantitative Genetic Analysis of Morphological Variation in an Antarctic Diatom Grown at Two Light Intensities. *Journal of Phycology,* Vol. 23, p. 42-54.

Yanagisawa, Y., and Akiba, F., 1998. Refined Neogene diatom biostratigraphy for the northwest Pacific around Japan, with an introduction of code numbers for selected diatom biohorizons. *Journal of the Geological Society of Japan.* 104:395–414.

Yin, Q.Z, and Berger, A., 2012. Individual contribution of insolation and CO_2 to the interglacial climates of the past 800,000 years. *Climate Dynamics*, Vol. 38, p. 709-724. DOI 10.1007/s00382-011-1013-5.

APPENDICES

Table A1. Diatom count data for all samples from Hole C9001C.

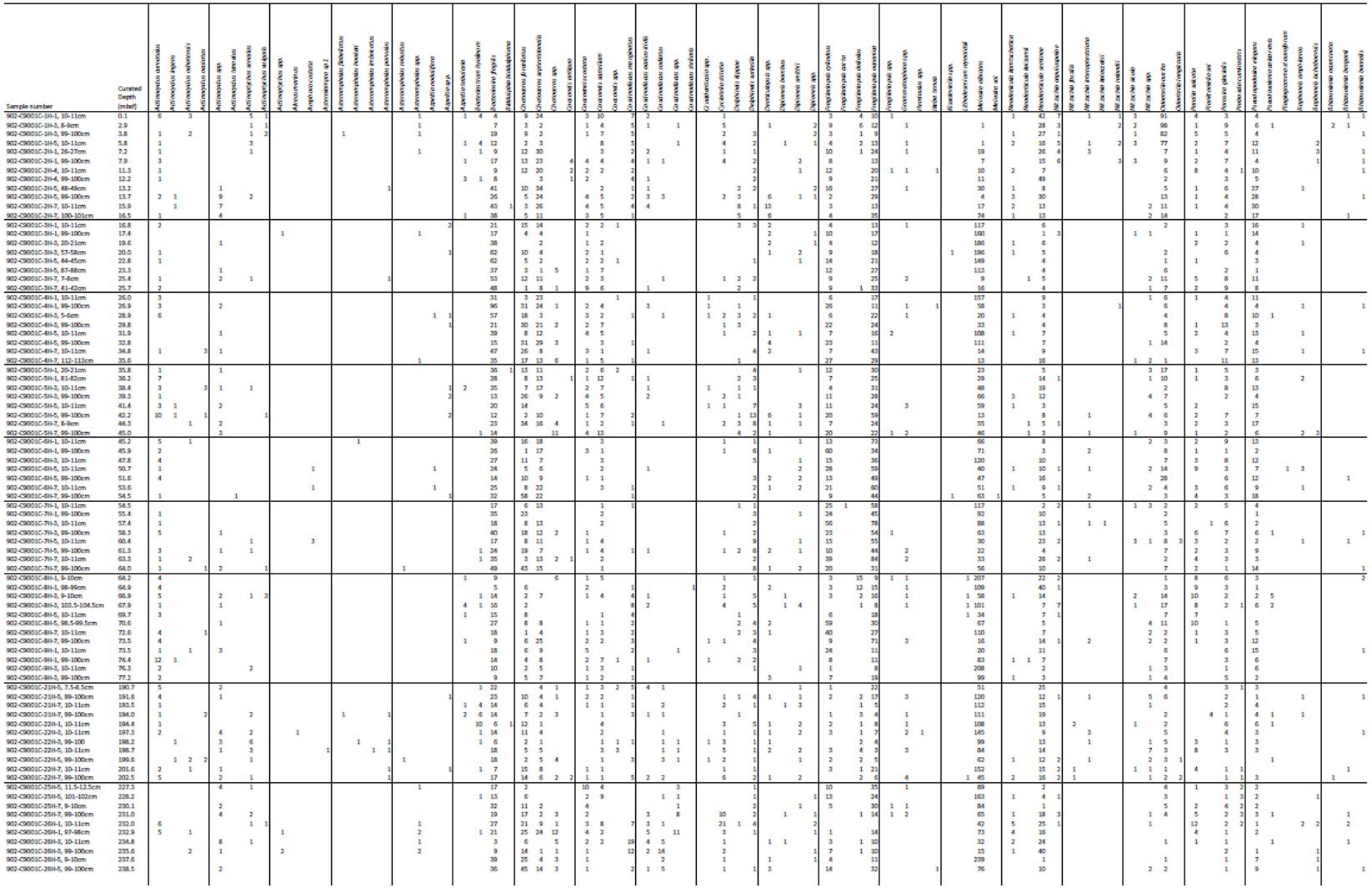

Table A1 (continued).

Sample number	Curated Depth (mbsf)	Rhizosolenia hebetata f. hiemalis	Rhizosolenia hebetata f. semispina	Rhizosolenia setigera	Rhizosolenia spp.	Rhizosolenia styliformis	Roperia tesselata	Stephanopyxis turris	Synedropsis recta	Synedropsis [illegible]	Terpsinoe spp.	Thalassionema bacillaris	Thalassionema frauenfeldii	Thalassionema nitzschioides	Thalassionema spp.	Thalassiosira antarctica	Thalassiosira sp. A	Thalassiosira sp. B	Thalassiosira decipiens	Thalassiosira eccentrica	Thalassiosira ferelineata	Thalassiosira gravida	Thalassiosira hyalina	Thalassiosira jouseae	Thalassiosira kryophila	Thalassiosira leptopus	Thalassiosira lineata	Thalassiosira [illegible]	Thalassiosira [illegible]	Thalassiosira nidulus	Thalassiosira nordenskioeldii	Thalassiosira oestrupii	Thalassiosira pacifica	Thalassiosira punctigera	Thalassiosira spp.	Thalassiosira trifulta	Thalassiothrix longissima	Total valves counted
902-C9001C-1H-1, 10-11cm	0.1	2	1	1	3	2						8		96		11				18		1	4			1	15	7			12	4		1	10	2	1	458
902-C9001C-1H-3, 8-9cm	2.9			2		2		2			5	4		101		25				20	1	7	9				15	1			83	2		2	15	8		521
902-C9001C-1H-3, 99-100cm	3.8	1	2	8	4	6					5	8		133		19				24	3	5					19	4			25	6			13	6	2	491
902-C9001C-1H-5, 10-11cm	5.8	2	6		4	4		1			6	10		129	1	8			2	14		10	5				10	3			43	5			10	5	2	478
902-C9001C-2H-1, 26-27cm	7.2		3	1		2					4	5		113		15			8	43		11	49				20	1			107	1			10	8	2	582
902-C9001C-2H-1, 99-100cm	7.9			6	4	2		6			5	8		82		11			5	31		5	32				22				60	1		1	21	12		476
902-C9001C-2H-4, 10-11cm	11.3			4		2		2			2			56		43				32		3	32			33	12	5			97	2			15	9		486
902-C9001C-2H-4, 99-100cm	12.2	1	1	6	2	6		7			5			91		29				52	4	21	12			13	22	2			31				19	16	2	468
902-C9001C-2H-5, 48-49cm	13.2	1	1	1	1	1					11	1		39		54			1	41	1	22	23	1		1	8				14				10	18	1	481
902-C9001C-2H-5, 99-100cm	13.7	1				3		14	9		14			36		74			1	22	1	39	14				8	3			2				12	52	2	521
902-C9001C-2H-7, 10-11cm	15.9				1	3		10	5		14			19		37			3	39	2	52	34	2			7	3			28	1			10	25	1	512
902-C9001C-2H-7, 100-101cm	16.5		1		2	7		1	1		18	1		26		12			2	49	1	55	10			1		1			30				4	8	2	475
902-C9001C-3H-1, 10-11cm	16.8							4			6			20		3			2	8		48	11			1	10				103				5	6		457
902-C9001C-3H-1, 99-100cm	17.4		2			2			1		10			18		10			16	16		38	25				1	1			74				4	5	1	464
902-C9001C-3H-3, 20-21cm	19.6			1				1			6			50		7	2		22	16		13	23				3				40				5	5		459
902-C9001C-3H-3, 57-58cm	20.0							2	13		8			23		10	8		8	4	1	10	6			2					30				9	3	1	464
902-C9001C-3H-5, 44-45cm	22.8		1					2	3		4			40		12	11		9	12	1	9	11			3	5				55				10		2	460
902-C9001C-3H-5, 87-88cm	23.3	1		1	1	2		2	2		7			51		16	5		7	20		14	45			5	2				80				6	7		494
902-C9001C-3H-7, 7-8cm	25.4	1	1					5	1		13	1		58		41	5		8	10		11	23			1	27				48				16	9	2	461
902-C9001C-3H-7, 41-42cm	25.7				1	1		6	1		4			65	1	29			3	23		19	45			1	14	1			66				8	7	2	465
902-C9001C-4H-1, 10-11cm	26.0					3		2	3		10	1	1	26		12	2		3	11		20	24			1	11				44				13	7	1	470
902-C9001C-4H-1, 99-100cm	26.9							2	4		14			47		14			4	15		21	69			3	9				47						1	535
902-C9001C-4H-3, 5-6cm	28.9		1			1			6		12			86		13	7		9	10		18	19			2	20				59	1			14	8	1	466
902-C9001C-4H-3, 99-100cm	29.8				1				1		14	1		74		11	5		2	7		31	59			1	7	3			82	2			4	5	1	507
902-C9001C-4H-5, 10-11cm	31.9					1		1	9		14			72		18	4		3	1		16	45				2				29				4	1	1	461
902-C9001C-4H-5, 99-100cm	32.8								10		12	1		75		14	4		4	12		10	66			2	8				63				4	6		550
902-C9001C-4H-7, 10-11cm	34.8		1			4		5			4	1	2	81		34	26		5			11	20			2	20				45				11	8	1	478
902-C9001C-4H-7, 112-113cm	35.6		1			1		5			6	2		105		16	4			13		10	23				2	1			103	3				9	1	498
902-C9001C-5H-1, 20-21cm	35.8	1	1					1	3		12			96		10	12		5	4		25	24			1	13	2			50	1			11	11		460
902-C9001C-5H-1, 81-82cm	36.2	1	3	2		1		8	2		15			96		20	3		2	15		17	29			2	11				56	3			14	8	2	486
902-C9001C-5H-3, 10-11cm	38.4	1				1			3		10		1	79		20	8		10	19		24	28			3	34				53				9	8	1	520
902-C9001C-5H-3, 99-100cm	39.3	1						5	3		13			93		17	4		3	14		16	58			6	12	2			39				7	13	5	515
902-C9001C-5H-5, 10-11cm	41.4		2					4			16			64		14	1	1	8	5		16	17				19				89	1			4	4	1	452
902-C9001C-5H-5, 99-100cm	42.2	3						3	4		16	1		85	1	36				20		7	7				17	3			20	2			9	15	5	441
902-C9001C-5H-7, 8-9cm	44.3		1			1		2	6	3	27		1	57		4	2	3	4	7		4	60				7				43	1	1		6	3	1	462
902-C9001C-5H-7, 99-100cm	45.0		4			2		1	7		18			70	1	7			5	13		8	79				3	1			48				12	3	1	456
902-C9001C-6H-1, 10-11cm	45.2		1	1	1			1	5		10	2		40		8	1		4	1		10	36				10	1			46	1			5	8	1	468
902-C9001C-6H-1, 99-100cm	45.9			1		1		1	4		18	2		41		4			11	16		1	88				1		2		49				8			488
902-C9001C-6H-3, 10-11cm	47.8	1	2	3				3	4	4	4	1		49		9	7		3	6		4	38				4	1			41	1				9	1	464
902-C9001C-6H-5, 10-11cm	50.7	1	2			1		2			6	6		75		28			4	20		8	20				2				41	1			9	5	1	454
902-C9001C-6H-5, 99-100cm	51.6	1	4	4		3		1		3	6	6	1	89		23			5	8		14	13			3	8	1			25	3		2	10	10	1	458
902-C9001C-6H-7, 10-11cm	53.6	1		1		2		1	5		6	1		37		55	1			13		14	40				15				32	1			2	4	1	466
902-C9001C-6H-7, 99-100cm	54.5		1						2	6	5	1		44		50	3	4				6	41					1			23	2			4	1		465
902-C9001C-7H-1, 10-11cm	54.5		2			1		1			1	2		43		12	2		6	6		4	28				6				88				1	1		467
902-C9001C-7H-1, 99-100cm	55.4	2						2		19	5	1		38		31	1	5	1	5		10	30				6	1			69				1	4		470
902-C9001C-7H-3, 10-11cm	57.4			1				2	1		6			50		22	8			4		17	51				1				47			1	3	2	1	513
902-C9001C-7H-3, 99-100cm	58.3		5	1		1				4	3			39		21	9	2	1	3		10	20			1	2				66				5	11		464
902-C9001C-7H-5, 10-11cm	60.4		4	4	2	1					7	9		116		11				10		9	12				4	1			83	1			5	8	1	492
902-C9001C-7H-5, 99-100cm	61.3	2	1	6		5		6	9		13			92		105	2	1		5		11	7				6	2			12			1	6	6	1	477
902-C9001C-7H-7, 10-11cm	63.3		1	7		2			2		4	4		92		16	2			5		8	5				9	1			37	1		1	1	2		461
902-C9001C-7H-7, 99-100cm	64.0			1		2		2	16	1	4			54		26	2			5		8	25				2				31			1	5	6	1	459
902-C9001C-8H-1, 9-10cm	64.2	2	2	2	1	1		4			3	3		37		21			1	11		7	7				7				36	1				2		457
902-C9001C-8H-1, 98-99cm	64.9		2	11	1	3		8			5	4		83		12			2	13	1	4	5		2		9	2			59	3			4	11	2	466
902-C9001C-8H-3, 9-10cm	65.9	1	12	17	7	18		19			8	8		98	2	14			3	28		6	2		1	1	2	1			21	8				11	2	473
902-C9001C-8H-3, 103.5-104.5cm	67.9	2	8	4	2	13	1	4			6	11		118	1	30			13	37		6	6				6				8	13			9	15	4	529
902-C9001C-8H-5, 10-11cm	69.7		4	14		2		11	1		5	1		103		10			54	40		16	10				2	1			34	1			7	19	1	450
902-C9001C-8H-5, 98.5-99.5cm	70.6		1			2		3	6		7			81		70			2	11		3	10				2				7	1			3	5		462
902-C9001C-8H-7, 10-11cm	72.6		2					4	5		9			63		45			10	29		8	42				7				32	1			3	7	1	505
902-C9001C-8H-7, 99-100cm	73.5		5	1		1		5	1					80		13			15	54		5	27	1			8				74		1		10	8	1	504
902-C9001C-9H-1, 10-11cm	73.5	1				1		21			5			61		27			6	28		11	23				8	2			92	1			12	16	3	461
902-C9001C-9H-1, 99-100cm	74.4		2			2		25	1		7	2		71		31			6	17		2	13				9	1			65				9	17	1	463
902-C9001C-9H-3, 10-11cm	76.3		1					50			5			51		25			20	14		6	11				4	3			17				5	4	1	475
902-C9001C-9H-3, 99-100cm	77.2	2						40	3		2	1		53		31			17	25		19	8	1			17	5			52				11	20	1	479
902-C9001C-21H-5, 7.5-8.5cm	190.7	1	10	2	1	5	2	12			2			46		80			2	11		3	2	26		2	26	6		2	17	5			15	16	3	459
902-C9001C-21H-5, 99-100cm	191.6		11	1	1	7		10			9	3		45		30	1		6	11		16	8	21			18			2	15	6			12	5	1	470
902-C9001C-21H-7, 10-11cm	193.5		9	1	3	5	1	13			5	3		34		28			4	23		17	3	28			52			1	19	7		2	7	6	1	454
902-C9001C-21H-7, 99-100cm	194.0		10	4	4	6	1	19			9	3		45		22			2	19		18	2	19			32			2	13	9		1	11	19	3	473
902-C9001C-22H-1, 10-11cm	194.4		6		1	5	4	23			16	3	3	65		12			5	8		13	2	20		1	30			1	15	6			10	11	4	461
902-C9001C-22H-3, 10-11cm	197.3		6	1		8		22	2		7	1	1	49		22			7	4		10	5	12			42	3			5	4			13	3	5	463
902-C9001C-22H-3, 99-100	198.2		8		3	12	1	21	1		9	1	3	41		20			9	11	1	6	3	13			77	1			19	7			11	5	1	449
902-C9001C-22H-5, 10-11cm	198.7	1	2		2	20	3	26			8	4	1	42		32			6	18		18	1	19			21				8	10			11	10	3	454
902-C9001C-22H-5, 99-100cm	199.6	3	7		2	8		22			7	2		54		34			3	18		20	8	24			79				17	5			14	10	2	482
902-C9001C-22H-7, 10-11cm	201.6		6		1	3		9			9	3		46	1	11			5	14		12	4	36			22	1		2	15	6			7	4	2	465
902-C9001C-22H-7, 99-100cm	202.5	1	2	1		4		41			16	3		44		26			3	15		17	5	20			51			4	16	8			10	10	1	460
902-C9001C-25H-5, 11.5-12.5cm	227.3		4	1		1		19	7		4	1		112		25			9	13		6	28	7				2			11				18	1	2	463
902-C9001C-25H-5, 101-102cm	228.2		2			1		6	13		9			79		16			24	10		4	19	17			1				25				16		1	494
902-C9001C-25H-7, 9-10cm	230.1		3			2		9	9		5			104		21			42	14		3	27	7				1			8				11	2	1	461
902-C9001C-25H-7, 99-100cm	231.0	2	5			8	1	16			18	6		57		40			2	25		19	7	17			1				6	3			9	11	2	454
902-C9001C-26H-1, 10-11cm	232.0	6	19	8	2	24		23			18	14		54		22			2	20		14	5	30			3	2			12	9			9	8	2	530
902-C9001C-26H-1, 97-98cm	232.9	4	13	1	1	22		13			6	9		41		49	1			31	1	11	3	26			8	1			28	14			11	4	4	536
902-C9001C-26H-3, 10-11cm	234.8		13	1		2		29			13	5		134	1	29				22		2	19	12			6				13	10			11	10		468
902-C9001C-26H-3, 99-100cm	235.6	3	17			8		51			3	2		139		17	1			28		4	5	4			11				5	3			11	15	5	474
902-C9001C-26H-5, 9-10cm	237.6							4	3		1			33		11			50	6	2		6	26			1				3				4	4		496
902-C9001C-26H-5, 99-100cm	238.5	1	4			2		10	3		5	2		62		58			14	14	3	1	10	94			1				2	3			5			557

Table A2. Tabulated calculations for each sample based on the diatom flora.

Sample	Curated Depth (mbsf)	Diatom Valves Counted	Total diatom abundance	Abundance (%) cold-water diatoms (*Xc*, XC)	Abundance (%) warm-water diatoms (*Xw*, XW)	*Td'*	Calculated SST (°C)
902-C9001C-1H-1, 10-11cm	0.1	458	2,781,273	24.0	5.9	19.7	14.8
902-C9001C-1H-3, 8-9cm	2.9	521	6,267,351	34.7	5.2	13.0	13.2
902-C9001C-1H-3, 99-100cm	3.8	491	3,581,665	23.8	5.9	19.9	14.9
902-C9001C-1H-5, 10-11cm	5.8	478	2,849,003	26.2	5.2	16.7	14.2
902-C9001C-2H-1, 26-27cm	7.2	582	7,099,895	45.5	4.8	9.6	12.2
902-C9001C-2H-1, 99-100cm	7.9	476	3,802,993	39.9	5.0	11.2	12.7
902-C9001C-2H-4, 10-11cm	11.3	486	313,386	42.8	2.9	6.3	10.9
902-C9001C-2H-4, 99-100cm	12.2	468	1,406,003	37.8	5.6	12.8	13.2
902-C9001C-2H-5, 48-49cm	13.2	481	1,282,503	39.1	1.9	4.6	9.9
902-C9001C-2H-5, 99-100cm	13.7	521	320,420	40.5	1.5	3.7	9.4
902-C9001C-2H-7, 10-11cm	15.9	512	977,210	44.1	1.6	3.4	9.2
902-C9001C-2H-7, 100-101cm	16.5	475	1,299,160	42.5	0.6	1.5	7.3
902-C9001C-3H-1, 10-11cm	16.8	457	14,144,591	50.8	2.2	4.1	9.7
902-C9001C-3H-1, 99-100cm	17.4	464	7,002,046	41.4	0.6	1.5	7.4
902-C9001C-3H-3, 20-21cm	19.6	459	3,904,929	31.2	0.7	2.1	8.0
902-C9001C-3H-3, 57-58cm	20.0	464	6,518,395	34.5	0.0	0.0	0.0
902-C9001C-3H-5, 44-45cm	22.8	460	13,816,467	39.6	1.3	3.2	9.0
902-C9001C-3H-5, 87-88cm	23.3	494	5,821,528	47.0	0.4	0.9	6.3
902-C9001C-3H-7, 7-8cm	25.4	462	4,492,823	44.5	6.1	12.0	13.0
902-C9001C-3H-7, 41-42cm	25.7	465	3,097,318	52.5	3.2	5.8	10.6
902-C9001C-4H-1, 10-11cm	26.0	470	12,451,036	35.7	2.3	6.1	10.8
902-C9001C-4H-1, 99-100cm	26.9	535	6,485,724	58.7	1.7	2.8	8.7
902-C9001C-4H-3, 5-6cm	28.9	466	12,131,710	48.5	5.2	9.6	12.2
902-C9001C-4H-3, 99-100cm	29.8	507	7,336,951	57.4	1.8	3.0	8.9
902-C9001C-4H-5, 10-11cm	31.9	461	11,295,885	37.3	0.4	1.1	6.8
902-C9001C-4H-5, 99-100cm	32.8	550	8,001,946	42.7	1.5	3.3	9.1
902-C9001C-4H-7, 10-11cm	34.8	478	11,228,787	47.1	4.4	8.5	11.8
902-C9001C-4H-7, 112-113cm	35.6	498	7,072,851	49.9	1.1	2.1	8.0
902-C9001C-5H-1, 20-21cm	35.8	460	6,192,533	46.3	3.3	6.6	11.0
902-C9001C-5H-1, 81-82cm	36.2	486	528,812	42.2	3.5	7.7	11.5
902-C9001C-5H-3, 10-11cm	38.4	520	8,419,011	42.7	6.9	14.0	13.5
902-C9001C-5H-3, 99-100cm	39.3	515	960,593	43.1	2.3	5.1	10.3
902-C9001C-5H-5, 10-11cm	41.4	452	5,450,096	44.5	4.9	9.9	12.3
902-C9001C-5H-5, 99-100cm	42.2	441	161,558	39.0	4.5	10.4	12.5
902-C9001C-5H-7, 8-9cm	44.3	462	9,890,570	45.0	1.9	4.1	9.7
902-C9001C-5H-7, 99-100cm	45.0	456	6,352,933	43.6	1.8	3.9	9.5
902-C9001C-6H-1, 10-11cm	45.2	468	14,133,755	56.4	2.6	4.3	9.8
902-C9001C-6H-1, 99-100cm	45.9	488	10,988,333	54.3	0.6	1.1	6.8
902-C9001C-6H-3, 10-11cm	47.8	464	4,524,109	44.0	1.5	3.3	9.1
902-C9001C-6H-5, 10-11cm	50.7	454	8,972,875	45.4	1.5	3.3	9.1
902-C9001C-6H-5, 99-100cm	51.6	458	7,299,377	38.2	3.5	8.4	11.7
902-C9001C-6H-7, 10-11cm	53.6	466	15,547,649	47.4	3.6	7.1	11.2
902-C9001C-6H-7, 99-100cm	54.5	465	6,810,690	48.2	1.1	2.2	8.1
902-C9001C-7H-1, 10-11cm	54.5	467	29,238,739	50.3	1.9	3.7	9.4
902-C9001C-7H-1, 99-100cm	55.4	470	13,608,811	53.8	1.3	2.3	8.3
902-C9001C-7H-3, 10-11cm	57.4	513	11,728,279	57.9	0.8	1.3	7.1
902-C9001C-7H-3, 99-100cm	58.3	464	26,250,025	57.5	1.7	2.9	8.8
902-C9001C-7H-5, 10-11cm	60.4	492	10,692,396	47.2	2.0	4.1	9.7
902-C9001C-7H-5, 99-100cm	61.3	477	5,689,318	30.8	1.5	4.5	9.9
902-C9001C-7H-7, 10-11cm	63.3	461	2,081,023	53.1	2.6	4.7	10.0
902-C9001C-7H-7, 99-100cm	64.0	459	5,515,148	49.2	0.4	0.9	6.3
902-C9001C-8H-1, 9-10cm	64.2	457	3,211,452	23.4	5.7	19.5	14.7
902-C9001C-8H-1, 98-99cm	64.9	466	2,479,978	33.9	5.6	14.1	13.3
902-C9001C-8H-3, 9-10cm	66.9	473	2,210,813	21.8	6.1	22.0	13.2
902-C9001C-8H-3, 103.5-104.5cm	67.9	529	2,117,595	15.7	6.6	29.7	15.8

Table A2. (continued)

Sample	Curated Depth (mbsf)	Diatom Valves Counted	Total diatom abundance	Abundance (%) cold-water diatoms (*Xc*, XC)	Abundance (%) warm-water diatoms (*Xw*, XW)	*Td'*	Calculated SST (°C)
902-C9001C-8H-5, 10-11cm	69.7	450	3,574,574	31.1	1.8	5.4	8.8
902-C9001C-8H-5, 98.5-99.5cm	70.6	462	1,992,310	34.0	0.9	2.5	8.5
902-C9001C-8H-7, 10-11cm	72.6	505	4,063,163	37.8	2.0	5.0	9.6
902-C9001C-8H-7, 99-100cm	73.5	504	8,337,168	46.2	3.2	6.1	10.2
902-C9001C-9H-1, 10-11cm	73.5	461	527,354	48.4	2.0	3.9	9.8
902-C9001C-9H-1, 99-100cm	74.4	463	1,514,060	33.9	2.4	6.5	10.5
902-C9001C-9H-3, 10-11cm	76.3	475	1,951,765	13.7	1.1	7.1	10.7
902-C9001C-9H-3, 99-100cm	77.2	479	1,293,801	31.7	3.5	10.1	12.4
902-C9001C-21H-5, 7.5-8.5cm	190.7	459	7,474,841	27.5	9.4	25.4	15.9
902-C9001C-21H-5, 99-100cm	191.6	470	5,145,145	24.5	8.1	24.8	15.8
902-C9001C-21H-7, 10-11cm	193.5	454	10,199,127	19.6	15.6	44.4	18.5
902-C9001C-21H-7, 99-100cm	194.0	473	7,172,726	21.8	13.3	38.0	17.7
902-C9001C-22H-1, 10-11cm	194.4	461	10,054,204	19.3	10.4	35.0	17.3
902-C9001C-22H-3, 10-11cm	197.3	463	5,042,356	15.8	12.1	43.8	18.4
902-C9001C-22H-3, 99-100	198.2	449	6,853,436	13.4	21.4	61.5	20.2
902-C9001C-22H-5, 10-11cm	198.7	454	8,108,190	18.5	9.0	32.8	17.0
902-C9001C-22H-5, 99-100cm	199.6	482	5,162,900	21.4	19.7	48.0	18.9
902-C9001C-22H-7, 10-11cm	201.6	465	9,098,188	21.5	7.7	26.5	16.1
902-C9001C-22H-7, 99-100cm	202.5	460	4,714,819	25.0	13.9	35.8	17.4
902-C9001C-25H-5, 11.5-12.5cm	227.3	463	4,888,694	24.8	0.9	4.1	9.6
902-C9001C-25H-5, 101-102cm	228.2	494	7,611,798	22.1	0.6	2.8	8.7
902-C9001C-25H-7, 9-10cm	230.1	461	5,032,171	26.7	0.7	2.5	8.5
902-C9001C-25H-7, 99-100cm	231.0	454	1,569,815	26.0	2.9	10.2	12.4
902-C9001C-26H-1, 10-11cm	232.0	520	2,123,348	26.2	6.3	19.5	14.8
902-C9001C-26H-1, 97-98cm	232.9	536	3,262,413	25.9	6.5	21.0	15.1
902-C9001C-26H-3, 10-11cm	234.8	468	3,511,729	24.4	6.8	22.9	15.4
902-C9001C-26H-3, 99-100cm	235.6	474	9,960,159	27.4	6.8	20.4	15.0
902-C9001C-26H-5, 9-10cm	237.6	496	22,298,035	19.0	0.2	1.1	6.8
902-C9001C-26H-5, 99-100cm	238.5	557	9,081,662	27.8	1.4	5.6	10.5